1979

Wind Turbine Tower Wake Interface

J. Turnberg

Duane E. Cromack

PC67025F
UC-60
UM-WF-TR-79-7

WIND TURBINE TOWER WAKE INTERFERENCE

Technical Report

By

J. Turnberg and D. Cromack

Energy Alternatives Program
University of Massachusetts
Amherst, Massachusetts 01003

August, 1979

Prepared for
Rockwell International Corporation
Energy Systems Group
Rocky Flats Plant
Wind Systems Program
P.O. Box 464
Golden, CO 80401

As a part of the
U.S. DEPARTMENT OF ENERGY
DIVISION OF DISTRIBUTED SOLAR TECHNOLOGY
FEDERAL WIND ENERGY PROGRAM

DISCLAIMER

PATENT STATUS

TECHNICAL STATUS

EXECUTIVE SUMMARY

The response of a wind turbine when the blades travel through the wake of its supporting tower is an important consideration in the design of a wind energy conversion system. This tower induced flow perturbation, commonly known as tower shadow, has the cyclic effect of unloading a blade for a short period of time with each rotor revolution. A periodic force of this nature has the capability of exciting vibratory responses and exhibiting a fatigue affect on the long range operation of the turbine.

For this study, the response of the rotor to the unsteady loading is examined using two analytical models that deal with an isolated turbine blade. One model assumes the blade to be rigid and hinged at the hub, while the other model assumes a flexible blade cantilevered at the hub. Two approaches were chosen because each has certain advantages. The rigid model is simple and linearized yet offers insight into the problem, while the flexible blade model includes many non-linear terms and provides an in-depth analysis of the blade motion. Each model is solved to identify general trends that occur under normal wind turbine operation.

The wake that perturbs the blade is quite complex because a wind turbine pipe tower is a cylindrical bluff body that produces a wake with features common to most bluff bodies. The wake is generally unstable giving it a variable structure. Flow features change with windspeed, tower diameter, turbulence, and a host of other physical parameters. It is not feasible to account for all aspects of the complex wake flow; thus, a simple wake model is used as an approximation. The main features of the

wake required to preserve the nature of the blade interaction are the wake width and loss of wind speed. These features are approximated by using a rectangular velocity decrement occuring behind the tower. This tower shadow model is shown in Figure 1. The velocity decrement has strength (w_o), width (ζ) and it maintains the periodic frequency of blade passage. A simple momentun analysis of the wake velocity yields the result,

$$w_o = \frac{V}{V_o} = 1 - \frac{C_D}{2}$$

for estimating the velocity decrement. Since the Reynolds Number is usually high, the largest velocity decrement permitted by this model is $w_o = .5$, meaning the windspeed behind the tower is half the free stream velocity.

In modeling the turbine so that the tower shadow affect is clearly portrayed, it is necessary to isolate the wake-blade interaction from the many other unsteady variables. The variables that will be neglected in the force system are changes in wind speed and rotational speed of the rotor, wind shear, and gravity. This leaves a system that is periodically perturbed by the tower wake.

One model used for the simplified analysis consists of a rigid slender beam attached to the rotor hub by a hinge-spring. This model is known as an off-set hinge model and has been used extensively for helocopter studies as well as having been successfully adopted to wind turbines in many recent studies [7]. The model is shown in Figure 2.

The governing equation of motion for the isolated blade represents a periodically forced single degree of freedom system. The governing

FIGURE 3.5

TOWER SHADOW MODEL

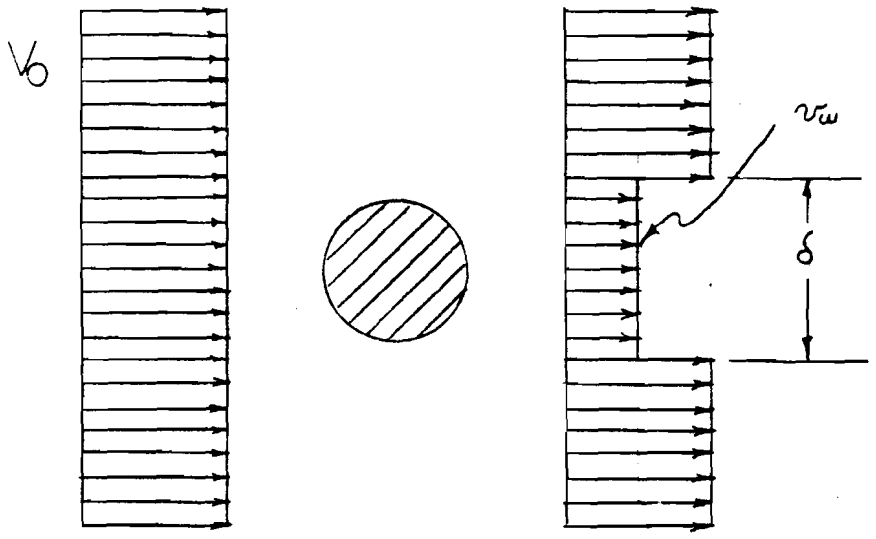

RECTANGULAR PULSE APPROXIMATION

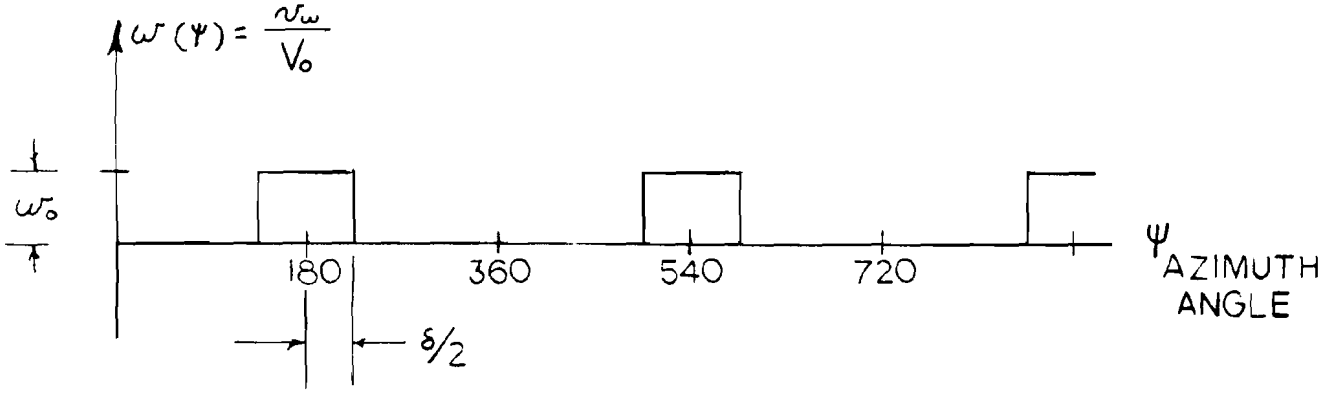

Figure 4.3

Blade Flapping Diagram

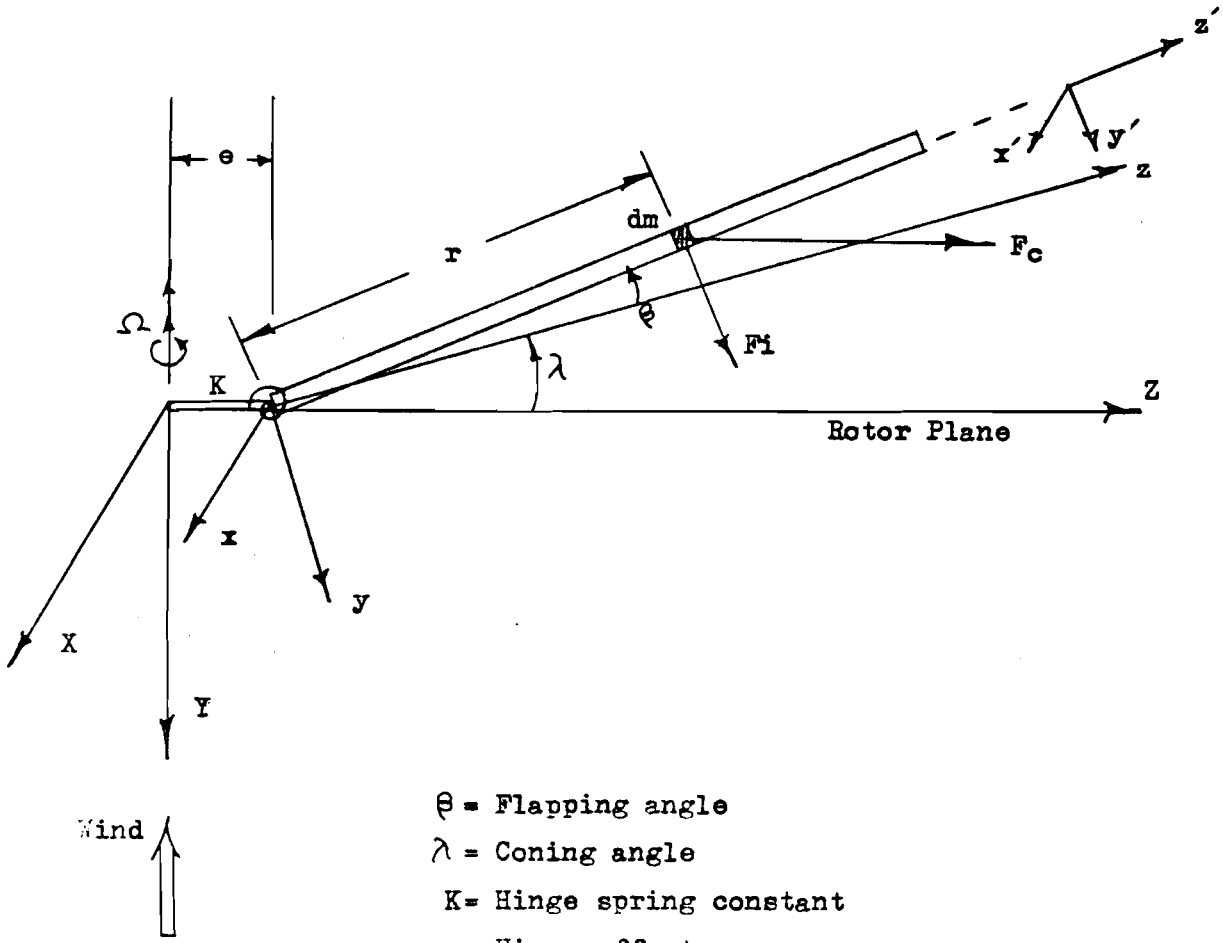

β = Flapping angle

λ = Coning angle

K= Hinge spring constant

e= Hinge offset

$Fi = r\ddot{\beta}\,dm$ Inertial force

$Fc = (eR + r\cos(\beta + \lambda))\Omega^2 dm$ Centrifugal force

equation is given by the following expressions:

$$\beta'' + \frac{\gamma}{8}\beta' + \frac{\omega_n^2}{\Omega^2} = \frac{\gamma}{2}\frac{\mu o}{3}(1-w(\psi)) - \frac{\lambda i}{3} - \frac{\theta p}{4} - \frac{\theta o}{20} + M_c$$

where: $\mu_o = \frac{V_o}{\Omega R}$; 1/tip-speed ratio

$\lambda_i = \frac{v_i}{\Omega R}$; induced velocity ratio

$\eta = r/R$; station span

$\gamma = \frac{\rho c l \alpha C R^4}{I}$; Lock's inertia term

$\beta' = \frac{d\beta}{d\psi} = \frac{\beta}{\Omega}$; flapping speed

θ_o = blade twist

θ_p = blade pitch

$w(\psi)$ = wake strength

and

$$M_C = \Omega^2(\epsilon \sin\lambda + \cos\lambda \sin\lambda)$$

$$\omega_n^2 = \Omega^2(\epsilon \cos\lambda + \cos^2\lambda - \sin^2\lambda) + \frac{K_\beta}{2}$$

with

Ω = rotational speed

K_β = hinge spring constant

ϵ = hinge offset constant

λ = coning angle

I = mass moment of inertia

An equivalent wake is determined by setting the shaded area behind the tower equal to the area of a sector swept by the blade;

$$\delta\psi = \frac{2D}{R}$$

This definition for the wake assumes that the velocity change depends only on the blade asimuth angle, so the wake acts instantaneously over the entire blade when the shadow is encountered.

As an example of the blade response, a solution is determined for the steady state operation of the WF-I is a 9 m/s (20 mph) wind. During rotation, the tower shadow deficit occurs between ($\delta\psi$ + 180°) and ($\delta\psi$ - 180°), but the resulting response is not significant until the blade begins its ascent from the bottom of rotation. The turbine blade follows an oscillating path as it rotates about the wind shaft. The oscillating pattern is similar for all windspeeds because the damping remains less critical. The blade root bending moment for the example case illustrates the response (Figure 3).

Oscillations of the blade root bending moments are the most important feature of the response. These oscillations are best described by their maximum (M_{max}) and minimum values (M_{min}). Figure 4 shows the maximum, minimum and steady moments encountered over the entire operating range of wind speeds for WF-I. The magnitude of the steady root moment drops quickly when the operational mode is changed to constant rotational speed. A more subtle change occurs in the magnitude of the oscillations. If the steady moment is removed from the response, a clear picture of the tower shadow perturbation results (Figure 5). The flatwise moment variation increases at a faster rate under constant rotational speed (region III) operation, than would have occured if constant tip-speed-ratio has been maintained.

FIGURE 4.7

RIGID PREDICTION

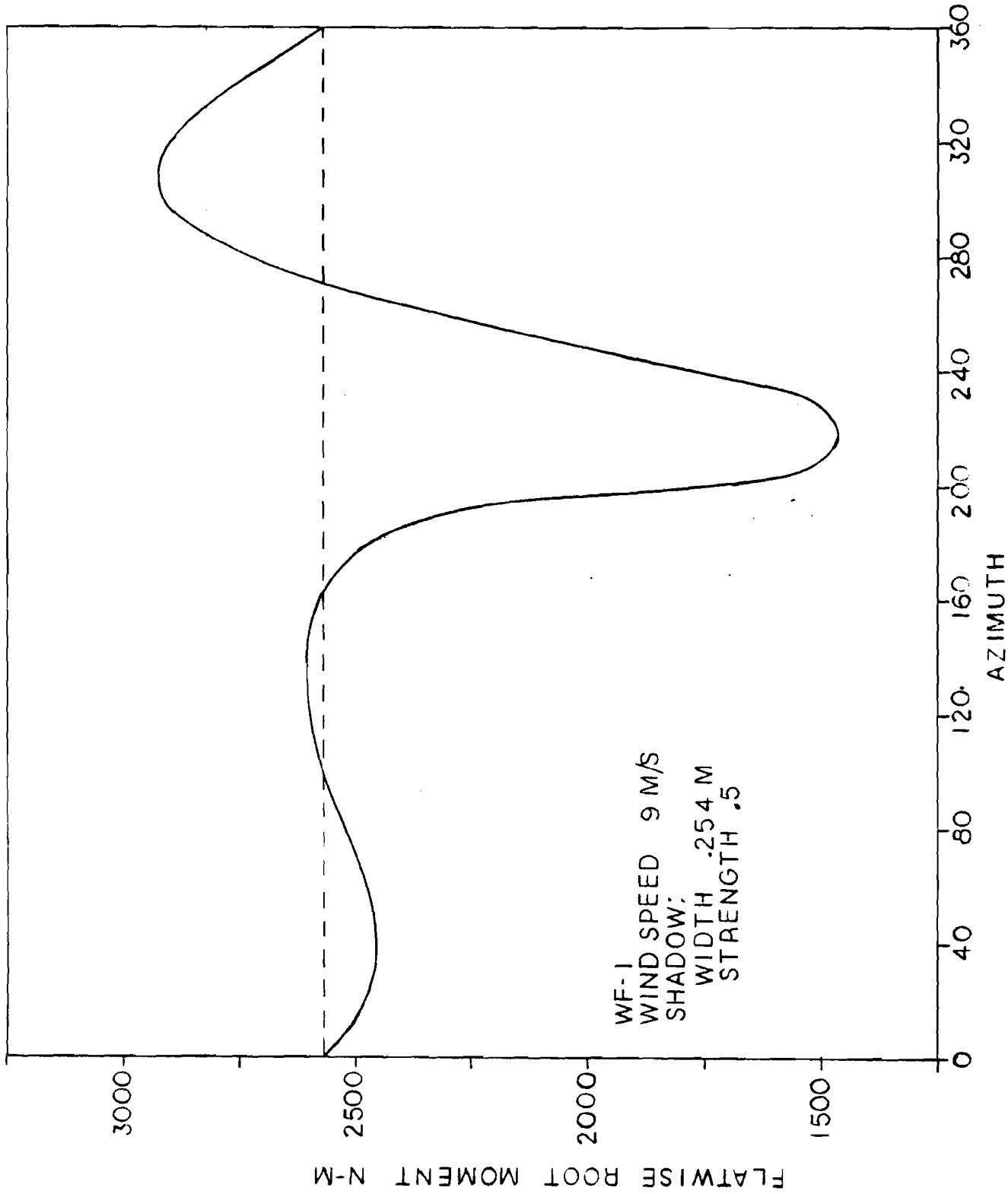

FIGURE 4.8

OPERATING RANGE

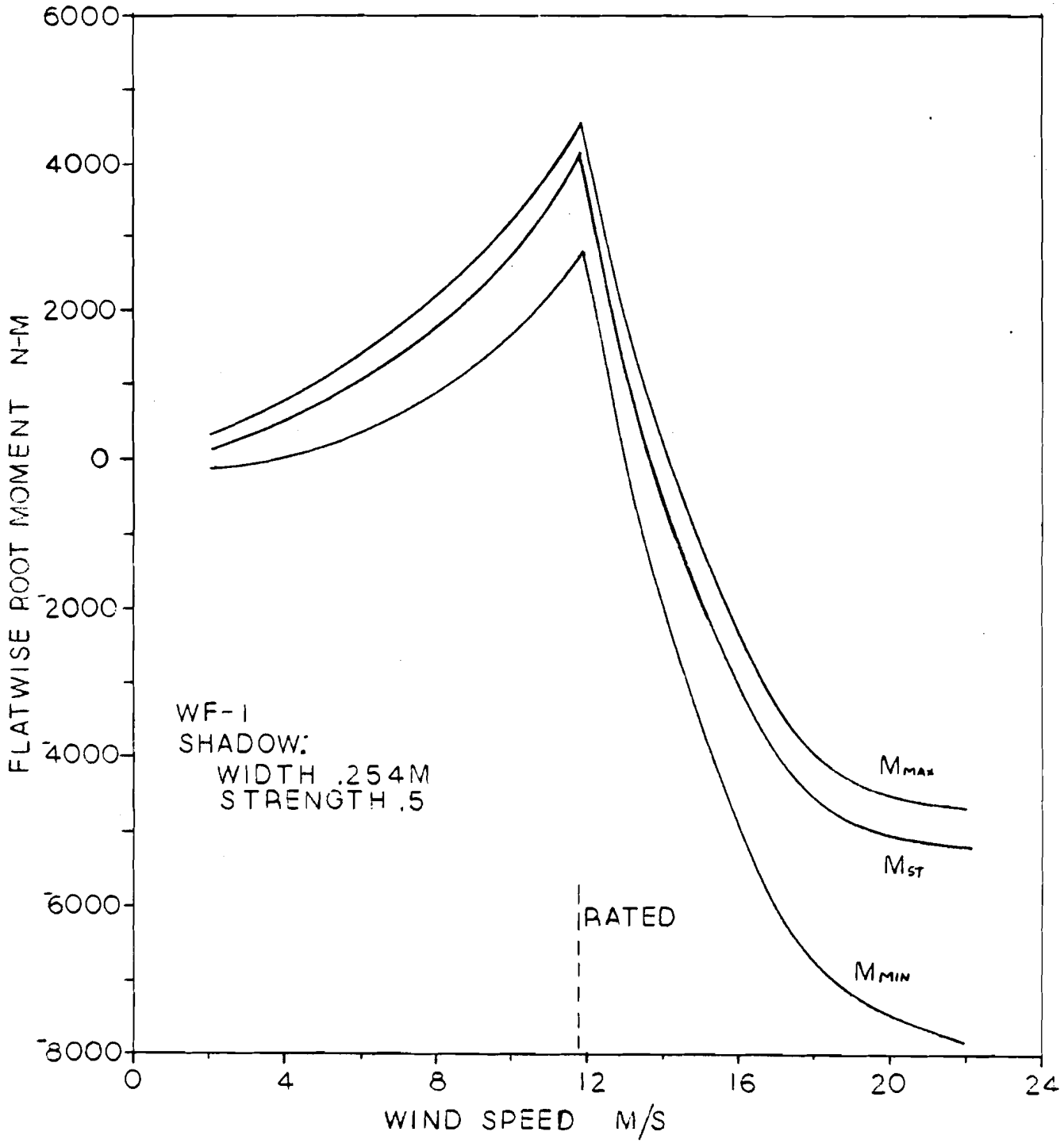

FIGURE 4.9

CYCLIC LOADS

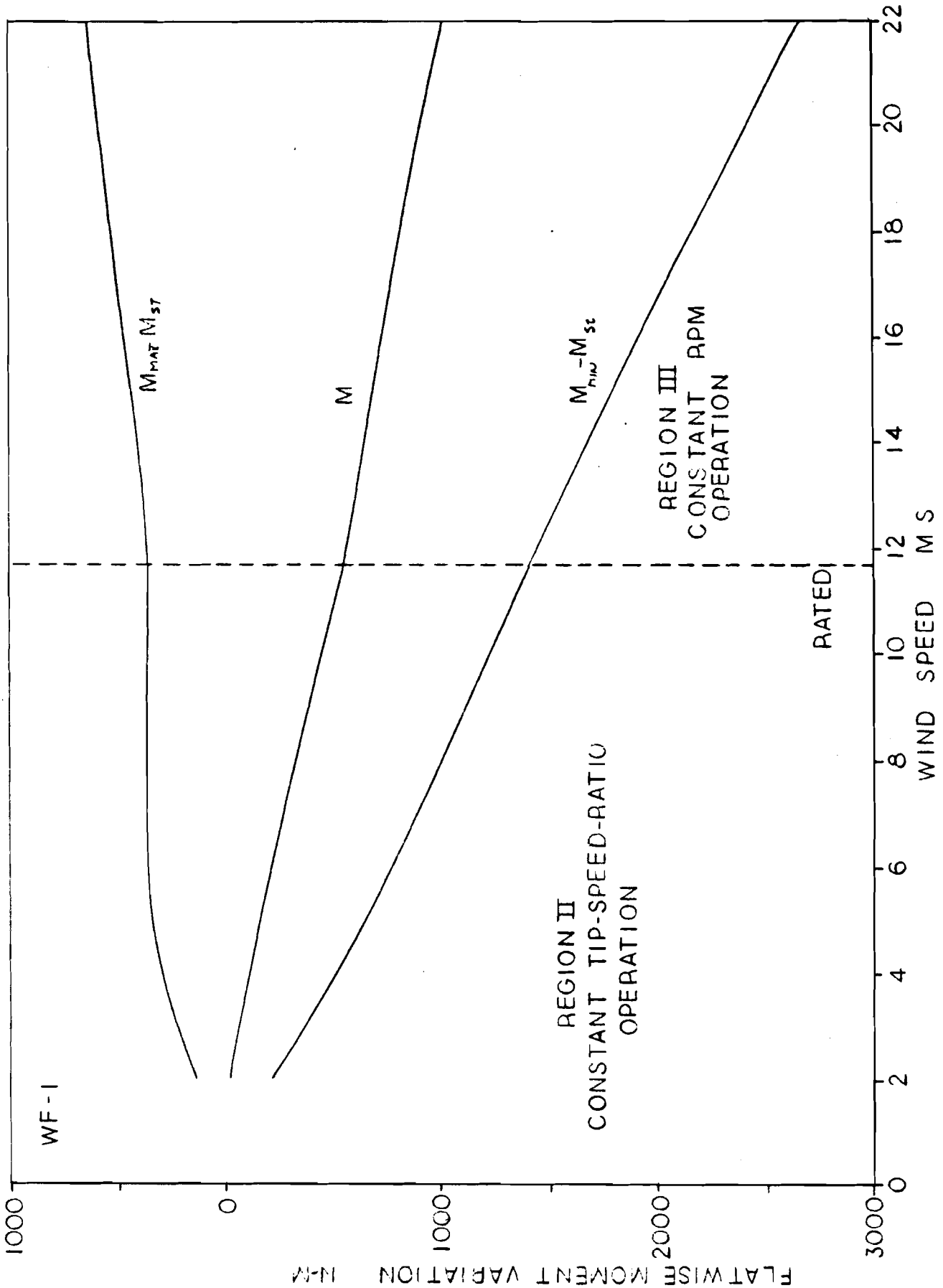

In addition to blade root bending moment variations, the wake contributes to the yaw motion experienced by the turbine. During high winds, WF-I has been observed to oscillate about a position slightly yawed away from the wind direction. A motion of this nature is indicated by the predicted shadow data when the blade moments for the entire rotor are resolved about the yaw axis. An example of the resulting yaw moments occuring in a 20 m/s (44 mph) wind are shown in Figure 6. The yaw moment has a frequency of three times the rotational speed with an amplitude variation about a positive mean yaw moment.

The previous simple rigid blade model is not adequate for an analysis of the force distribution along the blade. The rigid model is useful for determining many dynamic affects caused by the tower shadow, but the rigid model lacks the ability to handle blade flexibility and a complex geometry. A wind turbine blade is a non-uniform non-homogenious beam and the entire motion of the blade is needed for a detailed analysis of loading and moments.

The equation of motion for a differential element of a flexible rotor blade is;

$$\frac{\partial^2}{\partial z^2}\left[E \left(\frac{\partial^2 x}{\partial z^2} I_{xy} + \frac{\partial^2 y}{\partial z^2} I_{xx}\right) \right] - \frac{\partial}{\partial z}\left(G \frac{\partial y}{\partial z}\right) + m \frac{\partial^2 y}{\partial t^2} = F_y$$

$$\frac{\partial^2}{\partial z^2}\left[E \left(\frac{\partial^2 y}{\partial z^2} I_{xy} + \frac{\partial^2 x}{\partial z^2} I_{yy}\right) \right] - \frac{\partial}{\partial z}\left(G \frac{\partial x}{\partial z}\right) + m \frac{\partial^2 x}{\partial t^2} = F_x$$

where;

$$G = \int_z^R mr^2 z dz \quad = \text{blade tension}$$

E = Elastic modulus

FIGURE 4.11

YAW MOMENTS

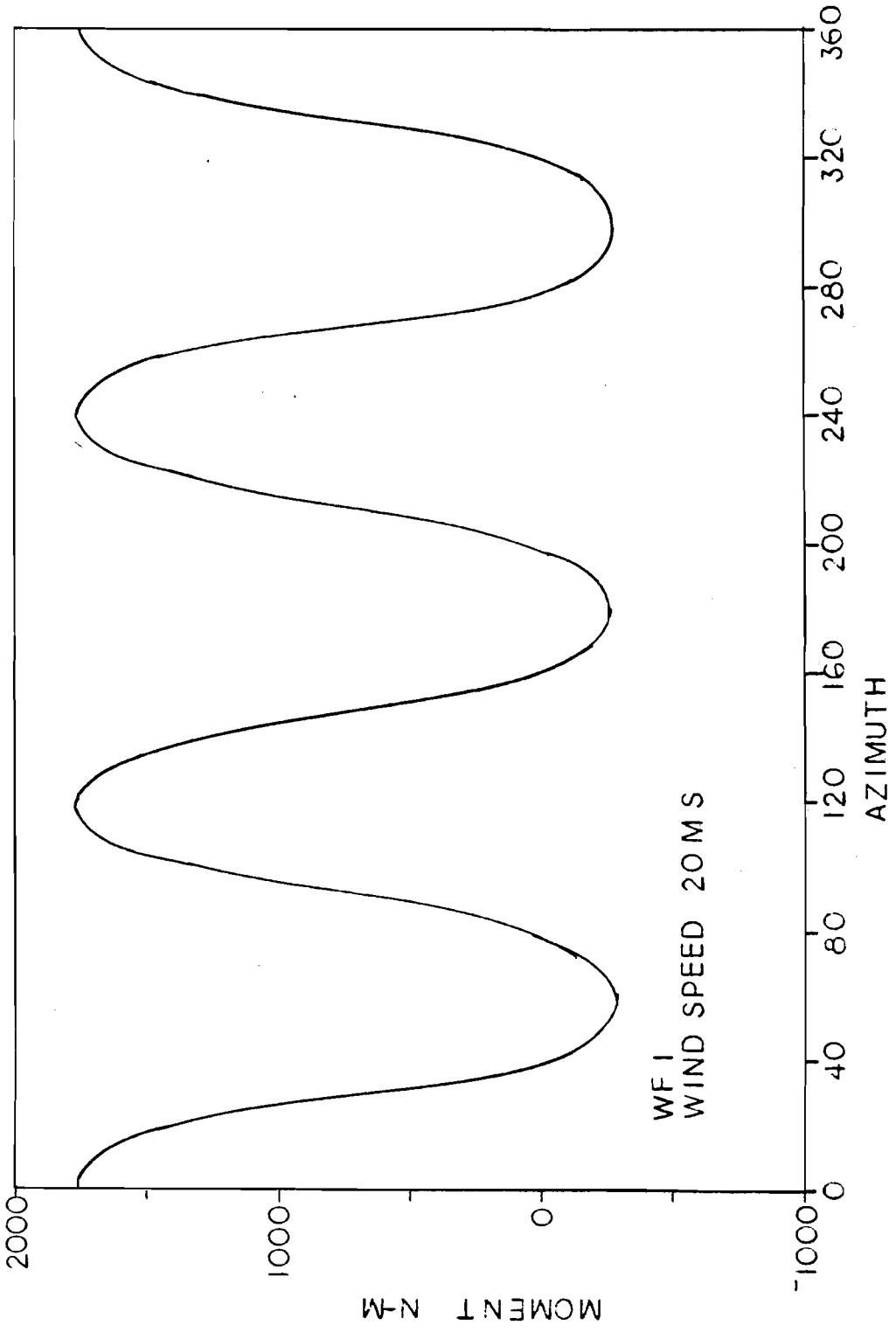

M = lineal mass

I_{xx}, I_{yy}, I_{xy} = aero moments of inertia

F_y, F_x = aerodynamic and centrifugal loads

It is evident by examination of these equations that the blade motion is coupled in the lag and flapping planes. There is no closed form solution for the expression, so an approximate method for solution is required. A modal analysis is chosen as the preferred solution technique since the equations are uncoupled in the modal frame of reference.

For this model, tower shadow is represented by a rectangular pulse that is both a function of azimuth angle and blade radius. Therefore, the velocity deficit is applied gradually starting at the blade root as the blade encounters the wake.

Rated conditions were also chosen to show the typical response of the blade when tower shadow perturbation is disrupting the flow. Figure 7 shows the blade root bending moment prediction for the flexible blade. The blade response has many similarities to the rigid blade analysis in that the shadow response occurs after the blade passes behind the tower and the recovery from the shadow indicates a damped oscillation. Bending moments are not severe because the tower shadow is applied and removed gradually. The gradual loading of the blade is believed to be a realistic model of the physical situation.

Part of the output from the solution of the equations of motion includes the steady-state forces that would exist for a uniform flow field. The

FIGURE 5.8

MODAL PREDICTION

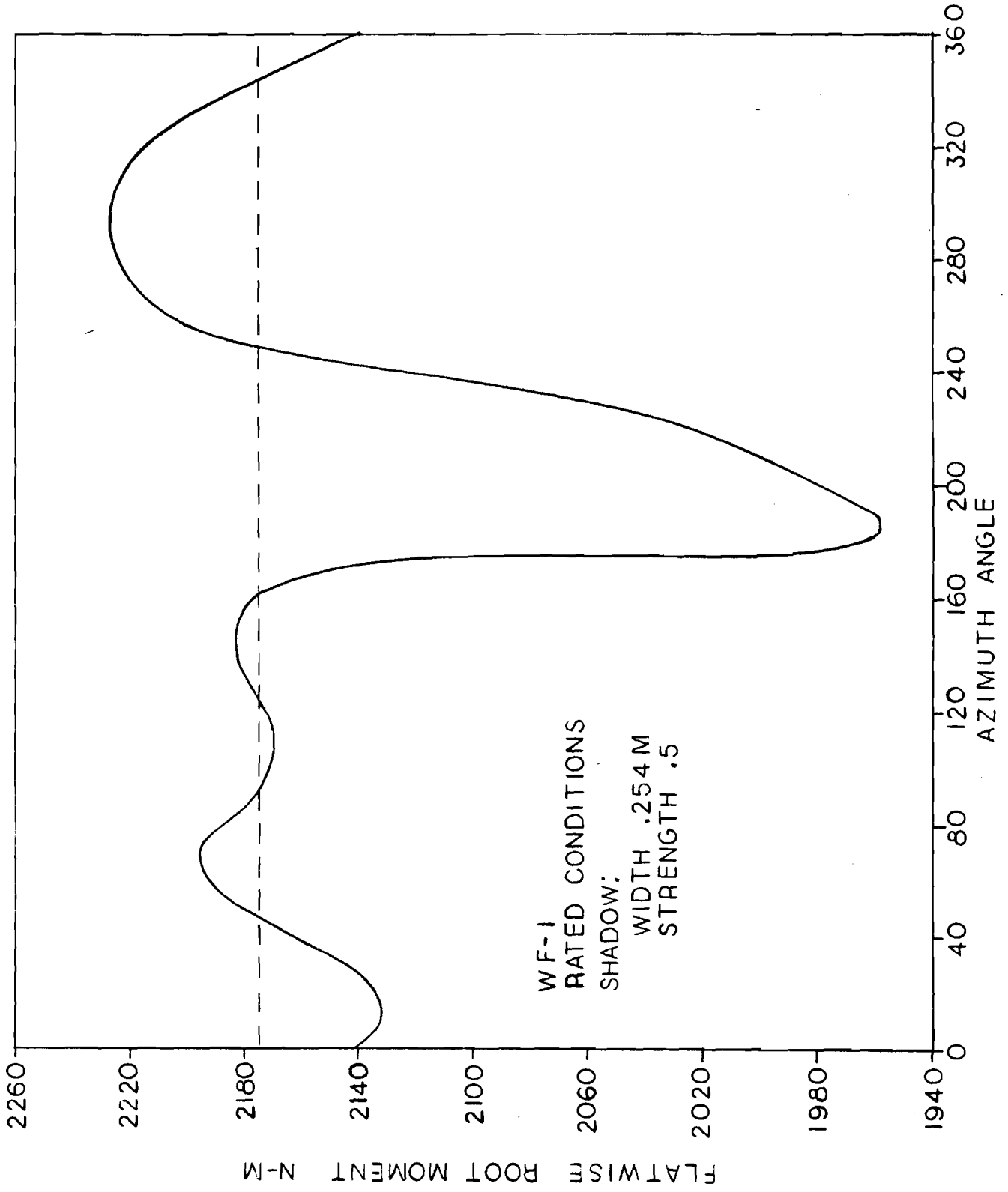

maximum bending moments on the blade occur between the .5 and .7 blade radius stations. The stress occurring on this section of the blade should be a maximum because the cross-sectional area decreases towards the tip. Figure 8 shows the affect that pre-coning the blade 10 degrees has on the bending moment distribution. Centrifugal relief reduces the total moment by more than half, which is a significant reduction of the steady applied loads.

In summary, both models indicate that the tower wake imparts a force that causes the blade to have a damped oscillatory motion with large deflection amplitudes occuring on the upswing of the blade ($\psi > 180°$). The major discrepancy between the two model predictions involves the magnitude of the resulting forces. Larger cyclic forces are always predicted by the simple rigid model because the shadow is assumed to encompass the entire blade instantaneously, while the complex model assumes a gradual application of the shadow.

Of the two approaches, the rigid system solved by computer code RIGID proved to be easier and less time consuming than its flexible counterpart solved by computer code DYNAMICS. Since the simple model predicts a more drastic response, it serves to make conservation estimates of the blade loading. The more complex model serves the purpose of defining a detailed loading distribution along the blade. For design applications, the simple system will indicate problem areas and the complex system will define the loads at those problem areas.

FIGURE 5.6

CENTRIFUGAL RELIEF

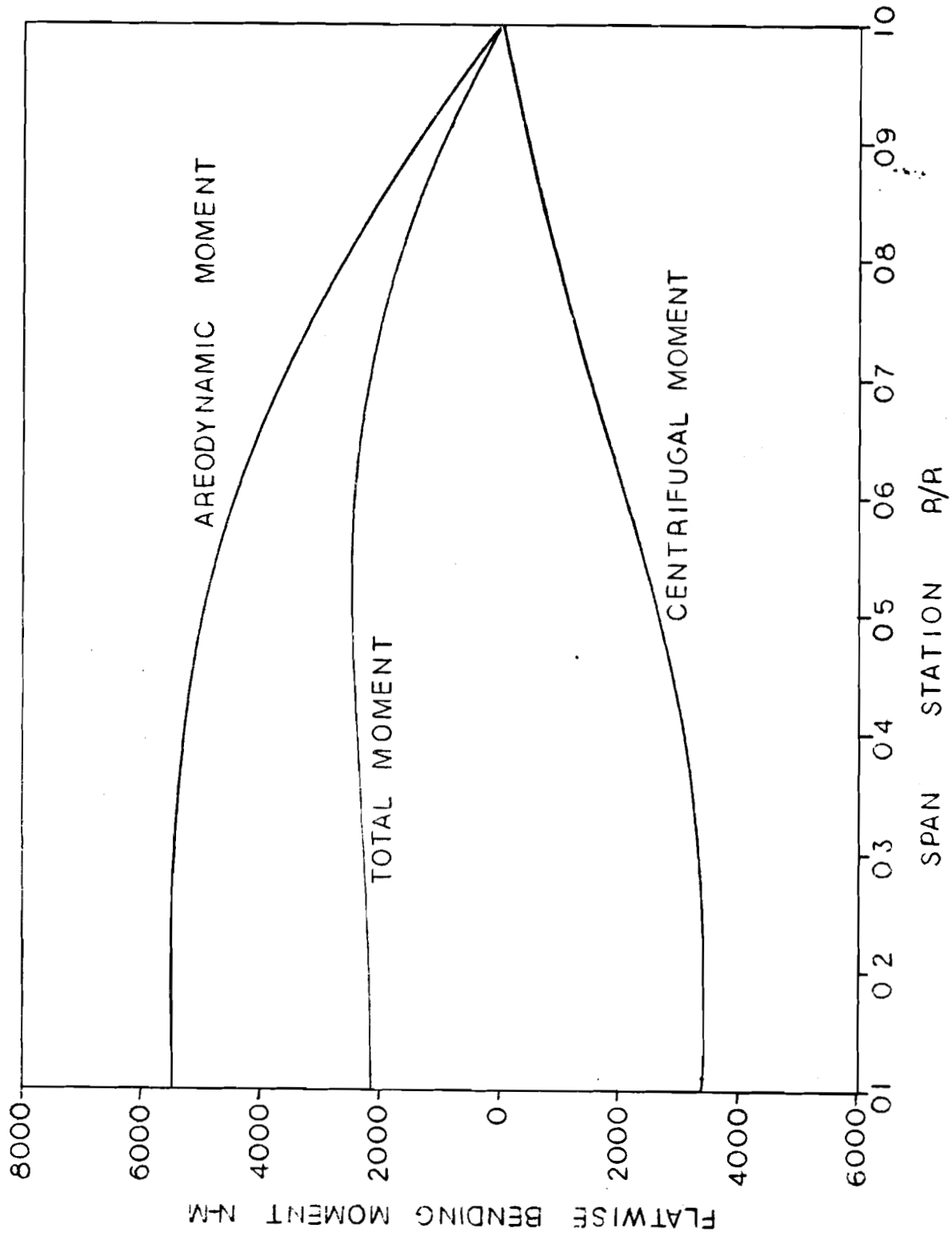

ABSTRACT

The design of a wind turbine involves the combination of many parameters, one of which is the determination of the dynamic load cases affecting the blades. The dynamic loads include many periodic and random fluctuations. Of these loads, the cyclic loading of the blade as it passes through the wake of the wind turbines supporting tower is the subject of this paper.

The tower wake and/or shadow causes a change in the deflection pattern of the blade on a once per revolution per blade basis. Analytical predictions developed for this project show that the blade exhibits an oscillatory motion. The amplitude of oscillation ranges from a maximum on the upswing of the blade to near zero amplitude immediately before the tower wake is encountered on the downswing.

The magnitude of the tower induced load variation is an essential part of a wind turbine design because cyclic load variations have a fatiguing effect on structural components that must be included in the design process. Therefore, the enclosed analysis offers a procedure for predicting the wind turbine blade response to tower shadow for use in preliminary design applications.

TABLE OF CONTENTS

LIST OF FIGURES

LIST OF TABLES

INTRODUCTION

The response of wind turbine when the blades travel through the wake of its supporting tower is an important consideration in the design of a wind energy conversion system. This tower induced flow perturbation, commonly known as tower shadow, has the cyclic effect of unloading a blade for a short period of time with each rotor revolution. A periodic force of this nature has the capability of exciting vibratory responses and exhibiting a fatigue affect on the long range operation of the turbine. Therefore, the tower shadow must be taken into account to assure structural integrity.

The extent of tower interference is primarily determined by the geometry of the support. There are two major types of support structures commonly employed, the truss tower and the pole tower. Little has been accomplished to qualify the affect of a pole tower wake disturbance. The majority of available data has been produced by the Department of Energy for the truss towers that support their large demonstration systems. The wake behind a truss tower is relatively stable and can be predicted using Prandtl's mixing length theory. The wake behind a pole tower is only well behaved for low wind speeds. At moderate and high wind speeds, the wake becomes unstable because the near wake is in the region of vortex formation. Even without the added complication of blade motion, present theory cannot predict the detailed near wake structure for anything but low wind speeds.

The purpose of this project is to evaluate the affect of tower shadow on the turbine rotor. A wind turbine rotor blade is driven by forces that have inertial, elastic, and aerodynamic origins. Of these forces, the aerodynamic force is the result of the dynamic reaction of the blade to the air. Therefore, flow pertubations caused by the tower result in unsteady forces that produce blade motion.

The response of the rotor to the unsteady loading is examined using two analytical models that deal with an isolated turbine blade. One model assumes the blade is rigid and hinged to the hub, while the other model assumes a flexible blade cantilevered into the hub. Two approaches were chosen because each has advantages. The rigid model is simple and linearized so that it offers insight into the problem, while the flexible blade model includes many non-linear terms that complicate the system. Each model is solved to identify general trends that occur with normal wind turbine operation.

It is hoped that the results of this research will give a designer insight into the tower shadow phenomenon to assist him with design decisions, because an understanding of tower shadow is vital to the cost, safety, and reliability conditions necessary for the economic generation of power from the wind.

CHAPTER 2

THE UNIVERSITY OF MASSACHUSETTS WIND FURNACE I

2.1 Operational Aspects

To facilitate the investigation of tower shadow, the wind turbine operating at the University of Massachusetts is used as a typical example of a high speed horizontal axis windmill. This wind turbine, known as the Wind Furnace I (WF-I), is used for the space heating of a home, Solar Habitat I. WF-I has a downwind configuration with a three bladed 9.9 m (32.5 ft.) diameter rotor, and the torque developed by the rotor is transmitted to a 31.5 kW a.c. synchronous generator. The entire rotor-generator system is mounted atop a 18.3 m (60 ft.) stayed pole mast. The turbine has a design capacity of 25 kW at 11.7 m/s (26 mph) wind speed.

Operation of the WF-I is defined by four regions: (1) start-up; (2) constant tip-speed-ratio; (3) constant rotational speed; and (4) shut down. These operational regions are shown in Figure 2.1, a representation of power output as a function of windspeed. Power production is controlled with changes in blade pitch angle and generator excitation. Pitch angle and excitation are set by a pre-programmed microprocessor based on rotor speed. Figure 2.2 shows the pitch changes that occur from start-up to shut down as a function of wind speed.

In region I, start-up, the blades are pitched to 40° to produce maximum start-up torque. The wind speed must be sufficient to turn the rotor at 40 rpm before the blades are pitched to 6.0° for region II operation. Throughout region II, the aerodynamic conditions needed to extract the maximum power from the wind are maintained by keeping the

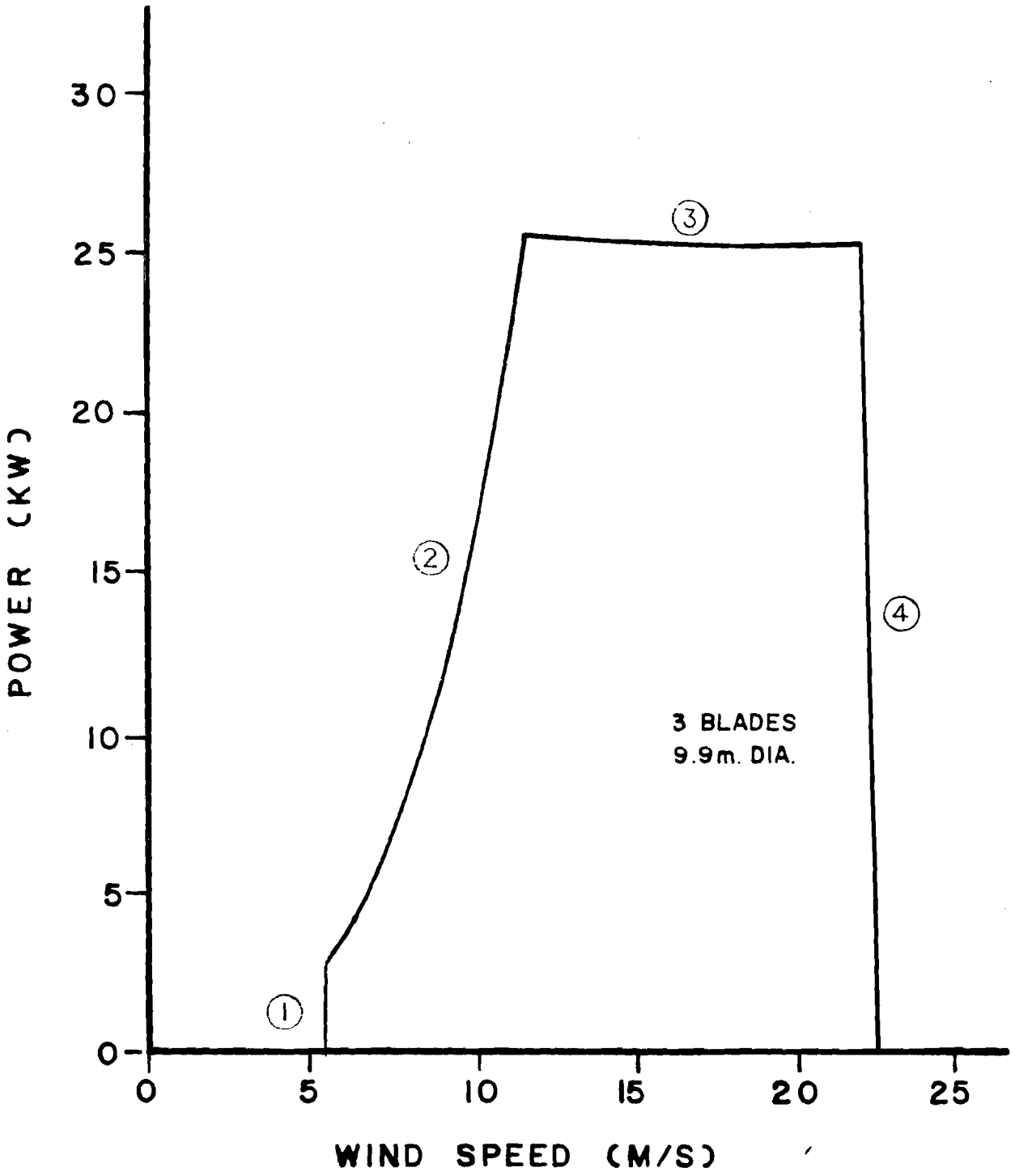

PREDICTED PERFORMANCE

FIGURE 2.1

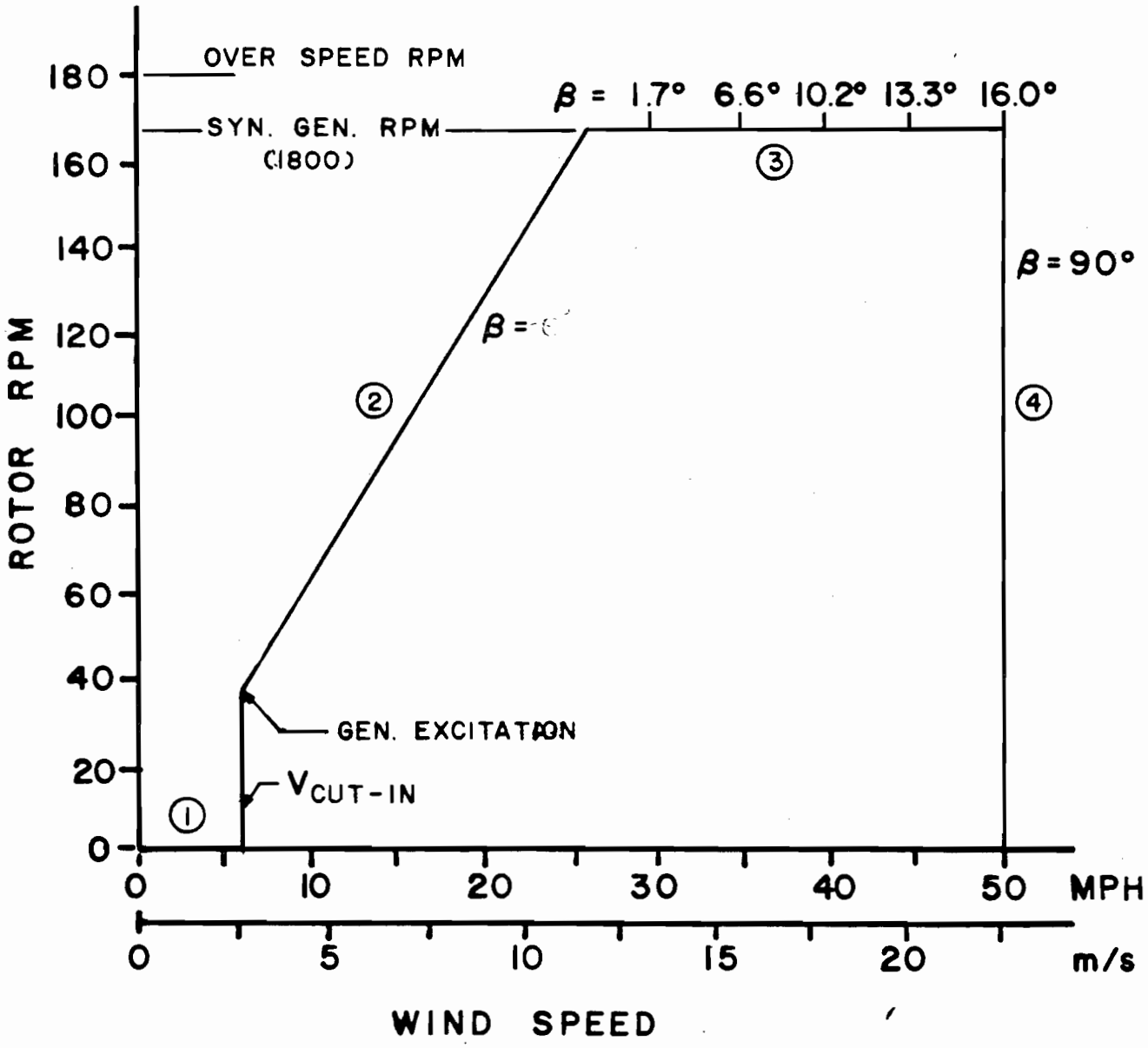

ROTOR RPM AS A FUNCTION OF WIND SPEED

FIGURE 2.2

tip-speed-ratio at a constant value of 7.5. Tip-speed-ratio is the ratio of rotor speed to wind speed;

$$\mu = \frac{\Omega R}{V_o} \tag{2.1}$$

where: Ω = rotor rotational speed

R = rotor radius

V_o = wind speed

The generator excitation is used during constant tip-speed operation to control the rotor rpm so that the power will follow a cubic relationship with increasing wind speed.

When the rotational speed reaches 167 rpm at rated conditions, region III operation begins. The rotor speed and power remain constant throughout region III because the blades are pitched to "spill the wind." This control of speed and power is maintained until the turbine is shut down. Region IV, shut-down, is brought about by pitching the blades to an angle of 90° or full feather.

2.2 Structural Parameters

The rotor blades are the primary components affected by the tower shadow. As elastic structures, the blades are continually subjected to a cyclic un-loading as they pass behind the tower. Sicne the un-loading pattern is periodic, fatigue and resonance problems will be a factor in any design. Therefore, the blade structural properties must be known before an analysis of the tower shadow perturbation can progress, since the aerodynamic, elastic, and inertial forces depend on the geometry and material composition of the blade.

The wind furnace blades are designed to have a twist and chord distribution near the optimum as predicted by aerodynamic theory and they are designed with an NACA 4415 airfoil section. The blades are constructed of glass reinforced plastic (GRP) molded into three structural members, the spar, skin, and trailing edge stiffener (Figure 2.3). The blade root stock is a steel sleeve which serves as a bearing support to cantilever the blade into the hub at a coning angle of ten degrees. The blade design is summarized in Table 2.1 [2]. These design parameters are then used as input to the structural computer codes, MOMENTS, and FREQ, developed by Perkins [2]. The output of these computer codes includes the following blade section structural properties: the mass distribution, mode shapes, and natural frequencies whose values are given in Table 2.2 with the modal coordinate system (Figure 2.4). A mode shape is the orientation of the blade when it oscillates at a natural frequency. For a flexible system there are an infinite number of natural frequencies, but only the lowest few frequencies are important to the response of a system.

2.3 Vibrational Considerations

The natural frequencies and blade properties presented in the previous section are sufficient to perform an elementary vibration analysis of possible resonant conditions. Resonance occurs when the frequency of the applied force system coincides with one of the natural frequencies of the body. At the resonant condition, large amplitudes may develope causing a loss in structural integrity. To determine the resonant frequencies, it is necessary to identify cases where the blades' natural

TABLE 2.1

BLADE DESIGN

WF-1 (Radius = 16.25 ft)

r/Radius (Station÷10)	Chord (ft)	Twist (degrees)	L.E. to Spar Web (ft)	Skin Thickness (in)	Spar Thickness (in)	Web Thickness (in)
.1	1.35	45	.54	.036	.238	.238
.2	1.46	25.6	.584	.036	.238	.238
.3	1.26	15.9	.504	.036	.205	.220
.4	1.02	10.4	.41	.036	.205	.150
.5	.85	7.4	.34	.036	.205	.050
.6	.73	4.5	.29	.127	.186	.050
.7	.63	2.7	.25	.027	.148	.050
.8	.55	1.4	.22	.018	.110	.050
.9	.45	.4	.18	.018	.072	.050
1.0	.35	0	.14	.018	.053	.050

$E_{skin} = 2.2 \times 10^6$ psi $\quad G_{skin} = .5 \times 10^6$ psi $\quad \rho_{skin} = .0555 \frac{lb}{in^3}$

$E_{spar} = 4.4 \times 10^6$ psi $\quad G_{spar} = .3 \times 10^6$ psi $\quad \rho_{spar} = .0501 \frac{lb}{in^3}$

FIG. 2.3

DESCRIPTION OF BLADE COMPONENTS

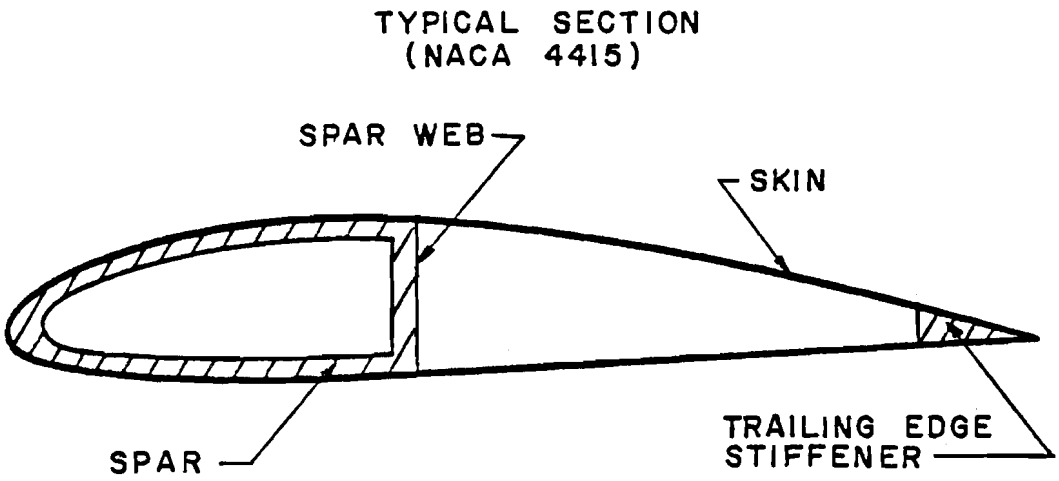

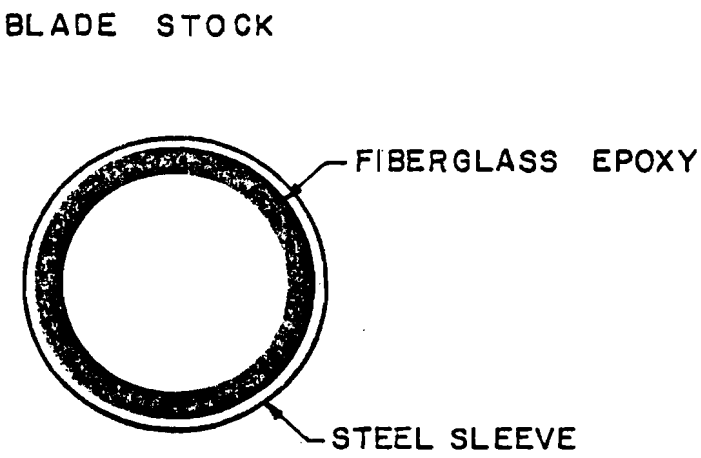

Table 2.2

STATION SPAN									
0.100	0.200	0.300	0.400	0.500	0.600	0.700	0.800	0.900	1.000
MASS DISTRIBUTION (KG)									
10.050	6.123	4.766	4.016	3.463	2.696	1.999	1.473	1.025	0.527
X MODAL COORDINATES									
0.000	0.000	-0.010	-0.020	-0.040	-0.060	-0.080	-0.110	-0.130	-0.160
0.000	0.010	0.050	0.110	0.180	0.290	0.430	0.600	0.790	1.000
0.000	-0.010	-0.020	-0.040	-0.060	-0.050	-0.030	0.030	0.120	0.150
Y MODAL COORDINATES									
0.000	0.010	0.030	0.090	0.170	0.290	0.430	0.600	0.790	0.990
0.000	0.000	0.000	0.000	0.000	0.020	0.060	0.110	0.180	0.250
0.000	0.030	0.090	0.180	0.270	0.280	0.140	-0.190	-0.700	-0.950

NATURAL FREQUENCY (RADIANS/SECOND)

28.430	64.450	99.550

Figure 2.4

MODAL COORDINATES

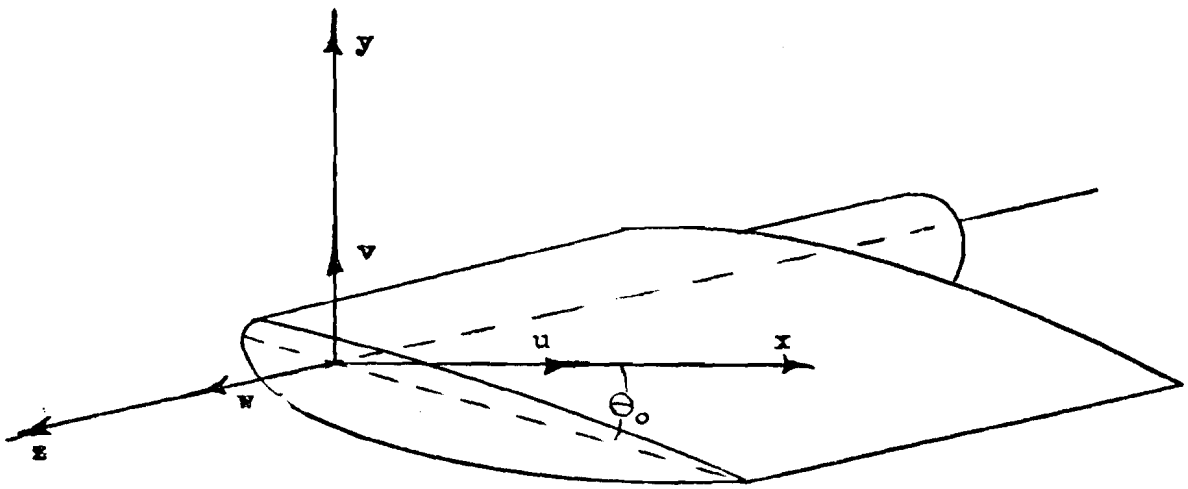

frequency coincides with the periodic force of the tower shadow.

Previously determined blade natural frequencies were developed for a non-rotating system. These frequencies will not be the same for a rotating system. The centrifugal force resulting from rotation stiffens the blade and thus raises the natural frequency. The increase in natural frequency is determined with the aid of the Theorem of Southwell, which is discussed in Appendix A. Briefly, this Theorem states that the frequency is divided into two parts, the non-rotating effect and the rotational effect. These two parts are combined using equation 2.2:

$$\omega^2 = \omega_n^2 + \alpha\Omega^2 \tag{2.2}$$

where: ω_n = non-rotating frequency

Ω = rotational speed

α = Southwell coefficient.

The Southwell coefficient (α) is found using the expression;

$$\alpha = \frac{\int_{R_o}^{R} Z \int_{R_o}^{Z} m \left(\frac{d\emptyset}{dZ}\right)^2 d z \, d z}{\int_{R_o}^{R} M \, \emptyset^2 \, d z} \tag{2.3}$$

where: R = rotor radius

R_o = hub radius

$\emptyset$ = mode shape

m = mass per unit length

The Southwell coefficients for the first three frequencies for the Wind Furnace blades have the values;

$\alpha_1 = 3.635$

$\alpha_2 = 3.458$

$\alpha_3 = 5.813$

These values are used in conjunction with eq. 2.2 for the evaluation of the natural frequency at any rotational speed.

Force frequencies are now needed to complete the frequency analysis. The un-loading of the rotor behind the tower produces a periodic force that has a primary harmonic component equal to the rotational speed (1P) on each blade and a three per revolution (3P) harmonic on the rotor. These two harmonics are largest in magnitude, but they are not the only components produced by the excitation. The nature of the tower shadow is periodic and unlike a sinusodal disturbance, a periodic force system can excite many frequencies. The forced frequencies occur at integer multiples of the rotor speed;

$$\omega = n\Omega \tag{2.4}$$

where: n = integer

In general the high harmonics have negligible effects on a system.

A comparison of the frequencies is clearly shown by the fan diagram (Campbell plot) in Figure 2.5. The straight lines extending from the origin indicate the various harmonics of rotor speed and the curved lines represent the natural frequencies. Each intersection of a harmonic line with a natural frequency line represents resonance. Since the occurance of resonance is generally unavoidable, its effect must be minimized. The safest region to have an occurance of resonance is when the rotor speed is variable, since the large amplitudes associated with resonance occur when the frequencies coincide for extended periods of time. Operational

FIGURE 2.5

WF-1 CAMBELL PLOT

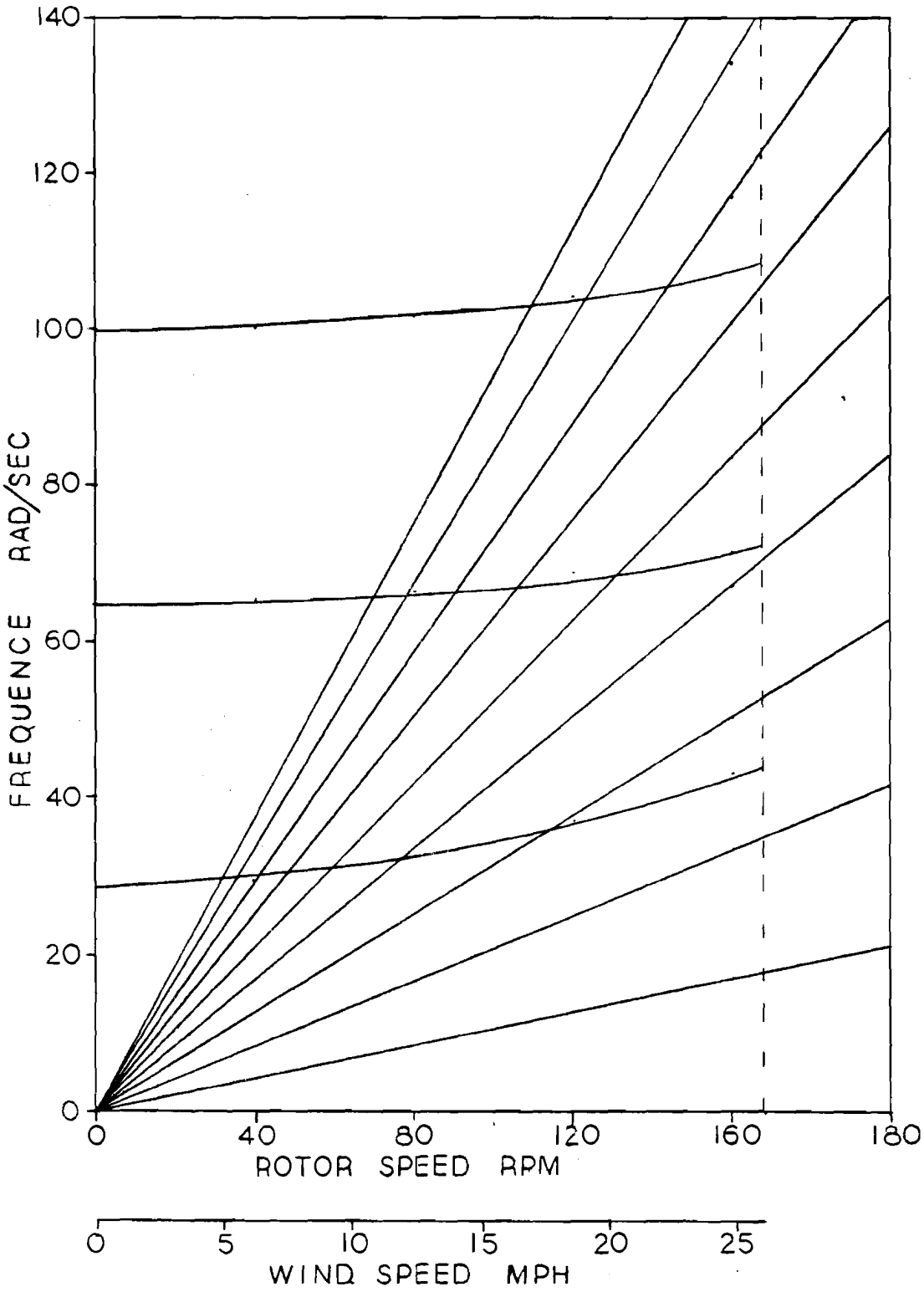

experience with the Wind Furnace indicates that the many resonant conditions occuring in region II operation do not affect the structure of the system. It should be emphasized that resonant conditions occuring at rated rpm will generally damage the turbine since the frequencies coincide for prolonged time periods. From this point, the analysis will involve the development of a wind turbine model that predicts the load variation induced by the tower shadow.

CHAPTER 3

FLOW BEHIND A PIPE TOWER

3.1 The Ideal Wake

A wind turbine pipe tower is a cylindrical bluff body that exhibits a wake with features common to most bluff bodies. One feature is that the wake close to the tower is strikingly different from that existing far downstream. The far-wake occuring more than 100 tower-diameters downstream is stable and predictable. Prandtls' mixing length theory serves as the analytical technique used to predict the velocity distribution in the far-wake. The near-wake is generally unstable giving it a variable structure. Flow features change with windspeed, tower diameter, turbulence, and a host of other physical parameters. The remainder of this chapter concentrates on the near-wake because it is this region that represents the tower shadow. In order to discuss the wake, it is convenient to divide the flow into classes that have similar properties. There are generally four classifications given to the wake: slow viscous, subcritical, critical, and supercritical [3]. Each class is experimentally determined and identified by a Reynold's Number regime, where the Reynold's Number is defined as the ratio of inertial to viscous forces:

$$R_e = \frac{V_o D}{\nu} \tag{3.1}$$

where: V_o = windspeed

D = tower diameter

ν = kinematic viscosity

When wind speeds are low, the wake is classified as that of slow viscous flow ($o < R_e < 40$). Under these low Reynolds Numbers, the wake

is stable because viscous forces dominate the flow. Although the wake is stable, gradual changes occur throughout the slow viscous regime. For Reynolds Numbers up to five, the flow stays attached to the tower. Above a Reynolds Number of five, the boundary layer separates from the surface of the tower creating two vorticies. These vorticies are side by side and remain stationary behind the cylindrical tower. These stationary vortices begin oscillating as the Reynolds Number increases beyond 40, because the fluid inertial forces now have a greater dominance over the flow. Further increases in the inertia of the flow causes the vorticies to periodically leave the cylinder one at a time from alternate sides. This periodic vortex shedding is the dominant feature of the sub-critical wake regime ($40 < R_e < 1.5x10^5$). The parameter used to describe the periodic production of vorticity is the Strouhal Number (S_t), defined as:

$$S_t = \frac{fD}{V_o} \tag{3.2}$$

where: f = frequency of vortex production (Hz)

and has a value in the neighborhood of .21 throughout the subcritical regime. In this region, the fluid boundary layer separates from the surface of the cylinder at approximately 82° from the up-wind stagnation point. Since separation occurs on the front portion of the tower, the wake directly behind the tower is wider than the diameter of the tower. The wide wake of the subcritical regime continues until the boundary layer becomes turbulent.

Transition to turbulence triggers the critical region of flow ($1.5x10^5 < R_e < 1.5x10^6$). Turbulence transfers momentum into the boundary layer causing the fluid to re-attach after initial separation.

Therefore, the point of separation moves to the back side of the tower. Re-attachment of the boundary layer is accompanied by the diminishing width of the wake and an increase in the Strouhal Number (S_t .44). When the Reynolds Number attains a high enough value, separation and subsequent re-attachment of the boundary is no longer present, so the flow is classified as supercritical ($R_e > 1.5 \times 10^6$). In this flow regime, separation occurs only once at about $\pm 120°$ from the up-stream stagnation point. The wake is wider than it was for the critical regime and the Strouhal Number decreases to an average value of .28. The drag coefficient acting on a cylinder is a good indicator of the four classes of flow, where drag coefficient is defined as:

$$C_d = \frac{F_d}{1/2 \ \rho V^2 A} \tag{3.3}$$

where: F_d = drag force on the body

ρ = fluid density

V = fluid velocity

A = cylinder area

Figure 3.1 shows the drag coefficient plotted as a function of the Reynolds Number. At low Reynolds numbers, high drag coefficients indicate the slow viscous regime. The drag coefficient then decreases and levels out in the viscinity of unity throughout the subcritical regime and then drops drastically in the critical regime.

When a Reynolds Number versus wind speed curve (Figure 3.2) is developed for an assortment of tower diameters, it becomes apparent that the tower Reynolds Number is generally high. The wake, therefore, is in the vicinity of the critical flow regime. Figure 3.3 is an example of

FIGURE 3.1

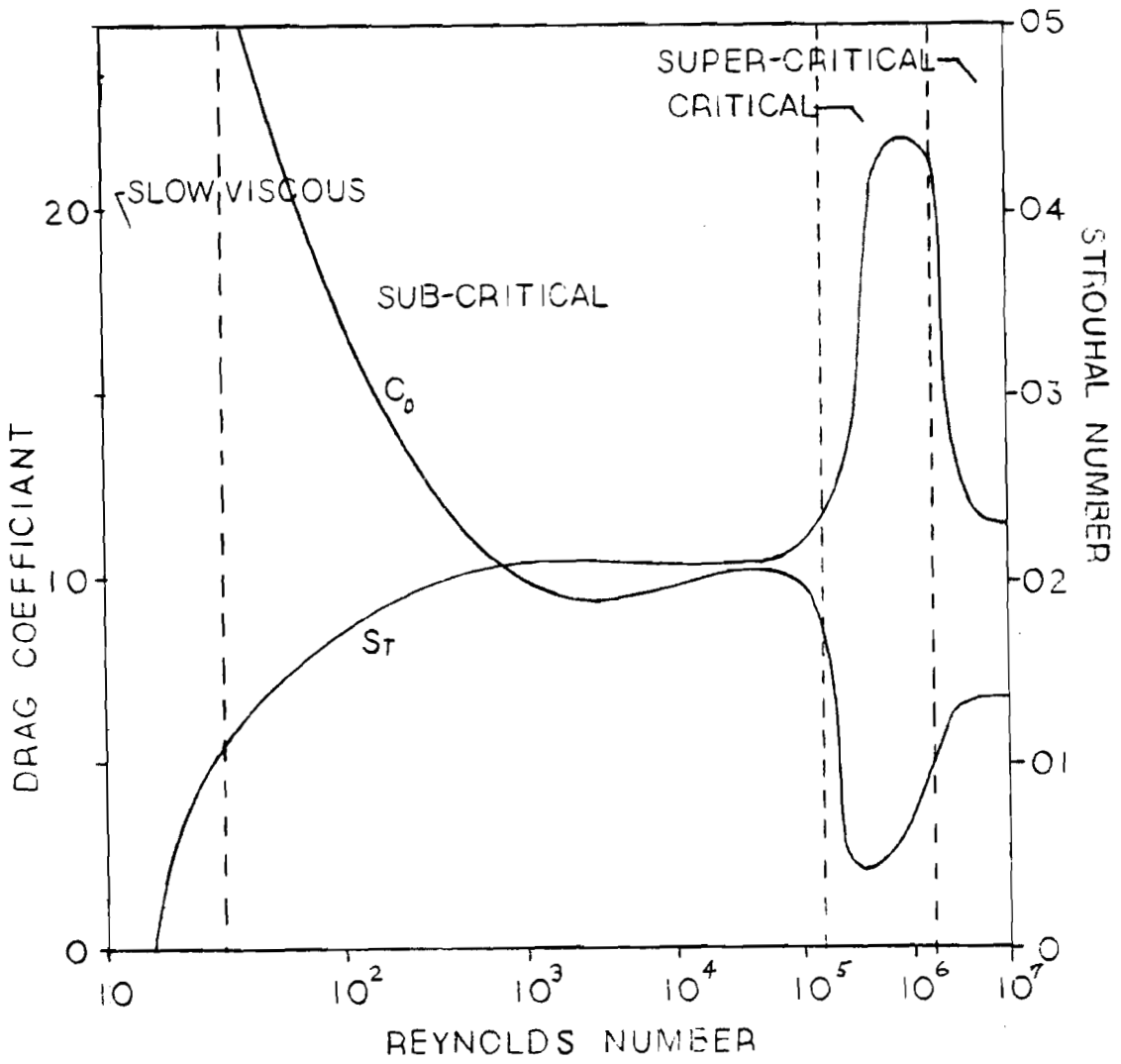

WAKE CATEGORIES

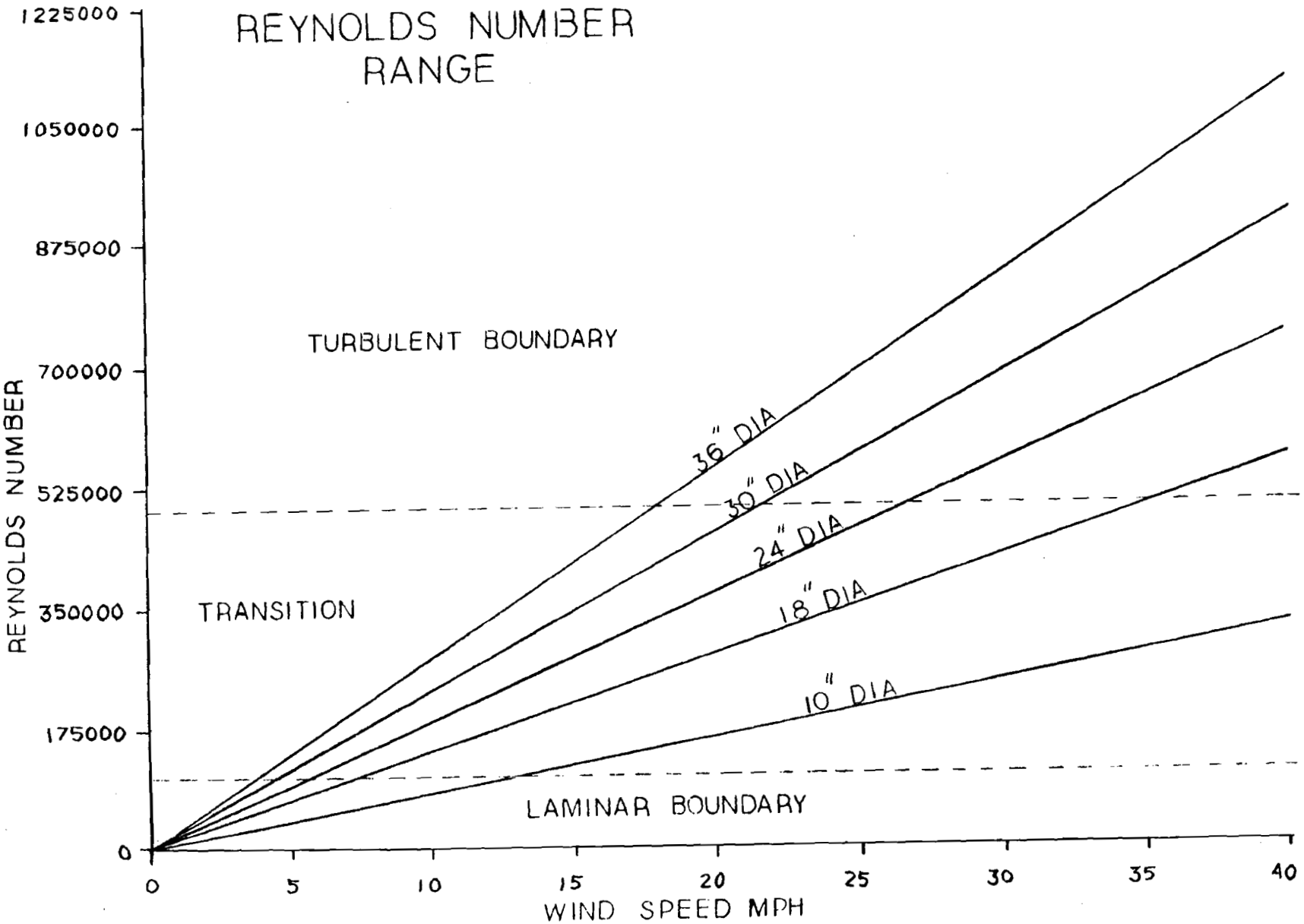
REYNOLDS NUMBER
RANGE
1225000
1050000
875000
700000
525000
350000
175000
0
REYNOLDS NUMBER
TURBULENT BOUNDARY
TRANSITION
LAMINAR BOUNDARY
36" DIA
30" DIA
24" DIA
18" DIA
10" DIA
0
5
10
15
20
25
30
35
40
WIND SPEED MPH

FIGURE 32

a time average of the velocity in the wake near the critical regime [4]. Because the averaging process masks the unstable nature of the wake, it has many features common to the flow occuring at Reynolds Numbers less than five. One notable feature in the figure is the region of stagnant fluid extending 1.2 diameters behind the tower. This stagnent region or tower shadow would impart a strong impulse to the blades if they were to pass through. In the more developed flow downstream, the shadow is less pronounced. At present, the WF-I blades rotate through the more developed flow since the tower is .254 m (10 in.) in diameter. If a .762 m (30 in.) tower were installed, the blades would travel through the stagnent region. The plane of rotor rotation for the present .254 m (10 in.) and the .762 m (30 in.) tower are superimposed on Figure 3.3 to emphasize the affect that changing the diameter has on the flow. Plans for changing the WF-I tower have been developed and Appendix I outlines the procedure.

3.2 Complications with a Wake Analysis

The categorization of the wake into distinct groups, identified by ranges in Reynolds Number, is only useful as a rough approximation. The four discrete regimes were developed using standard experimental conditions for the flow around cylindars. When conditions stray from the experimental standard, transitions between discrete categories occur at different Reynolds Numbers. The transition from subcritical to critical flow is particularly sensitive to deviations. It is unfortunate that the critical region is sensitive, because the tower wake occurs in the range of critical Reynolds Numbers for normal operation and a tower exposed to the environment is far from standard conditions.

The wake structure, occuring in the critical region, is due to a transformation of the boundary layer from laminar to turbulent. This

FIGURE 3.3

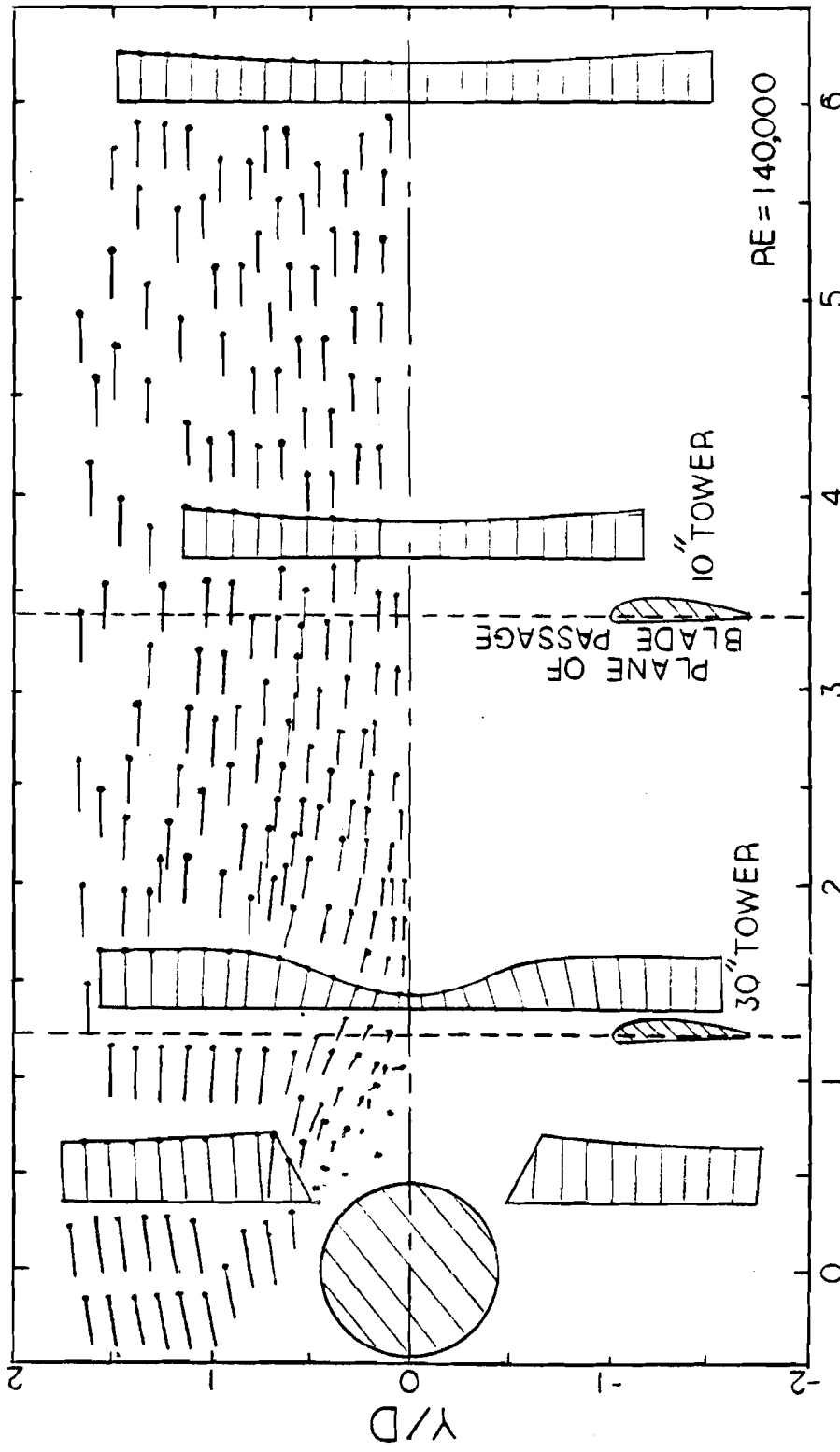

MEAN FLOW VECTORS

REF. B. CANTWELL

transition is determined by physical features of the wind and the tower. Tower roughness and wind turbulence have a major effect on the critical Reynolds Number. A rough tower and/or turbulent wind triggers the transition from the subcritical region at lower Reynolds Numbers while higher Reynolds Numbers are needed if the tower is smooth and/or wind is steady. Also, protrusions from the tower contribute to the wake. The orientation of guy wires, rungs, etc. create disturbances that may widen or otherwise significantly affect the wake in an unpredictable manner.

The rotor adds its own contribution to the wake because it slows the approaching wind and interferes with wake formation behind the tower. The result of downstream interference is indicated in Figure 3.4, which portrays the affect that a short splitter plate has on the wake of a cylinder. As the plate in moved downstream, the Stroukal Number and base pressure coefficient (C_{ps}) change. The drop in vortex shedding frequency and increase in pressure occur because the plate disturbs the formation of the vorticies. When the plate is moved beyond the region of vortex formation, the coefficients abruptly return to their normal values [5]. The rotor may affect the wake in a similar manner since it acts in this region of vortex formation.

These external parameters combine, creating a system which is not ameanable to a complete analytical or experimental analysis. Therefore, the next section serves to reduce this complex situation into a simple model representing the wake and tower shadow effect.

3.3 Wake Model

Since it is not feasible to account for all aspects of the complex wake flow, a simple wake model is used as an approximation. The main

Figure 3.4 Wake interference.

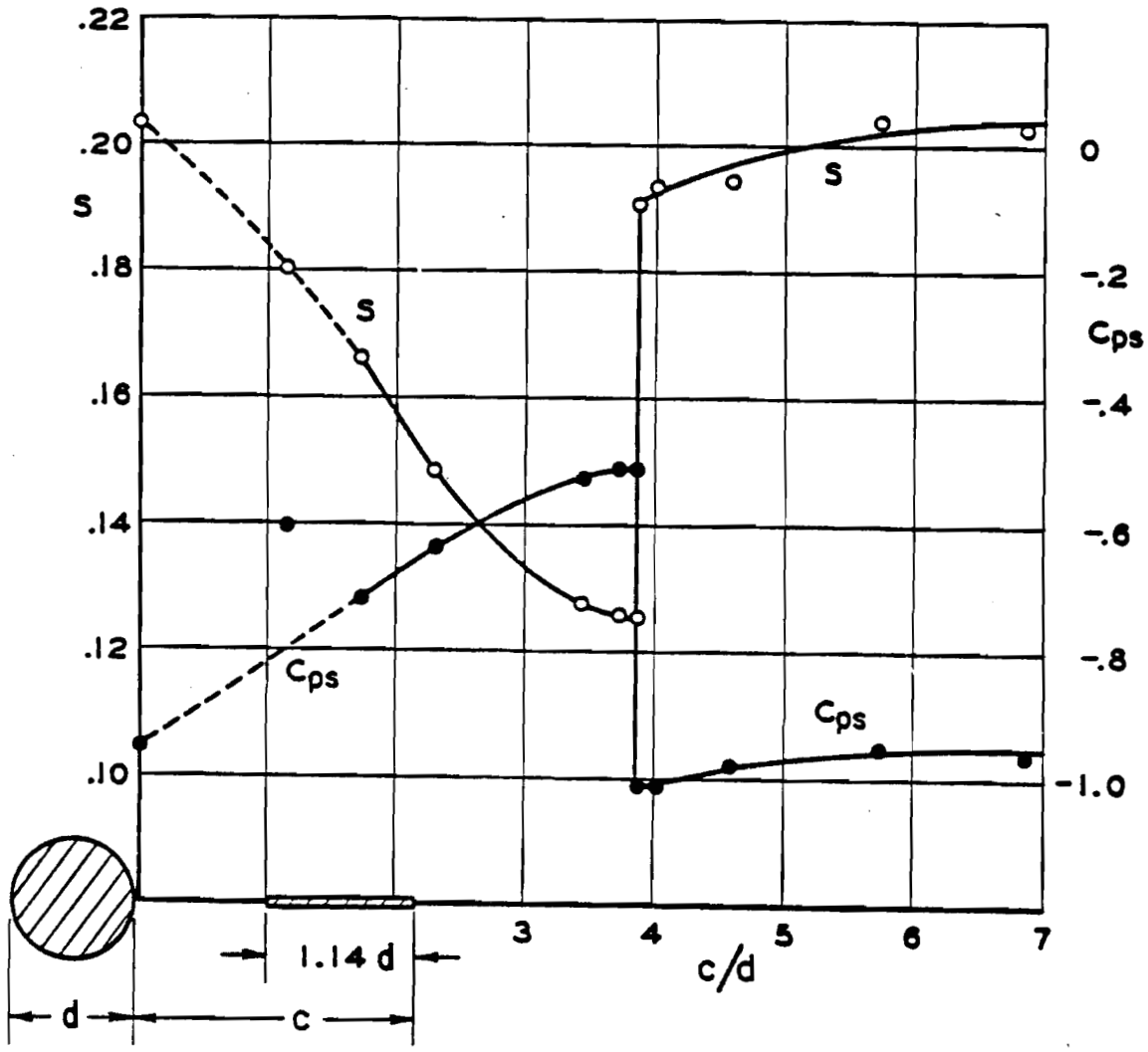

features of the wake required to preserve the nature of the wake - blade interaction are the wake width and loss of wind speed. These features are approximated by using a rectangular velocity decrement occuring behind the tower. This tower shadow model is shown in Figure 3.5. The velocity decrement has strength (w_o), width (δ) and it maintains the periodic frequency of blade passage. The rectangular pulse is chosen because it is simple and adaptable to analytical or numerical methods. A periodic pulse of this form can be modeled with a Fourier series. This series has the form:

$$(\psi) = a_o + \sum_{n=1}^{\infty} a_n \cos n\Psi \qquad (3.4)$$

where: $a_o = \frac{\omega o \, \delta}{2\pi}$

$a_n = \frac{2\omega_o}{n} \sin \frac{n\,\delta}{2}$

ψ = azimuth angle

One approximate method of calculating the velocity decrement and shadow width is by assuming that viscous effects are negligible and that the tower is a semi-permiable membrane. This assumed structure produces the same wake as previously modeled. The wake width is the same as the membrane width, which has a value equal to the tower diameter. The velocity decrement is found using the momentum theorem in conjunction with experimental data for the drag as a cylinder.

When a control volume is established around the tower, the momentun equation for the system has the form:

$$F_D = \rho Q (V_o - v) \qquad (3.5)$$

FIGURE 3.5

TOWER SHADOW MODEL

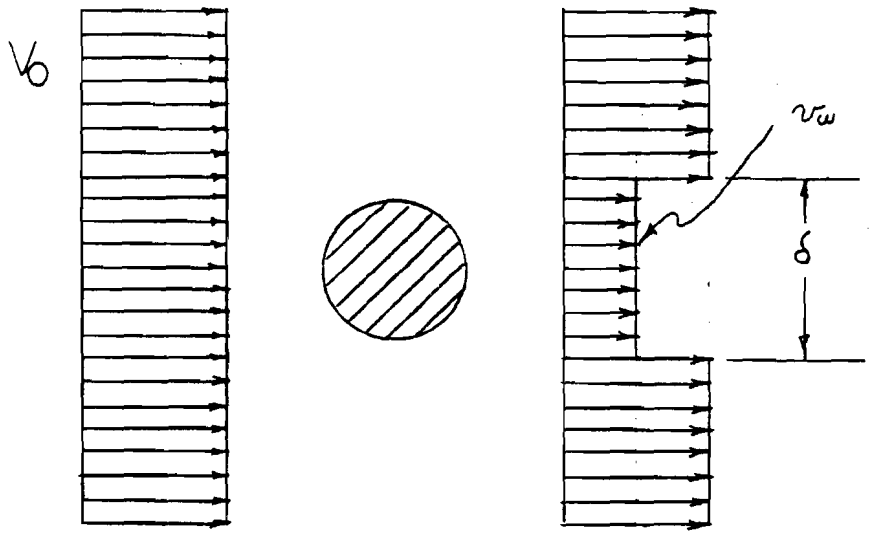

RECTANGULAR PULSE APPROXIMATION

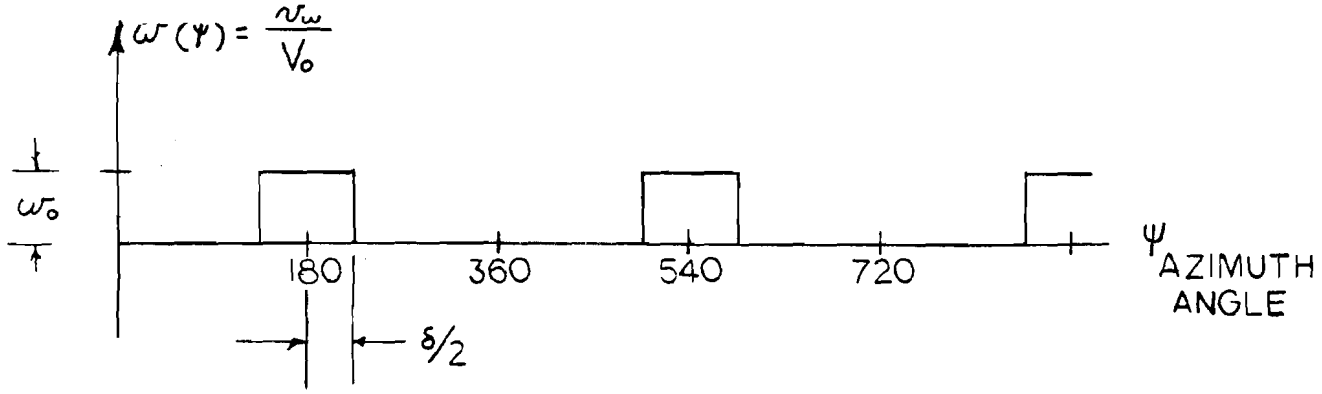

where: $F_T = 1/2\ \rho C_D V_o^2 D$ is tower drag force/unit length

ρ = density of air

$Q = V_o D$ is the flow rate/unit length

v = wake velocity

Re-arranging equation (3.4) yields the simple result for the velocity decrement as:

$$w_o = \frac{v}{V_o} = 1 - \frac{C_D}{2} \tag{3.6}$$

Since the Reynolds Number is usually high, the drag coefficient never has a value greater than one. Therefore, the largest velocity decrement permitted by this model is $w_o = .5$, meaning the windspeed behind the tower is half the free stream velocity. This simple model will serve as the wake representation for the estimation of the tower shadow effect performed in the following chapter.

CHAPTER 4

RIGID BLADE MODEL

4.1 Rational

The dyanmic response of a wind turbine rotor is a complex problem and tower shadow is only one facet. For a preliminary analysis of the tower shadow effect, this chapter presents a method to simplify the rotor system and clarify the dynamics. In general, the wind turbine has many degrees of freedom that are set into motion by a complex force system. The forces that act on the rotor are aerodynamic, gravitational, and inertial. Of these forces, the aerodynamic and inertial forces contribute to the blade response from tower shadow. Aerodynamic forces are due to the interaction of the air on the turbine blades and the inertial forces are the result of blade motion.

Ideally, the aerodynamic forces would be steady if the wind acted uniformly over the entire rotor at a constant speed with no gravitational affects. But this ideal situation never exists. Aside from gravity, wind variations like gusts, shear, and tower shadow result in an unsteady loading condition on the rotor which may have damaging results. The potentially damaging effects of tower shadow have already been proven by operational experience with the NASA MOD-0 wind turbine. With the initial tower configuration, the tower shadow resulted in excessive blade flapping and consequent material fatiguing. Subsequent removal of the stairs from within the tower structure significantly reduced the tower shadow [6].

In modeling the turbine so that the tower shadow effect is clearly portrayed, it is necessary to isolate the wake-blade interaction from the

many other unsteady variables. The variables that will be neglected in the force system are changes in wind speed and rotational speed of the rotor, wind shear, and gravity. This leaves a system that is periodically perturbed by the tower wake. Simplifications in the structural aspects of the rotor are also required when modeling the turbine. The rotor blade is assumed to act like a rigid slender beam with motion in the plane of rotation (edgwise) uncoupled from that perpendicular to the plane of rotation (flatwise). Of these, the edgewise motion is small and will be neglected since the aerodynamic requirements of the blade produce a structure that has small edgewise forces and a large edgewise stiffness.

Three coordinate systems are used to describe the turbine blade motion (Figure 4.1). The XYZ system that is attached to the hub and rotates with a constant speed (Ω). An X'Y'Z' system attached to the blade root and inclined by the coning angle (λ). The blade is then located by the XYZ system that is fixed to the blade, so that it moves through the flopping angle (β) measured from the (X'Y'Z') blade root system.

4.2 The Off-Set Hinge Model

The specific model used for the simplified analysis consists of a rigid slender beam attached to the rotor hub by a hinge-spring. This model is known as an off-set hinge model and has been used extensively for helicopter studies as well as having been successfully adopted to wind turbines in many recent studies [7]. The model gives a good approximation for the lowest mode of blade vibration in flapping. This approximation of the motion is shown in Figure 4.2 which displays the lowest mode shape for the WF-I and the hinged blade motion.

Figure 4.1

Coordinate Systems

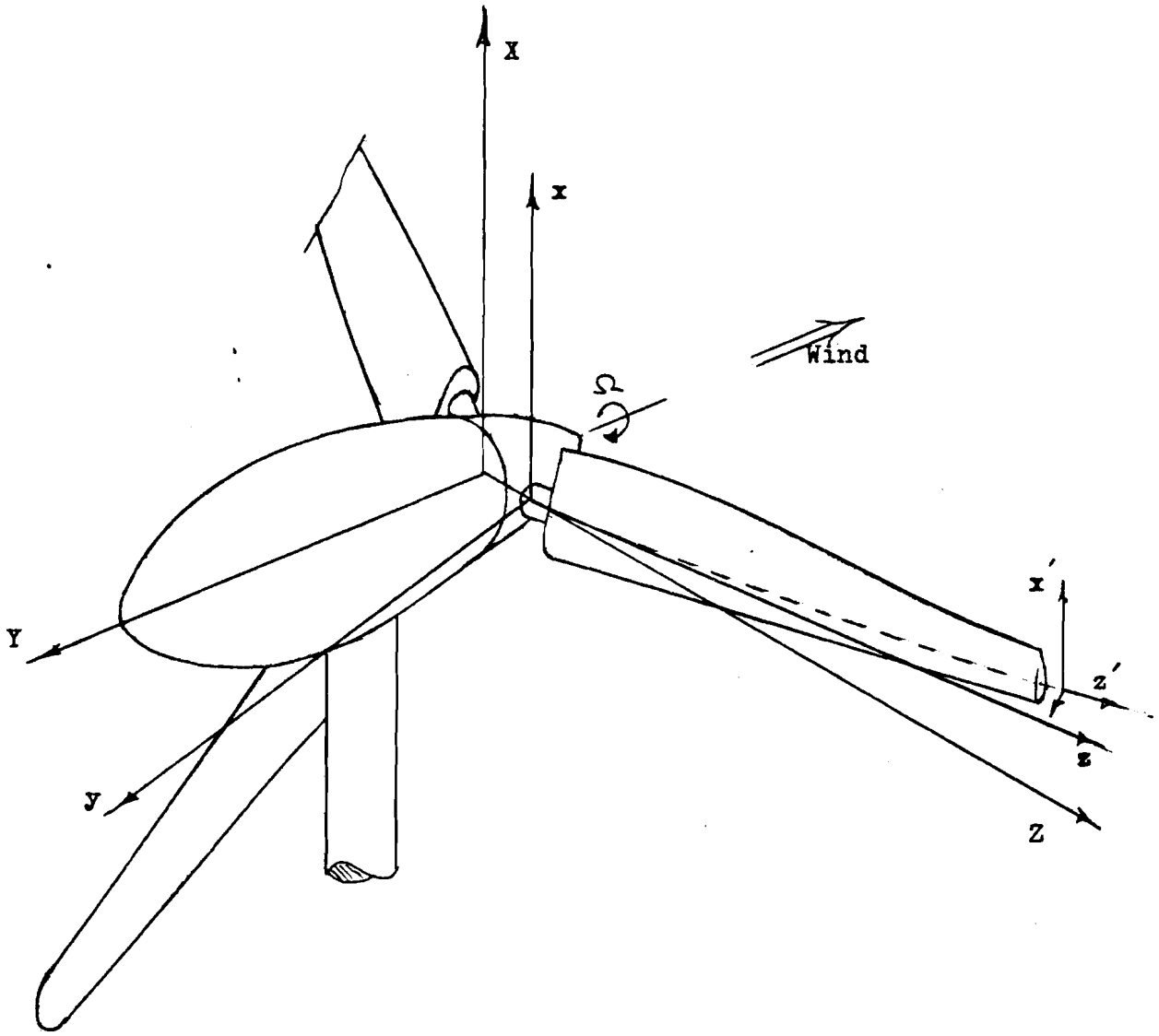

X Y Z system: Rotor hub coordinate system, it rotates at the machine rpm.

x y z system: Blade root coordinate system, it is inclined at the coning angle λ.

x´y´z´ system: Fixed to the blade, and inclined to the x y z system by the flapping angle β.

Ψ : Blade azimuth measured from the top of rotation.

FIGURE 42

COMPARISON OF MODE SHAPES

ACTUAL

1ST FLAPPING

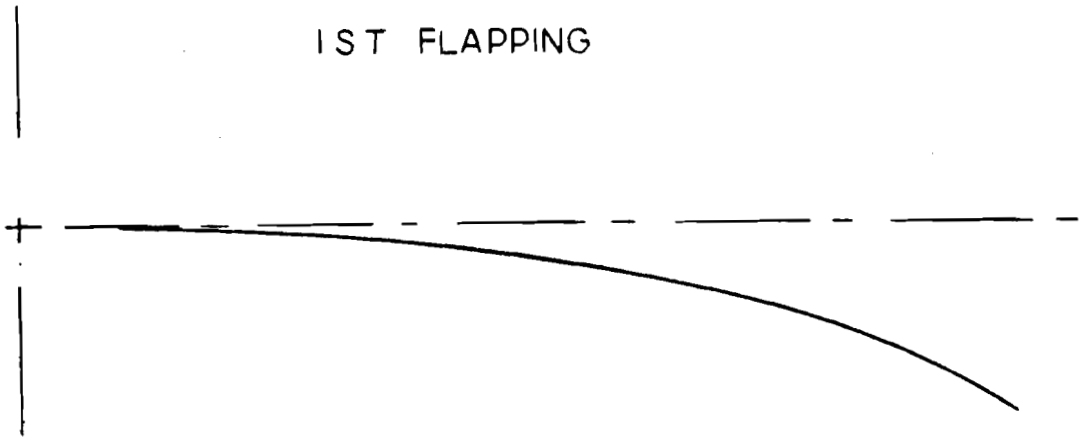

MODEL

FLAPPING

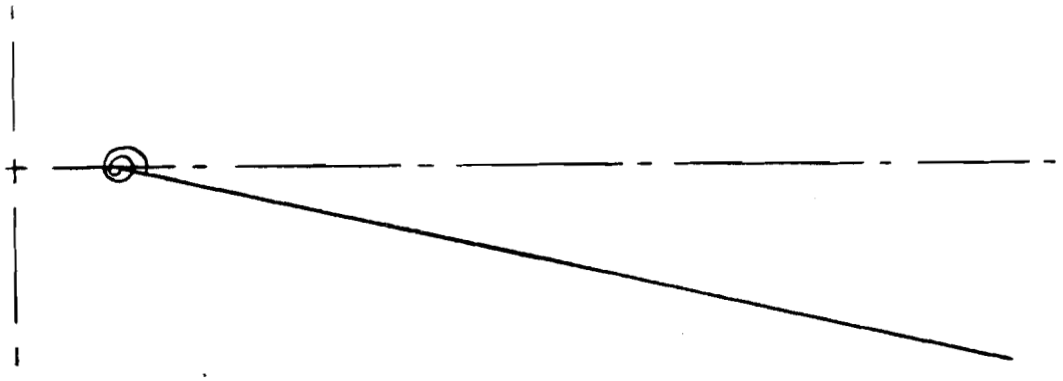

The governing equation for the free motion of this system is found using the free-body diagram of blade forces shown in Figure 4.3. When moments are resolved about the hinge spring, the equation takes the form;

$$I\ddot{\beta} + eR\, r_{cg}\, \Omega^2 M\, [\beta\cos\lambda + \sin\lambda] + I\Omega^2\, [\beta(\cos^2\lambda - \sin^2\lambda] + \cos\lambda\, \sin\lambda] + K_\beta\beta = 0 \qquad (4.1)$$

where: I = mass moment of inertia of a blade

M = mass of a blade

R = radius of the turbine

e = hinge effect

r_{cg} = center of gravity measured from the blade root

k_e = hinge spring stiffness

Ω = rotational speed

λ = coning angle

β = flop angle

Higer order terms in β have been neglected since this angle is generally small [7]. The equation of motion is more convenient when the offset hinge constant;

$$\varepsilon = \frac{M_e r_{cg}}{I} \qquad (4.2)$$

is introduced. Then eq. 4.1 becomes;

$$\ddot{\beta} + \beta[r^2(\varepsilon\cos\lambda + \cos^2\lambda - \sin^2\lambda) + \frac{K_\beta}{I}] + r^2\, (\varepsilon\sin\lambda + \cos\lambda\, \sin\lambda) = 0 \qquad (4.3)$$

The solution of eq. 4.3 represents the motion of a freely vibrating wind turbine blade with a natural frequency (ω_n) given by:

$$\omega_n^2 = \Omega^2(\varepsilon\cos\lambda + \cos^2\lambda - \sin^2\lambda) + \frac{K_\beta}{I} \tag{4.4}$$

The natural frequency exhibits the rotating and non-rotating components discussed in section 2.3,

$$\omega_n^2 = \omega^2_{\text{rotating}} + \omega^2_{\text{non-rotating}} \tag{2.2}$$

at rest, the turbine blade has a natural frequency of

$$\omega^2_{\text{non-rotating}} = \frac{K_\beta}{I} \tag{4.5}$$

Blade rotational speed causes the blades to stiffen, which increases the natural frequency by the amount

$$\omega^2_{\text{rotating}} = \Omega^2(\varepsilon\cos\lambda^2 + \cos^2\lambda - \sin^2\lambda) \tag{4.6}$$

A steady centrifugal force is also produced when a coned blade rotates. This centrifugal force creates a moment given by,

$$M_C = \Omega^2(\varepsilon\sin\lambda + \cos\lambda\sin\lambda) \tag{4.7}$$

that pulls the blade towards the plane of rotation. The action of this moment serves to relieve the aerodynamic moments that deflect the blade away from the plane of rotation.

4.3 Aerodynamic Loads

A wind turbine is driven by the dynamic reaction of the blades to the air. A blade acts as a lifting surface because it posses an airfoil

Figure 4.3
Blade Flapping Diagram

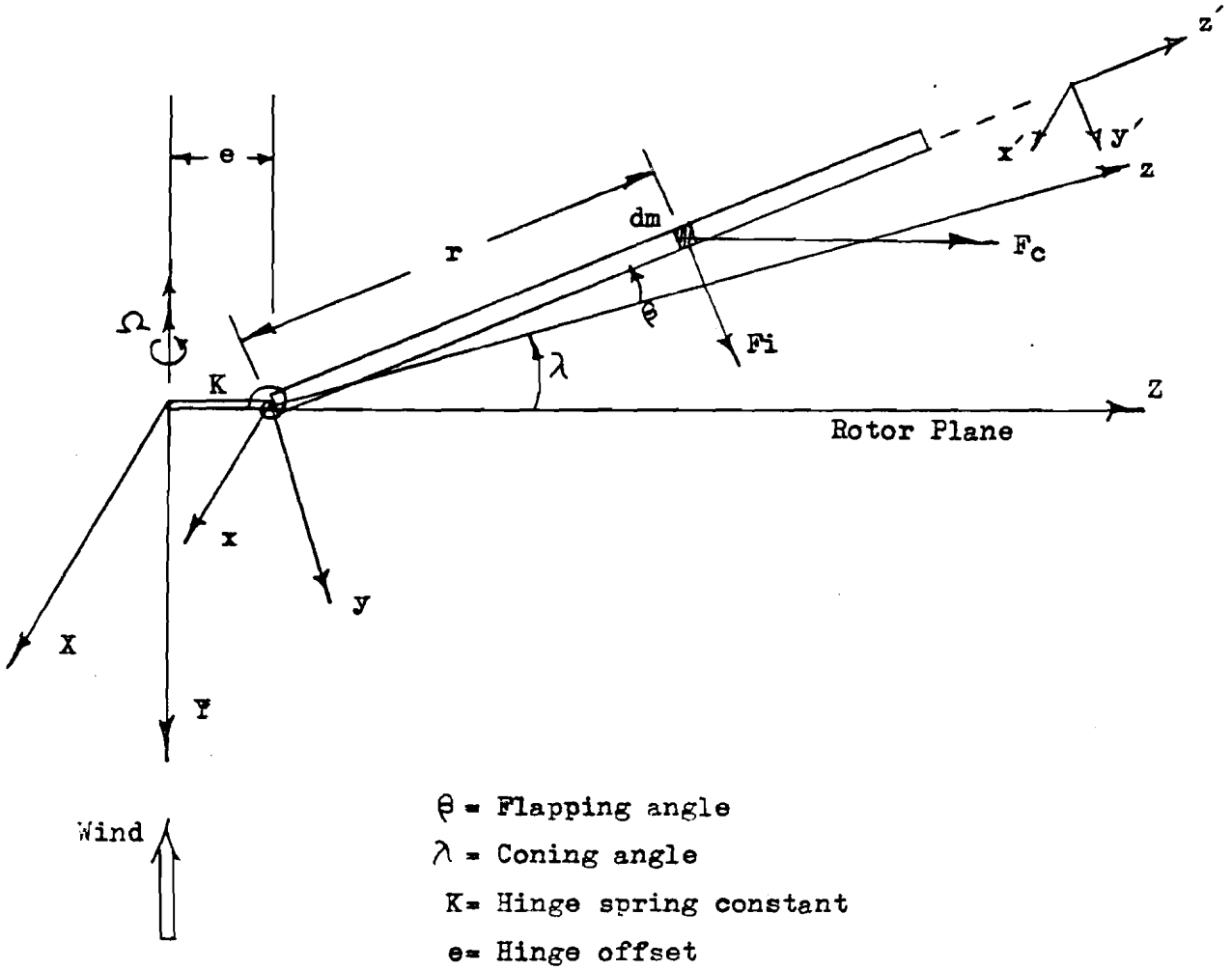

θ = Flapping angle
λ = Coning angle
K = Hinge spring constant
e = Hinge offset
$Fi = r\ddot{\theta}\,dm$ Inertial force
$Fc = (eR + r\cos(\theta + \lambda))\Omega^2 dm$ Centrifugal force

cross-section. The magnitude of the lift force depends on the blade orientation and the square of the air velocity acting parallel (U_p) and perpendicular (U_T) to the plane of rotation. Figure 4.4 shows the geometry of the forces and velocities acting on a blade cross-section used to express the equation for lift (L) per unit length;

$$L = \frac{1}{2}\rho Cl_\alpha C V_r^2 \alpha \tag{4.8}$$

Since the tower shadow changes, the perpendicular velocity encountered by the blade, it changes the lift and creates blade motions. Calculation of the velocity variations is essential to the force evaluation.

The simplified wake model developed in section 3.4 defines the velocity deficite created by the tower. Equation 3.3 is used directly if the wake width (δ) is replaced by an equivalent azimuth arc length ($\delta\psi$). An equivalent arc length is determined by setting the shaded area behind the tower equal to the area of a sector swept by blade (Figure 4.5) yielding the expression:

$$\delta\psi = \frac{2D}{R} \tag{4.9}$$

Therefore, equation 3.3 is re-wirtten as;

$$w(\psi) = \frac{w_o \delta\psi}{2\pi} + \sum_{n=1}^{\infty} \frac{2w_o}{n\pi} \sin \frac{n\delta\psi}{2} \tag{4.10}$$

This definition for the wake assumes that the velocity change depends only on the blade azimuth angle, so the wake acts instantaneously over the entire blade when the shadow is encountered.

Figure 4.4 Blade Element Diagram

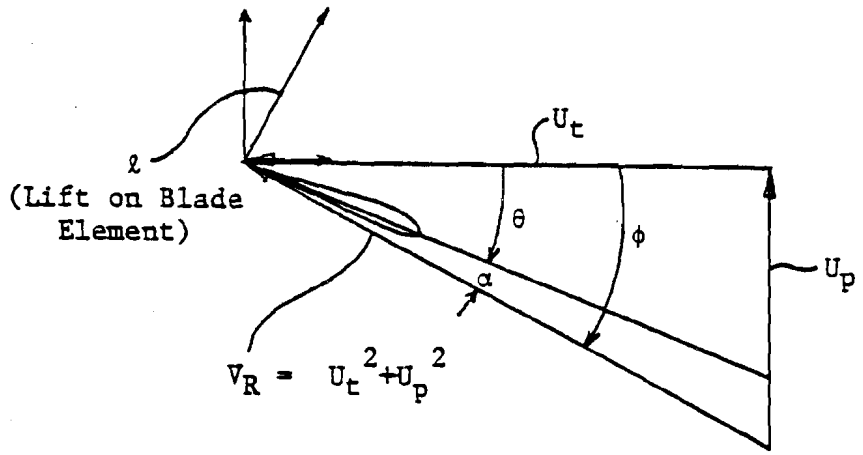

U_p = velocity perpendicular to the rotor plane

U_t = velocity tangential to the blade element

(This velocity is primarily due to rotation Ωr)

$V_R = \sqrt{U_t^2 + U_p^2}$ = resultant total velocity at blade element

ϕ = blade element angle = $\tan^{-1} \frac{U_p}{U_t}$

θ = blade element pitch angle

α = blade element angle of attack

ℓ = lift force per unit span

FIGURE 4.5
SHADOW MODEL

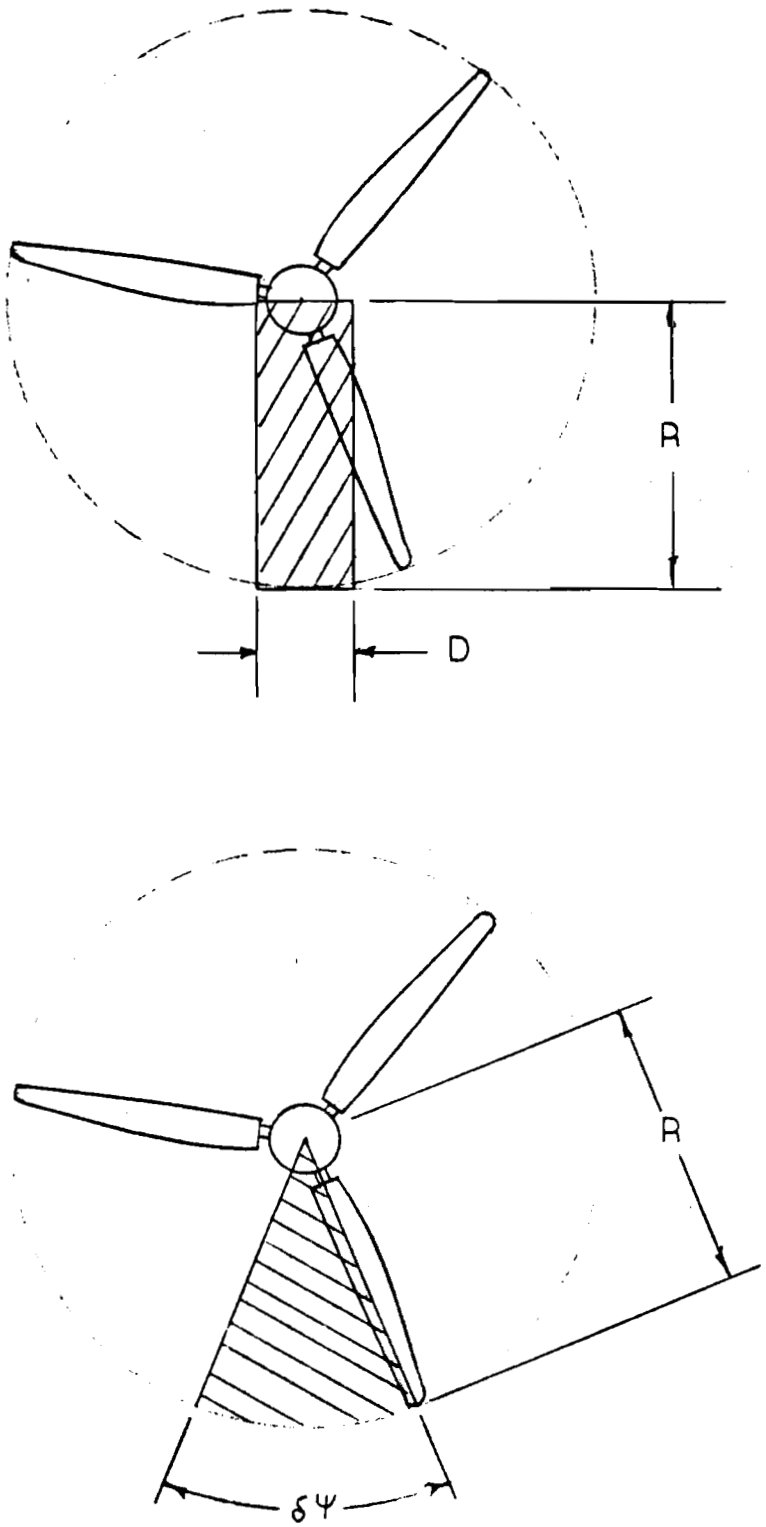

A simplified equation for the lift force variation due to velocity changes is developed in Appendix B and presented below by equation 4.11.

$$L = \frac{1}{2}\gamma I\,\Omega^2\,\frac{1}{R^2}\{\mu_o\eta(1-w(\psi))-\lambda_i\eta-\beta'\eta^2\cdot\eta^2\theta_o\,(1-\frac{\theta p}{\theta_o})+\eta^3\theta_o \qquad (4.11)$$

where: $\mu_o = \frac{V_o}{\Omega R}$; 1/tip-speed ratio

$\lambda_i = \frac{v_i}{\Omega R}$; induced velocity ratio

$\eta = r/R$; station span

$\gamma = \frac{\rho c l_\alpha C R^4}{4}$; Lack's inertia term

$\beta' = \frac{d\beta}{d\psi} = \frac{\dot{\beta}}{\Omega}$; flapping speed

θ_o = blade twist

θ_p = blade pitch

The variable velocity components in the lift equation are the tower shadow and blade motions.

An integration of the flatwise contribution of lift from the blade root to the blade tip determines the blade root bending moments ($M_{\beta A}$).

$$M_{\beta A} = \int_o^R L\cos\phi\cos\beta\, r dr = \int_o^1 LR^2\eta d\eta \qquad (4.12)$$

The result of the integration yields;

$$M_{\beta A} = \frac{1}{2}\gamma I\Omega^2\left[\frac{\mu o}{3}(1-w(\psi)) - \frac{\lambda i}{3} - \frac{\beta'}{4} - \frac{\theta p}{4} - \frac{\theta o}{20}\right] \qquad (4.13)$$

which is combined with the free vibration equation (eq. 4.3) to obtain the governing equation for the forced motion of a wind turbine blade.

$$\beta'' + \frac{\gamma}{8}\beta' + \frac{\omega_n^2}{\Omega^2}\beta = \frac{\gamma}{2}\left[\frac{\mu o}{3}(1-\omega(\psi)) - \frac{\lambda i}{3} - \frac{\theta p}{4} - \frac{\theta o}{20}\right] = M_C \qquad (4.15)$$

The motion implied by equation (4.15) and the solution for the expression will be discussed in the next section.

4.4 Solution of the Governing Equation

The governing equation of motion for the isolated blade represents a periodically forced single degree of freedom system. Equations of this type have been studied extensively in many vibrations texts and this section will draw from methods developed for vibration analysis to examine the tower shadow response [8]. The classical form for the differential equation of motion of a single degree of freedom system is given by;

$$\ddot{\beta} + 2\zeta\omega_n\dot{\beta} + \omega_n^2\beta = M(t) \qquad (4.16)$$

where: ζ = damping ratio

ω_n = natural frequency

$M(t)$ = applied moment

and it is useful to arrange equation (4.15) into this form.

In the time domain, the isolated blade equation is expressed by;

$$\frac{\ddot{\beta}}{\Omega^2} + \frac{\gamma}{8\Omega}\dot{\beta} + \frac{w_n^2}{\Omega}\beta =$$

$$\frac{\gamma}{2}\left[\frac{\mu o}{3}(1-w(\Omega t)) - \frac{\lambda i}{3} - \frac{\theta p}{4} - \frac{\theta o}{20}\right] - \frac{M_c}{\Omega^2} \qquad (4.17)$$

It is interesting to note that the system damping has an aerodynamic origin, as indicated by the coefficient of the flapping velocity ($\dot{\beta}$). The magnitude of the damping is related to the Lock Number (γ) and subsequent motion of the blade after it is perturbed depends of the amount of aerodynamic damping. If the damping is greater than or equal to a critical amount, the blade will not oscillate after it has been disturbed. The damping ratio (ζ) serves as an indicator for subsequent blade motion since it is the ratio of the actual damping divided by the critical damping. For this system, the damping ratio is given by;

$$\zeta = \frac{\alpha\Omega}{16\omega_n} \tag{4.18}$$

When this ratio is less than one, the blade oscillates. In general, the wind turbine blades will have a damping ratio less than one indicating that the blade exhibits a damped oscillation after the tower shadow has been encountered. The frequency of the damped oscillation is expressed as;

$$\omega_d = \omega_n \quad 1 - \zeta^2 \tag{4.19}$$

and the amplitude of oscilation decays exponentially, because the blade behaves like a damped single degree of freedom system.

A steady moment (M_{ST}) and the periodic moment (M_p) comprise the total moments acting on the blade root.

$$M(t) = M_{ST} - M_p \tag{4.20}$$

The steady moment, given by,

$$M_{ST} = \frac{1}{2}\gamma I r^2 \left[\frac{\mu o}{3} - \frac{\lambda i}{3} - \frac{\theta p}{4} - \frac{\theta o}{20}\right] - I\Omega^2[\epsilon \sin\lambda + \cos\lambda \sin\lambda] \qquad (4.21)$$

has no affect on the blade motion. It only serves to initially deflect the blade by the amount,

$$\beta_o = \frac{M_{ST}}{I\ \omega_n^2} \qquad (4.22)$$

and the proper choice of coning angle results in zero initial deflection for the blade. Blade motions are the result of the periodic moment caused by the tower shadow,

$$M_p = M_{po}\ w(\psi) = \frac{1}{2}\gamma\ I\Omega^2 \frac{\mu_o}{3} w(\psi) \qquad (4.23)$$

where the tower shadow has been represented by a Fourier Series. Now that the coefficients of equation (.16) have been defined, a solution can be obtained.

The steady state solution for the blade flapping deflection is expressed by a series, where each term in the series is the contribution to the deflection made by each harmonic of the Fourier tower shadow representation. Therefore, the total response of the blade is given by;

$$\beta = \beta_o + \frac{M_{po}}{I}\left[\frac{w_o \delta\psi}{4\pi\omega_n^2} + \sum_{n=1}^{\infty} \frac{\frac{2w_o}{n\pi}\sin\frac{n\delta\psi}{2}\cos(n\psi - \phi_n)}{(\omega_n^2 - n\Omega^2) + (2\omega_n \Omega n)^2}\right] \qquad (4.24a)$$

where the phase angle (ϕ_n) between contributions is;

$$\phi_n = \arctan\left[\frac{2\omega_n n}{\omega_n^2 - n\Omega^2}\right] \qquad (4.24b)$$

A practical evaluation of the response using equation (4.24) requires the truncation of the infinite series. The number of terms necessary to assure the desired accuracy of the solution depends on the width of the rectangular pulse ($\delta\psi$). If ($\delta\psi$) were close to π, the series would converge rapidly, but this is not the situation behind a pipe tower. The wake produced by a pipe tower is narrow, so that the solution does not converge rapidly to a steady deflection. Since the closed form solution of the equation of motion converges at a slow rate, numerical techniques are necessary. Computer code RIGID, listed in Appendix C, is used to solve the equation of motion using Eulers' time stepping integration.

4.5 Analysis of Wind Furnace I

The equations presented by the previous section will be used for the analysis of the WF-I. Since the WF-I does not have the specific geometry assumed by the off-set hinge model, an equivalent blade must be developed. The equivalent system retains the following turbine characteristics:

Blade radius	R = 4.95 m (16.25 ft.)
Hub radius	R_H = 0.495 m (19.25 in.)
Blade mass	M = 15.44 kg (34 lbs.)
Natural Frequency	ω_n = 25 rod/sec
Coning angle	λ = 10°

The slender rigid blades required by the model have mass moment of inertia equal to;

$$I = \frac{1}{3} m (R-R_H)^2 = 102.15 \text{ kgm}^2$$

This moment of inertia is then used with the blades' natural frequency to obtain a hinge spring constant;

$$k_\beta = \omega_n^2 I = 63843 \frac{n\text{-}m}{radius}$$

Aerodynamic loads are determined from mean values for the blade chord and twist distribution, because the blades have been modeled with a constant chord and linear twist. The equivalent chord has the value;

$$c = \frac{\sum_{n=1}^{\infty} C_n}{n} = .263 \text{ m}$$

and the equivalent twist is calculated in a similar manner as;

$$\theta_o = \frac{2 \sum_{n=1}^{\infty} \theta_o n}{n} = .262 \text{ radius}$$

As an example of the blade response, a solution is determined for the steady state operation of the WF-I is a 9 m/s (20 mph) wind. Equation 4.16, the governing equation of motion has coefficients equal to the quantities;

$$\omega_n = 28.814 \text{ rad/sec}$$
$$\zeta = 0.345$$
$$M_{ST} = 2569 \text{ n-m}$$
$$M_p = 4919.515 \text{ n-m}$$

and a solution for the equation of motion is performed by computer code RIGID. The blade tip deflection due to a .254 m (10") shadow width in a 9 m/s (20 mph) wind is shown in Figure 4.6. The blade root bending moment also shows the response (Figure 4.7). Moments will be used throughout the chapter because the blade stress is dependent on the

FIGURE 4.6

BLADE TIP DEFLECTION

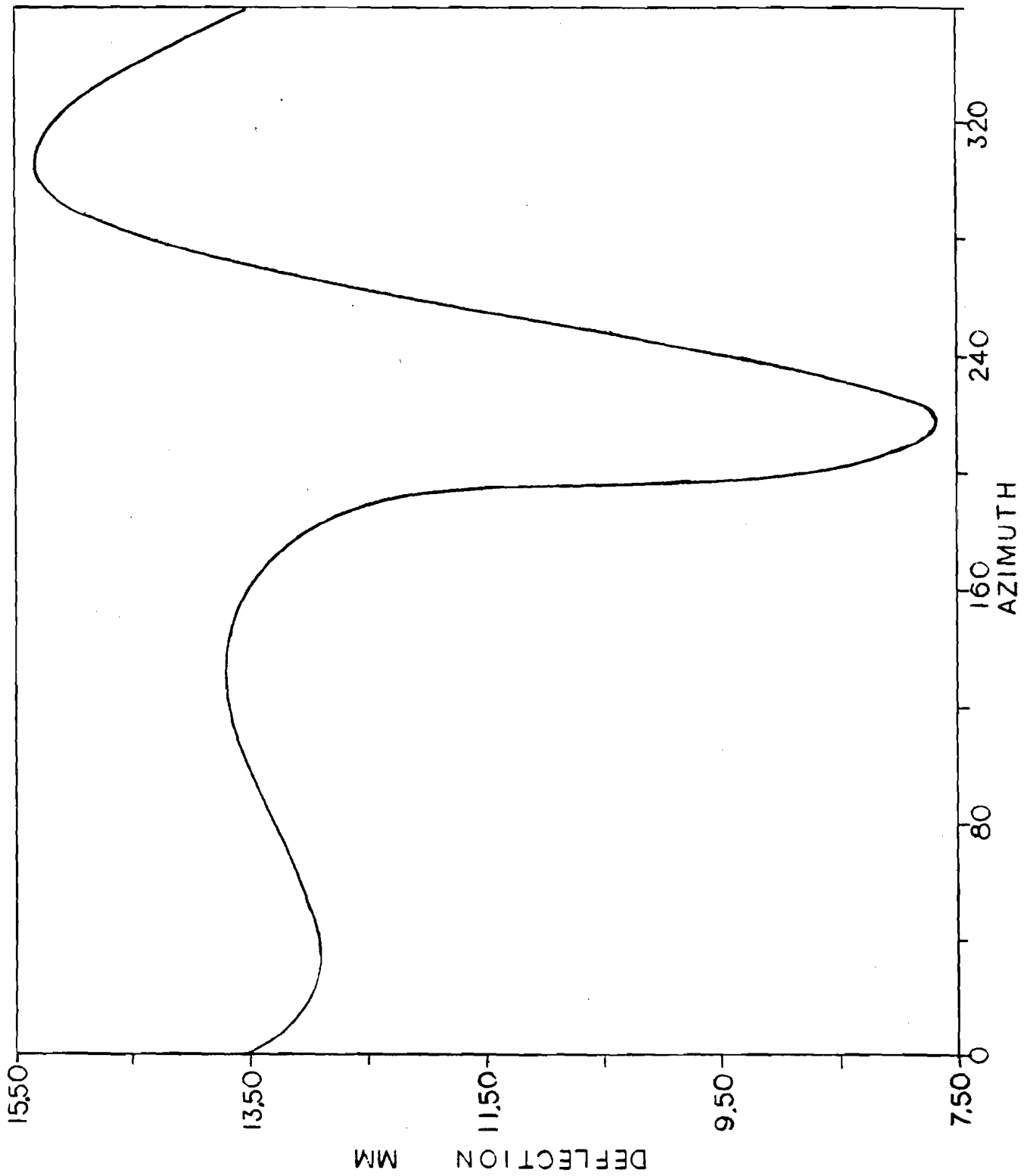

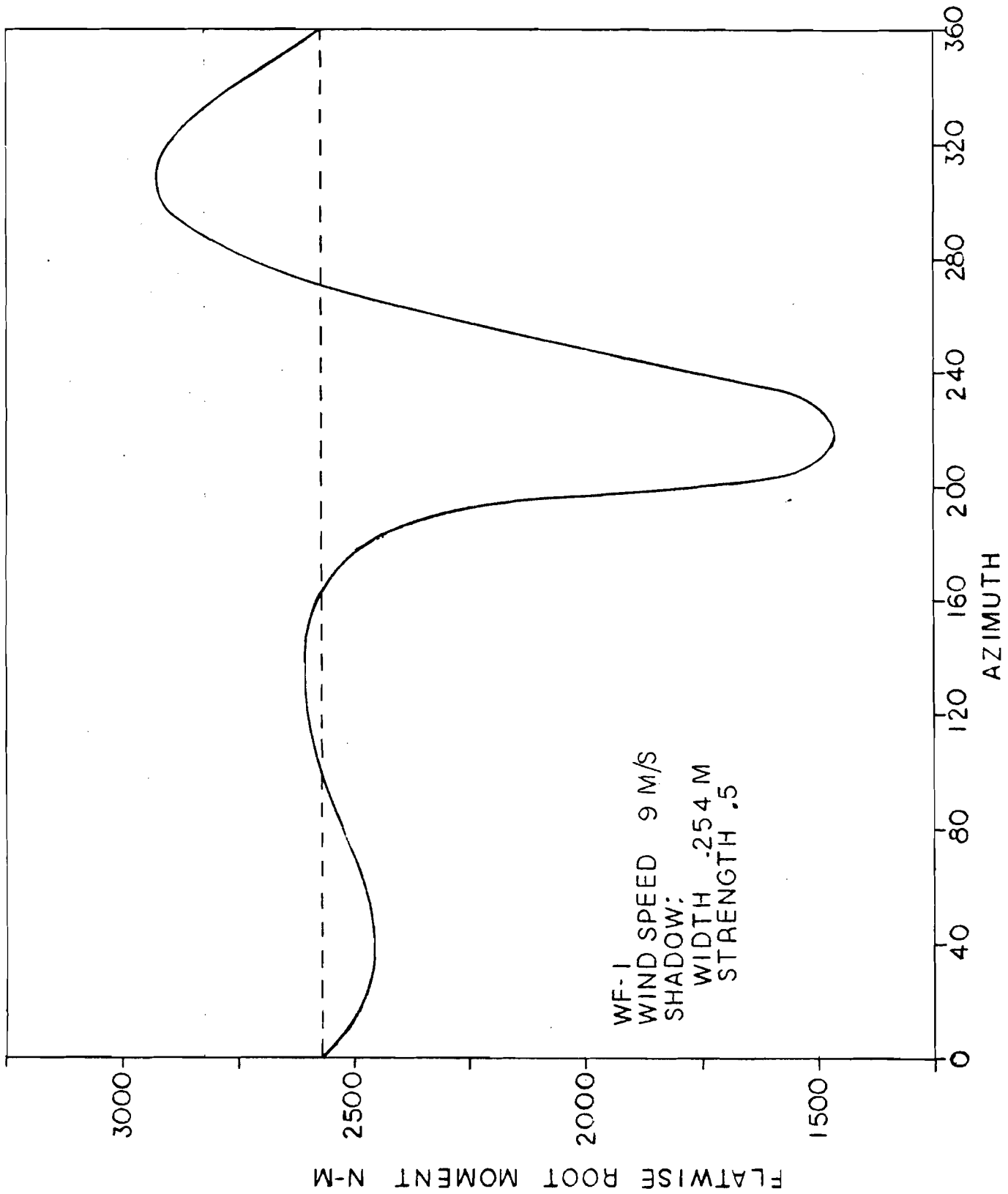
FLATWISE ROOT MOMENT N-M
3000
2500
2000
1500
0
40
80
120
160
200
240
280
320
360
AZIMUTH
WF-1
WIND SPEED 9 M/S
SHADOW:
WIDTH .254 M
STRENGTH .5

magnitude of the bending moments. During rotation, the twoer shadow deficit occur between ($\delta\psi$ + 180°) and ($\delta\psi$ - 180°), but the resulting response is not significant until the blade begins its ascent from the bottom of rotation. The turbine blade follows an oscillating path as it rotates about the wind shaft. This osciallating pattern is similar for all windspeeds because the damping ratio remains less than unity.

Oscillations of the blade root bending moments are the most important feature of the response. These oscillations are best described by their maximum (M_{max}) and minimum values (M_{min}). Figure 4.8 shows the maximum, minimum and steady moments encountered over the entire operating range of wind speeds for WF-1. The magnitude of the steady root moment drops quickly when the operational mode is changed to constant rotational speed. A more subtle change occurs in the magnitude of the oscillations. If the steady moment is removed from the response, a clear picture of the tower shadow pertabation results (Figure 4.9). The flatwise moment variation increases at a faster rate under constant rotational speed (region III) operation, then would have occured if constant tip-speed-ratio had been maintained.

Increases in the tower diameter also change the root bending moment due to changes in the tower shadow. Figure 4.10 shows the affect of tower diameter on the moment variation in a 9 m/s (20 mph) wind. The response due to the amount of blockage is small for a narrow tower and increases to a maximum as the tower diameter is enlarged. Increasing moment variation occurs because the response is a function of how long the blade remains shaded and the strength of the blockage. In the limit, the tower will shade the entire rotor and the periodic component of the bending moment will converge to steady value. Convergence occurs about

FIGURE 4.8

OPERATING RANGE

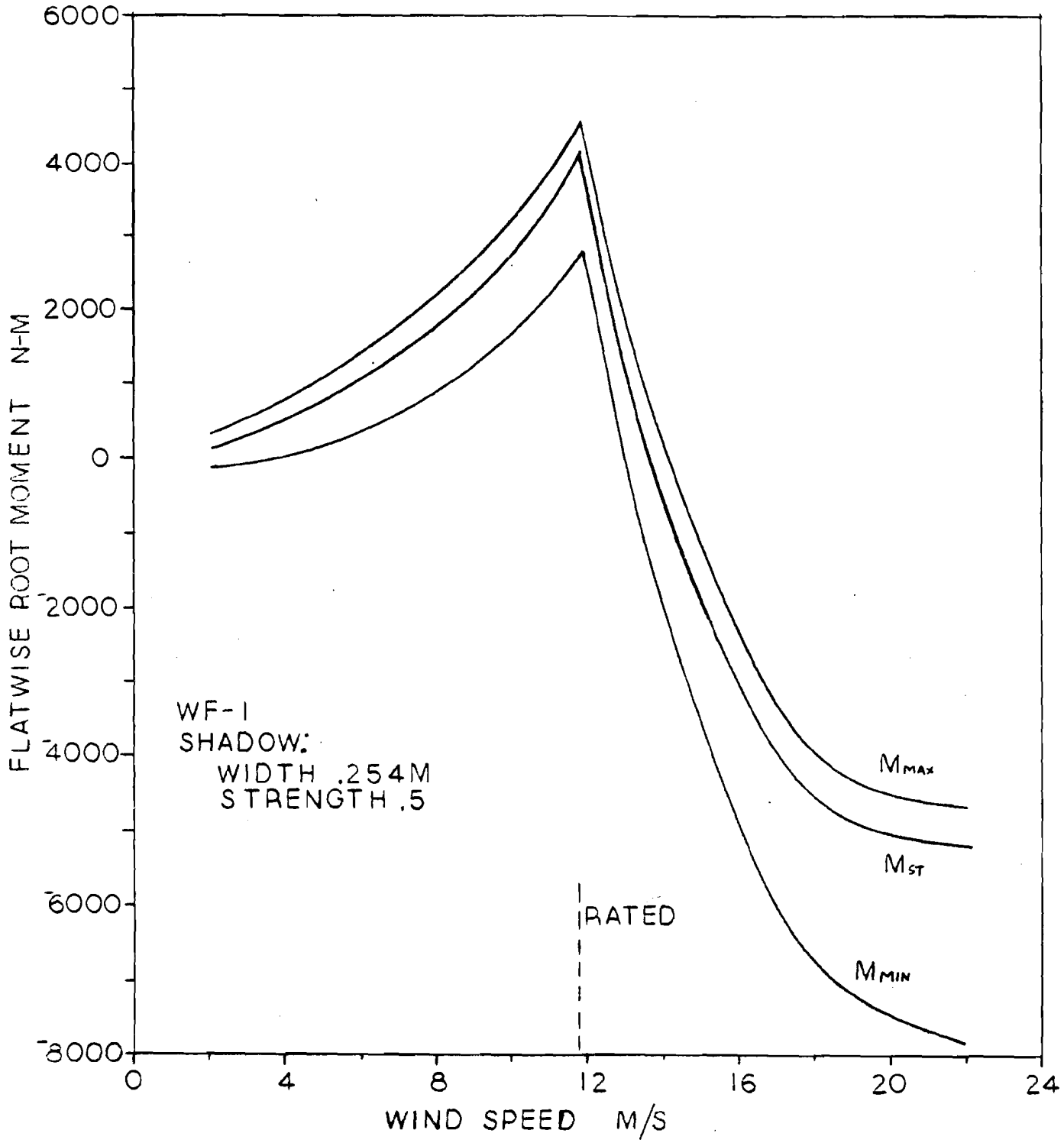

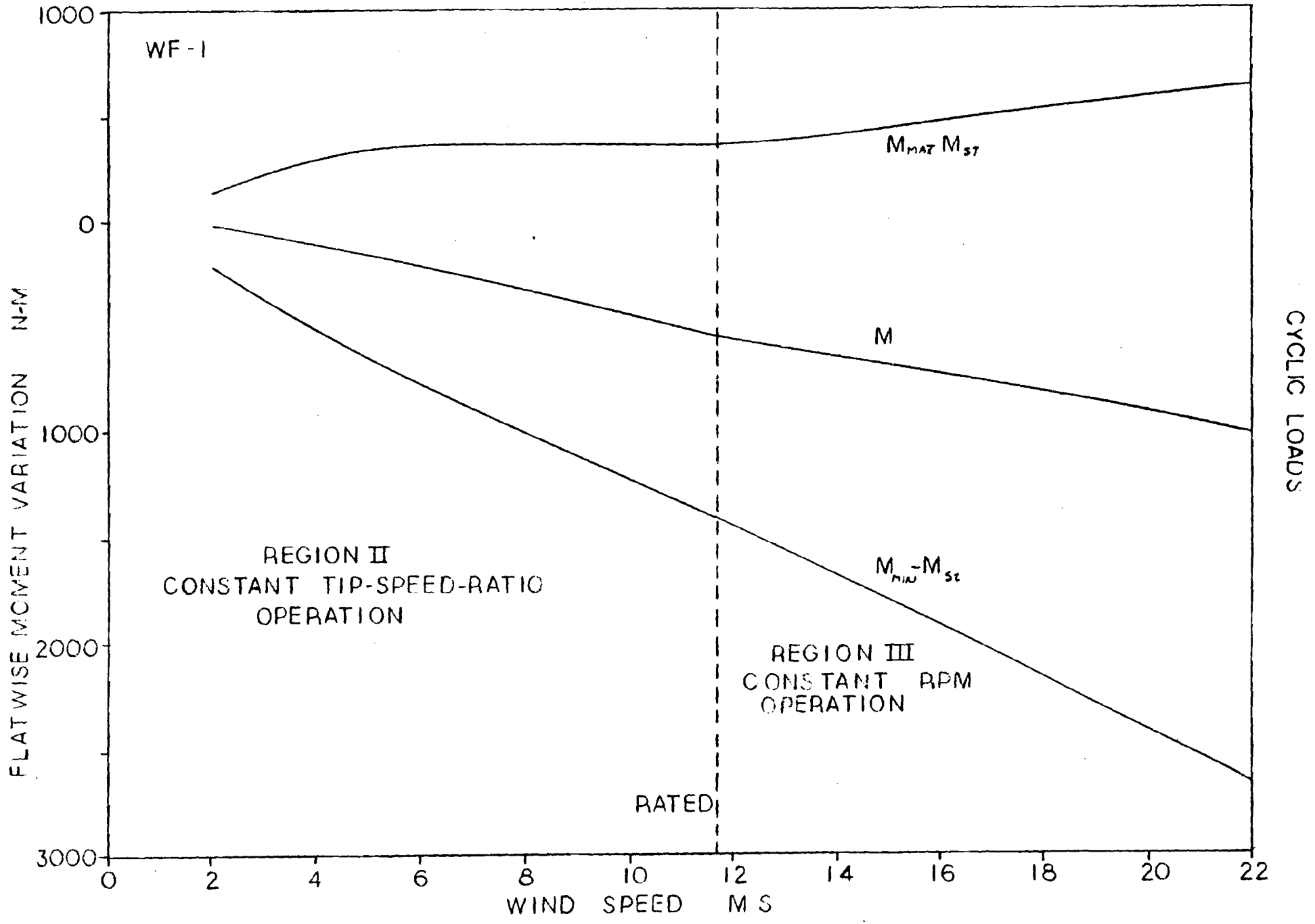
WF - 1
1000
0
1000
2000
3000
FLAT WISE MOMENT VARIATION N-M
M_{MAX} M_{ST}
M
M_{MIN}-M_{St}
REGION II
CONSTANT TIP-SPEED-RATIO
OPERATION
REGION III
CONSTANT RPM
OPERATION
RATED
0
2
4
6
8
10
12
14
16
18
20
22
WIND SPEED M S
CYCLIC LOADS

FIGURE 4.10
SHADOW WIDTH

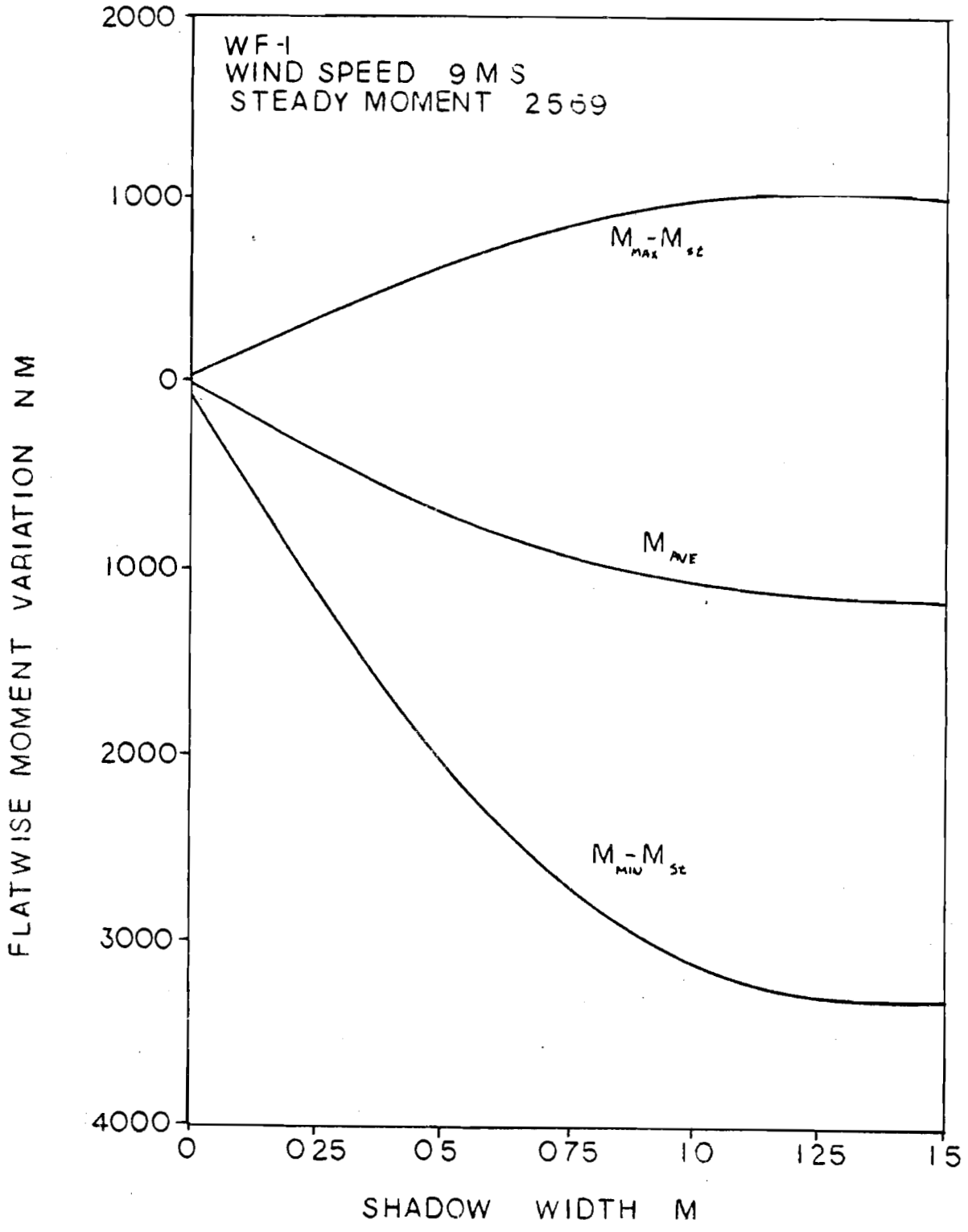

the steady moment due to wind speed minus the tower shadow deficite.

In addition to blade root bending moment variations, the wake contributes to the yaw motion experienced by the turbine. During high winds, WF-I has been observed to oscillate about a position slightly yawed away from the wind direction [9]. A motion of this nature is indicated by the predicted shadow data when the blade moments for the entire rotor are resolved about the yaw axis. An example of the resulting yaw moments occuring in a 20 m/s (44 mph) wind are shown in Figure 4.11. The yaw moment has a frequency of three times the rotational speed with an amplitude variation about a positive mean yaw moment. Experimental data has been collected at low windspeeds that verify the frequency of the tower shadow perturbation on the yaw characteristics of the turbine [9].

In summary, the off-set hinge representation of a wind turnine offers a simple technique to indicate elementary affects of tower shadow on the rotor dynamics. The next step in the analysis is the inclusion of a non-uniform flexible blade into the model so that the bending moment distribution along the blade can be determined. This more involved analysis will be presented in the next chapter.

FIGURE 4.11

YAW MOMENTS

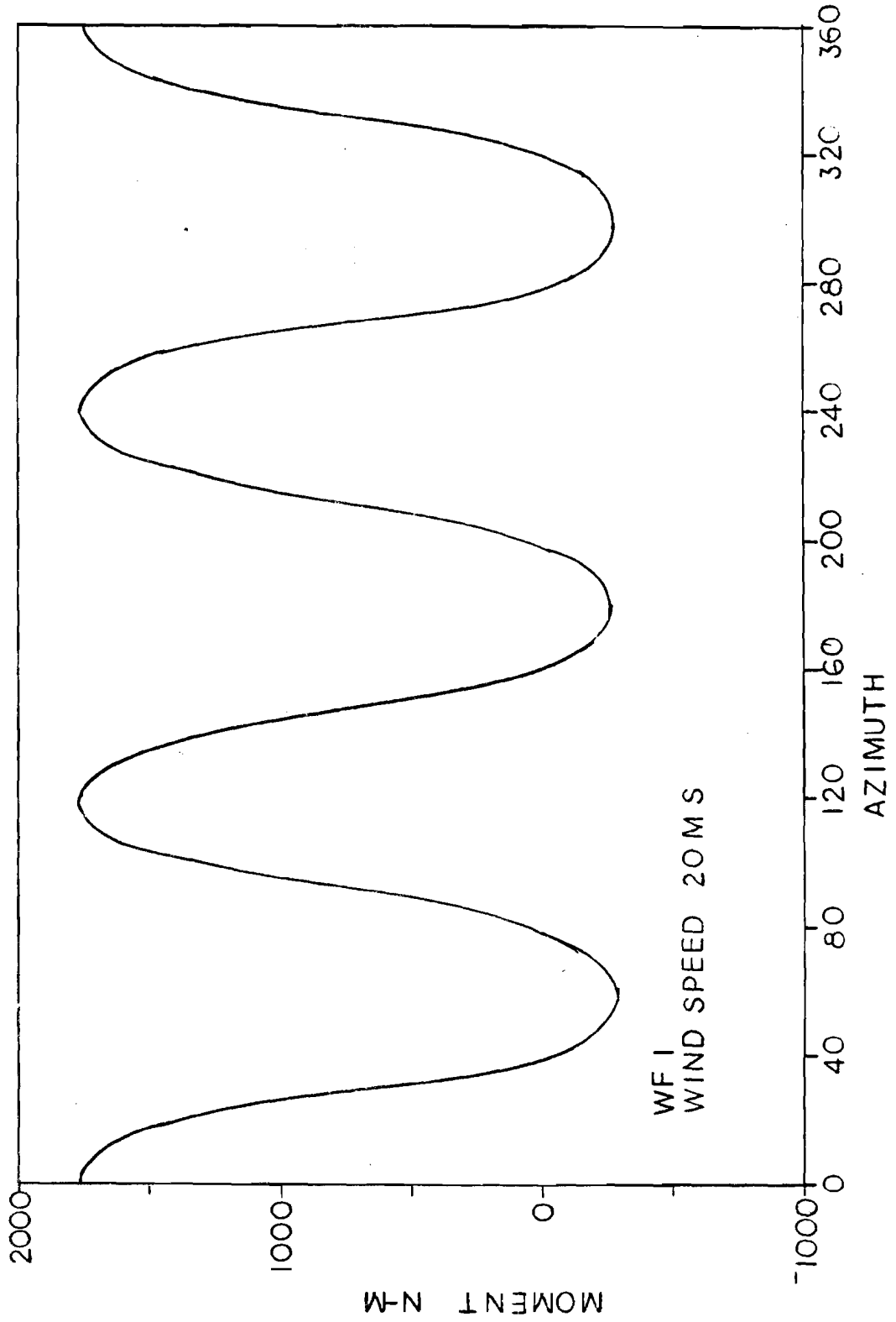

CHAPTER 5

COMBINED LEAD-LAG AND FLAPPING RESPONSE OF A WIND TURBINE ROTOR BLADE

5.1 Rational

The simple rigid blade model of the previous chapter is not adequate for an analysis of the force distribution along the blade. The rigid model is useful for determining many dynamic effects caused by the tower shadow, but the rigid model lacks the ability to handle blade flexibility and a complex geometry. A wind turbine blade is a non-uniform non-homogenious beam and the entire motion of the blade is needed for a detailed analysis of loading and moments.

The equation of motion for a differential element of the rotor blade is found using the same coordinate system developed for the rigid blade model. To simplify the derivation of the equation of motion, torsional effects are neglected. This leaves only coupled flatwise and edgewise motion. The forces and moments acting on a blade element are shown in Figure 5.1. These forces and moments are the local shear force (V), the bending moment (M), the aerodynamic load (F), and the centrifugal tension (G). Force equilibrium on the element requires that;

$$\Sigma F_z \qquad -\frac{\partial G}{\partial z} - mr^2 z = 0 \tag{5.1}$$

$$\Sigma F_x \qquad \frac{\partial V_x}{\partial z} - F_x + m\frac{\partial^2 x}{\partial t^2} = 0 \tag{5.2}$$

$$\Sigma F_y \qquad \frac{\partial V_y}{\partial z} - F_y + m\frac{\partial^2 y}{\partial t^2} = 0 \tag{5.3}$$

Integrating expression 5.1 with respect to z yields for the centrifugal tension G;

FIGURE 5.1

DIFFERENTIAL ELEMENT

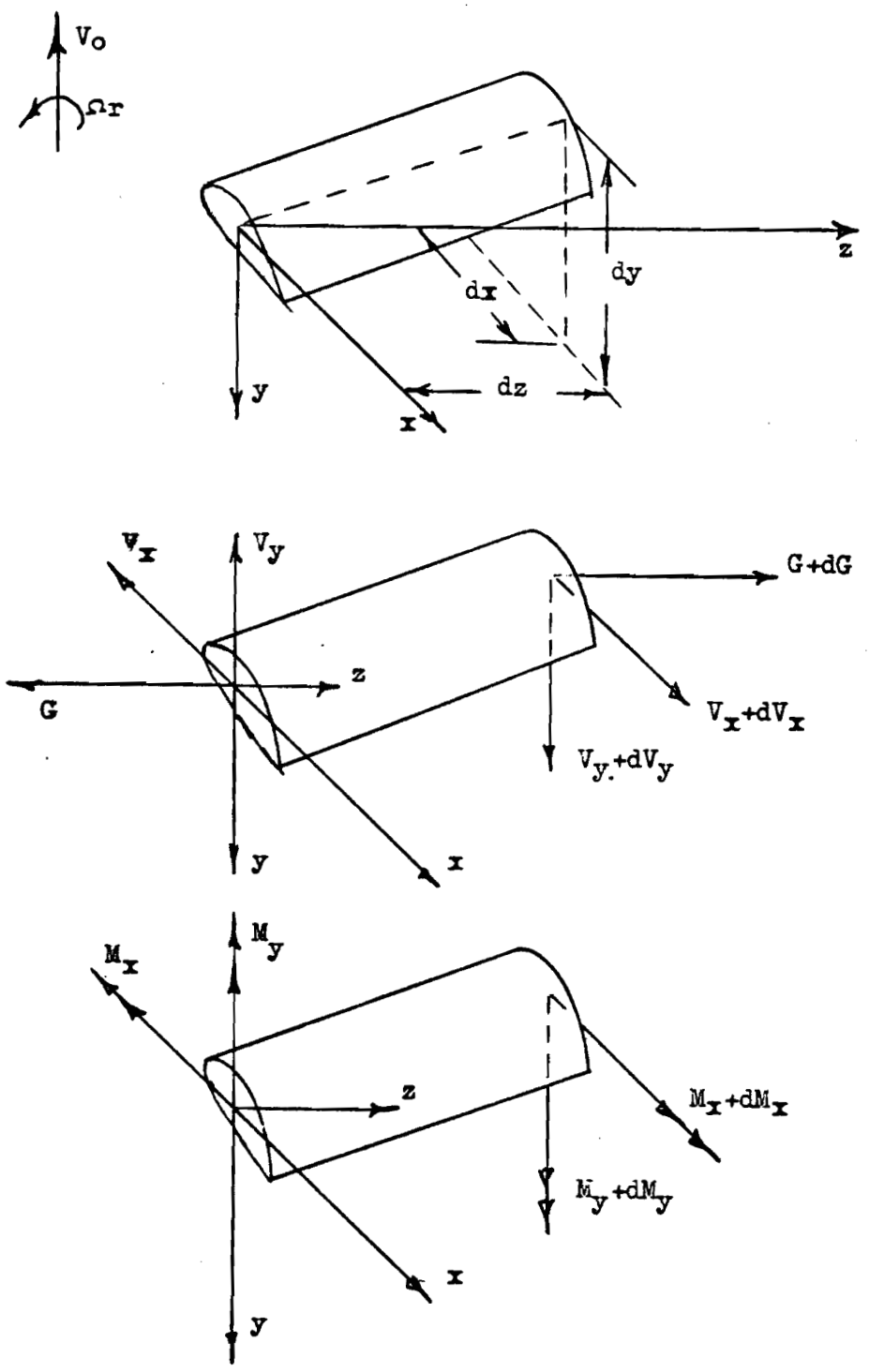

$$G = \int_z^R mr^2 z dz \tag{5.4}$$

The moment equilibrium for the element requires that

$$\Sigma M_y \qquad \frac{\partial M_x}{\partial z} + V_y + G\frac{\partial y}{\partial z} = 0 \tag{5.5}$$

$$\Sigma M_x \qquad \frac{\partial M_y}{\partial z} + V_x + G\frac{\partial x}{\partial z} = 0 \tag{5.6}$$

Differentiating the moment equations with respect to z gives;

$$\frac{\partial^2 M_x}{\partial z^2} + \frac{\partial V_y}{\partial z} + \frac{\partial}{\partial z}\left(G\frac{\partial y}{\partial z}\right) = 0 \tag{5.7}$$

$$\frac{\partial^2 M_y}{\partial z^2} + \frac{\partial V_x}{\partial z} + \frac{\partial}{\partial z}\left(G\frac{\partial x}{\partial z}\right) = 0 \tag{5.8}$$

A substitution from equations 5.2 and 5.3 into 5.7 and 5.8 yields;

$$\frac{\partial^2 M_x}{\partial z^2} + F_y - m\frac{\partial^2 y}{\partial t^2} + \frac{\partial}{\partial z}\left(G\frac{\partial y}{\partial z}\right) = 0 \tag{5.9}$$

$$\frac{\partial^2 M_y}{\partial z^2} + F_x - m\frac{\partial^2 x}{\partial t^2} + \frac{\partial}{\partial z}\left(G\frac{\partial x}{\partial z}\right) = 0 \tag{5.10}$$

Bending moments in equations 5.9 and 5.10 are given by the Euler-Bernoulli theory of bending [10]. For small displacements, the moment is related to the displacement by;

$$M_x = -E\left(\frac{\partial^2 x}{\partial z^2} I_{xy} + \frac{\partial y}{\partial z^2} I_{xx}\right) \tag{5.11}$$

$$M_y = -E\left(\frac{\partial^2 y}{\partial z^2} I_{xy} + \frac{\partial^2 x}{\partial z^2} I_{yy}\right) \tag{5.12}$$

When the bending moments are substituted into the equations of motion (5.9, 5.10), the following results;

$$\frac{\partial^2}{\partial z^2}\left[E \left(\frac{\partial^2 x}{\partial z^2} I_{xy} + \frac{\partial^2 y}{\partial z^2} I_{xx}\right) \right] - \frac{\partial}{\partial z}\left(G \frac{\partial y}{\partial z}\right) + m \frac{\partial^2 y}{\partial t^2} = F_y \tag{5.13a}$$

$$\frac{\partial^2}{\partial z^2}\left[E \left(\frac{\partial^2 y}{\partial z^2} I_{xy} + \frac{\partial^2 x}{\partial z^2} I_{yy}\right) \right] - \frac{\partial}{\partial z}\left(G \frac{\partial x}{\partial z}\right) + m \frac{\partial^2 x}{\partial t^2} = F_x \tag{5.13b}$$

It is evident by examination of these equations that the blade motion is coupled in the lead-lag and flapping planes. There is no closed form solution for the expression, so an approximate method is required. A modal analysis is chosen as the preferred solution technique since the equations are uncoupled in the modal frame of reference. The derivation of the uncoupled form is carried out in the next section and the solution is obtained using computer code DYNAMICS which may be found in Appendix D.

5.2 Modal Equations of Motion

Modal analysis is based on the assumption that the response of a system is determined by the linear combination of the orthogonal mode shape. The mode shape represents the deflection configuration of the system when it vibrates at a natural frequency. In other words, the mode shapes and natural frequencies are solutions to the free vibration equation. A further explanation of modes and their orthogonal properties can be found in most vibrations texts [11]. The combination of modes comprizing the response of the blade is represented by;

$$\begin{bmatrix} x \\ y \end{bmatrix} = \begin{bmatrix} \phi_1(x) \\ \phi_1(y) \end{bmatrix} g_1(t) + \begin{bmatrix} \phi_2(x) \\ \phi_2(y) \end{bmatrix} g_2(t) + \ldots \begin{bmatrix} \phi_n(x) \\ \phi_n(y) \end{bmatrix} g_n(t) \quad (5.14a)$$

where $\phi_n(x,y)$ is a mode shape and $g_n(t)$ is a modal amplitude. This equation is conveniently expressed in vector subscript notation by;

$$\xi_j = \phi_{ij}\, g_i \quad (5.14b)$$

where the summation is implied by repeated subscripts. This notation will be used throughout the chapter.

The governing equation of motion (eq. 5.13) has the following form in subscript notation;

$$(A_{ii}\, \xi_i'')'' + (B_{ii}\, \xi_i')'' + X_{ii}\, \ddot{\xi}_i = F_i \quad (5.15)$$

where:

$$A_{ii} = \begin{bmatrix} I_{yy} & I_{xy} \\ I_{xy} & I_{xx} \end{bmatrix} \qquad B_{ii} = \begin{bmatrix} G & 0 \\ G & 0 \end{bmatrix}$$

$$C_{ii} = \begin{bmatrix} M & 0 \\ 0 & M \end{bmatrix} \qquad F_i = \begin{bmatrix} F_x \\ F_y \end{bmatrix} \qquad \xi_i = \begin{bmatrix} x \\ y \end{bmatrix}$$

If the right hand side of equation (5.15) is zero, the equation representing the free vibration of the blade results;

$$(A_{ii}\, \xi_i'')'' + (B_{ii}\, \xi_i')'' + C_{ii}\, \xi_i = 0 \quad (5.16)$$

When a system oscillates in a normal mode (ϕ_{ij}) with a natural frequency (ω_j), every part of the system oscillates in phase or antiphase with every other part of the system. Thus, the typical displacement is expressed by;

$$\xi_i = \phi_{ij} \sin w_j t \tag{5.17}$$

There are an infinite number of these solutions for the freely vibrating blade. Since the equations of motion (5.15 and 5.16) and their solutions (5.14 and 5.17) are known, the modal equation can be determined.

The modal equation of motion represents the difference between the forced motion and the free motion. A substitution of eq. 5.14 into the governing equation generates;

$$(A_{ii}\, \phi_{ij}'')''\, g_j + (B_{ii}\, \phi_{ij}')'\, g_j + C_{ii}\, \phi_{ij}\, \ddot{g}_j = F_i \tag{5.18}$$

A substitution of eq. 5.17 into the free vibration equation yields;

$$(A_{ii}\, \phi_{ij}'')''\, g_j + (B_{ii}\, \phi_{ij}')'\, g_j - w_j^2\, C_{ii}\, \phi_{ij}\, g_j = 0 \tag{5.19}$$

When eq. 5.18 and 5.19 are pre-multiplied by the transpose of the mode shape (ϕ_{ji}) and subtracted from each other, a modal equation for the differential element results;

$$\phi_{ji}\, C_{ii}\, \phi_{ij}\, (\ddot{g}_j + w_j^2\, g_j) = \phi_{ji}\, F_i \tag{5.20}$$

All the coupled terms have been eliminated from the modal equation because of the orthogonality property of the mode shapes. The orthogonal condition stipulates that;

$$\phi_{ji}\, \phi_{ij} \neq 0 \text{ for } j = j \tag{5.21}$$

and

$$\phi_{ji}\, \phi_{ij} = 0 \text{ for } j \neq j \tag{5.22}$$

When eq. 5.20 is integrated from the blade root to the tip, the modal equation for the entire blade results as;

$$\int_{R_o}^{R} \phi_{ji}\, C_{ii}\, \phi_{ij}\, dz \quad (\ddot{g}_j + w_j^2\, g_j) = \int_{R_o}^{R} \phi_{ji}\, F_i\, dz \tag{5.23}$$

The first integral is named the modal mass;

$$M_{jj} = \int_{R_o}^{R} \phi_{ji}\, C_{ii}\, \phi_{ji}\, dz \tag{5.24}$$

and represents a diagonal mass matrix because of the orthononality conditions. The second integral is the generalized force;

$$Q_j = \int_{R_o}^{R} \phi_{ji}\, F_i\, dz \tag{5.25}$$

For an unconed turbine blade, the generalized force is composed of the aerodynamic forces on the blade, but if coning is present, it must include the additional centrifugal force. Therefore, the additional centrifugal component;

$$F_i = M\Omega Z^2 \tan \lambda \tag{5.26}$$

is added to the aerodynamic loads to obtain the generalized force as a coned turbine blade.

Therefore, the uncoupled modal equation;

$$M_{jj}\, (\ddot{g}_j + \omega_j^2\, g_j) = Q_j \tag{5.27}$$

and assumed response

$$\xi_i = \phi_{ij}\, g_j \tag{5.28}$$

represent the total motion of the wind turbine blade. An advantage of the modal equation is that a sufficiently accurate solution is obtained when only the first few modes of vibration are included in the analysis.

Usually the modal equation of motion (5.27) can be solved in the modal coordinate system. However, for the wind turbine rotor blades, the aerodynamic loads depend on blade velocities; therefore, the modal equations cannot be integrated directly. Thus, the solution involves the transformation between the modal coordinates and the physical coordinates to calculate the aerodynamic loading and the generalized forces. Computer code DYNAMICS listed in Appendix D is used to solve the modal equations for a wind turbine generator.

5.3 Aerodynamic Loads

In Chapter 4, a simplified expression for the aerodynamic loading on the rotor was presented. This expression excluded many higher order terms so that an analytical integration would be possible. Since numerical techniques are used for the modal analysis, the neglected variables can be included in the force system. Blade element theory is retained for the determination of the aerodynamic forces, but the blade element diagram shown in Figure 4.4 is modified to include drag (Figure 5.2).

Both lift and drag depend on the relative wind (V_R) and the angle of attack (α). The magnitude of these forces are given by the equations;

FIGURE 5.

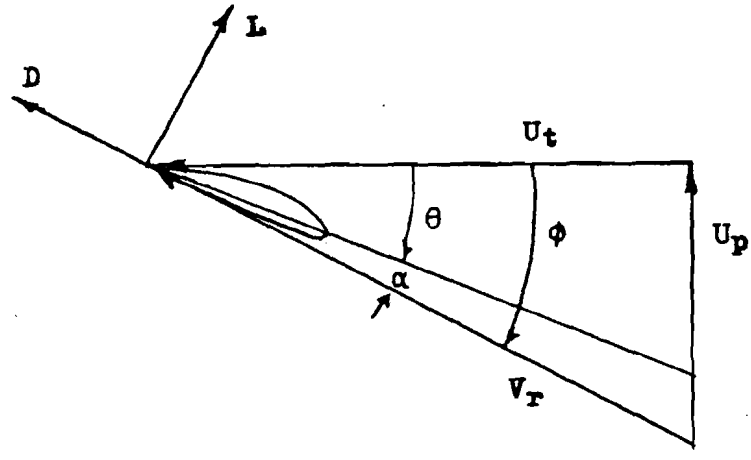

U_p = perpendicular velocity

U_t = tangential velocity

$V_r = U_t^2 + U_p^2$ = resultant velocity

ϕ = blade element angle

θ = blade pitch angle

α = angle of attack

L = lift

D = drag

$$L = \frac{1}{2} \rho \, C_{\ell} \, C \, V_R^2 \, \Delta r \tag{5.29}$$

and

$$D = \frac{1}{2} \rho \, C_D \, C \, V_R^2 \, \Delta r \tag{5.30}$$

The lift and drag coefficients, C_{ℓ} and C_D, are experimentally determined quantities that depend on the airfoil shape. These quantities are generally expressed graphically as shown in Figure 5.3, which shows the characteristics of the NACA 4415 airfoil used in the construction of the WF-I blades [12].

The relative velocity acting on the airfoil is composed of components perpendicular (U_p) and parallel (U_T) to the plane of rotation. These parallel and perpendicular velocities acting on an element of the blade are given by;

$$U_p = V_o \, (1 - (a+w(\psi)) - \dot{u} \tag{5.31}$$

$$U_T = \Omega r \, (1+b) - \dot{v} \tag{5.32}$$

where: V_o = wind speed

a = axial interference factor

b = radial interference factor

$w(\psi)$ = tower shadow factor

$\dot{u}$ = x blade velocity

$\dot{v}$ = y blade velocity

For this, modal tower shadow is represented by the rectangular pulse of section 3.4, but it is both a function of azimuth angle and blade radius. Therefore, the velocity deficit is applied gradually starting at the blade root as the blade encounteres the wake. Figure 5.4 displays this tower shadow approximation.

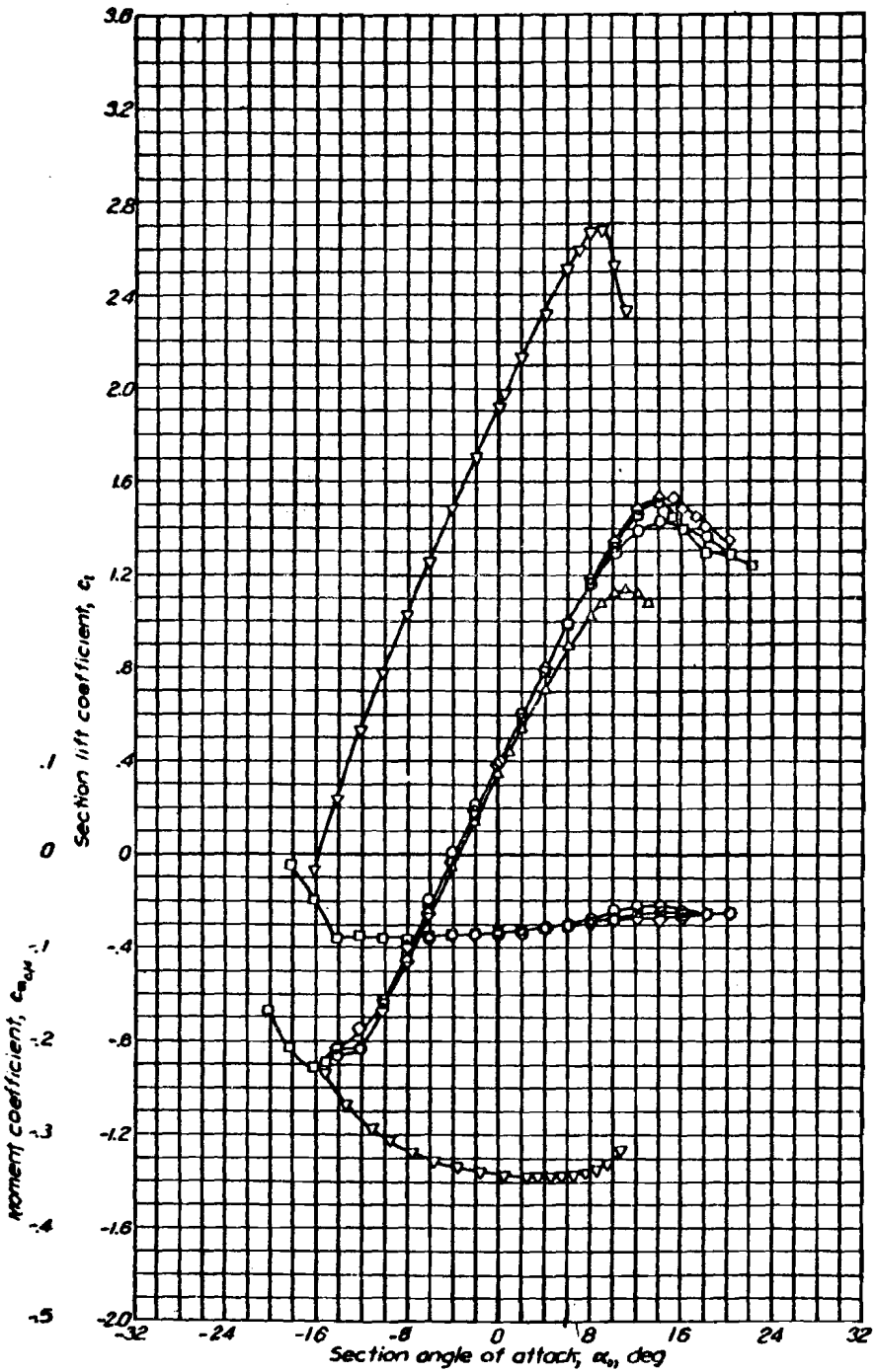

NACA 4418 Wing Section

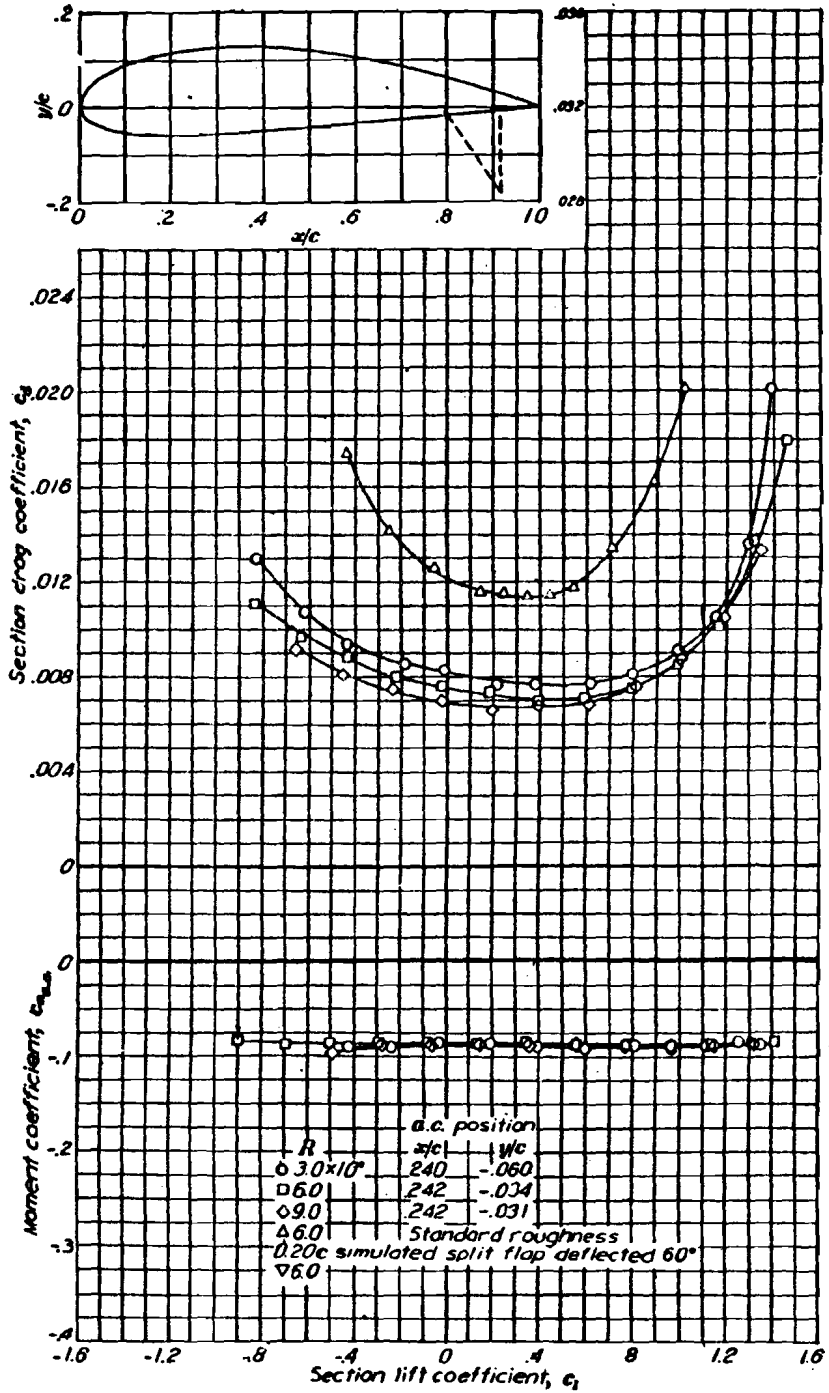

NACA 4418 Wing Section

FIGURE 5A
SHADOW MODEL

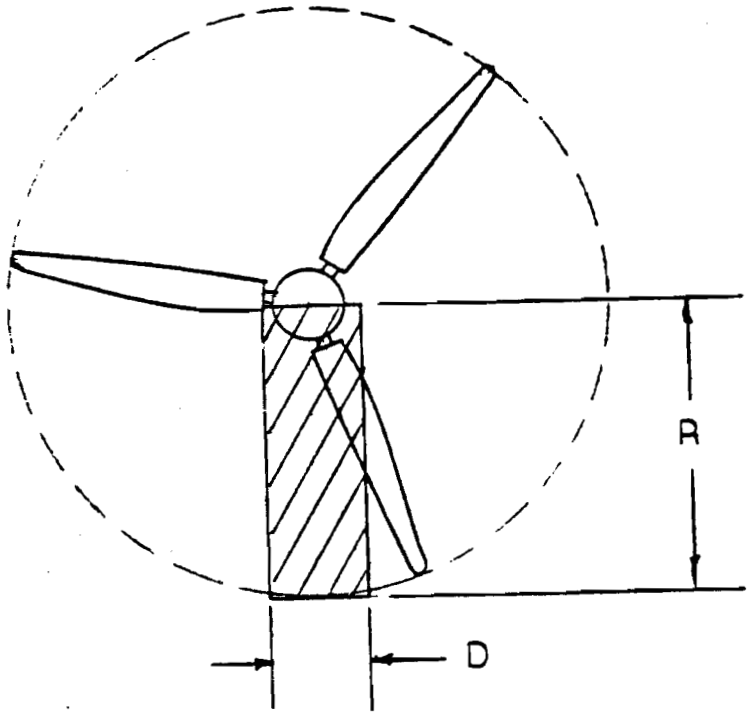

Rotor induced velocities are indicated by the axial and radial interference factors. No attempt is made to calculate these quantities for the dynamic system. They are assumed to be equivalent to the interference factors obtained from a steady state momentum analysis of the wind turbine. Momentum theory determines the axial and radial interference factors by iterating through the following equations until they converge upon the proper values [13].

$$\tan \phi = \frac{V_o}{\Omega r} \frac{1-a}{1+b} = \frac{1-a}{\mu(1+b)} \tag{5.33}$$

$$\frac{a}{1+a} = \frac{B\ c\ (C_l \cos \phi + C_D \sin \phi)}{8\pi\ r \sin^2 \phi} \tag{5.34}$$

$$\frac{b}{1-b} = \frac{B\ c\ (C_l \sin \phi - C_D \cos \phi)}{8\pi\ r \sin \phi \cos \phi} \tag{5.35}$$

In these equations (b) is the number of blades, (C) is the chord length, and (ϕ) is the relative pitch angle.

Once the velocity components are determined, they yield the angle of the attack (α), since;

$$\alpha = \phi - (\theta_o + \theta_p) \tag{5.36}$$

and

$$\phi = \arctan (U_p/U_t) \tag{5.37}$$

The angle of attack is then used with airfoil data (Figure 5.2) and eqs. 5.29 and 5.30 to determine the lift and drag on the blade element. The lift and drag forces are resolved into components parallel and perpendicular to the plane of rotation as;

$$F_x = -D \cos \phi + L \sin \phi \qquad (5.38)$$

$$F_y = D \sin \phi + L \cos \phi \qquad (5.39)$$

to serve as the aerodynamic input to the generalized forces defined by eq. 5.25.

5.4 Analysis of Wind Furnace I

An extensive analysis of the WF-I blades using computer code DYNAMICS has been performed and the results are presented in this section. The data necessary for the analysis has been listed in the previous sections, but an example of the input is condensed below for review and ease of reading.

```
      DATA
WIND SPEED (M/S).............  9.000
TIP SPEED RATIO..............  7.500
PITCH ANGLE (DEG)............. -6.000
CONING ANGLE (DEG)............ 10.000
SHADOW WIDTH (M).............  0.254
SHADOW STRENGTH V/V.........  0.500
BLADE RADIUS (M).............  4.953
STATION SPAN
  0.100  0.200  0.300  0.400  0.500  0.600  0.700  0.800  0.900  1.000
CHORD DISTRUBUTION (M)
  0.411  0.445  0.384  0.311  0.259  0.223  0.192  0.168  0.137  0.107
TWIST DISTRIBUTION (DEG)
 45.000 25.600 15.700 10.400  7.400  4.500  2.700  1.400  0.400  0.000
AXIAL INTERFERENCE FACTOR
  0.090  0.140  0.180  0.200  0.210  0.230  0.240  0.250  0.250  0.270
RADIAL INTERFERENCE FACTOR
  0.140  0.050  0.027  0.016  0.011  0.008  0.006  0.005  0.004  0.003
MASS DISTRIBUTION (KG)
 10.050  6.123  4.766  4.016  3.463  2.696  1.999  1.473  1.025  0.527
NATURAL FREQUENCY (RADIANS/SECOND)
          28.430            64.450            99.550
X MODAL COORDINATES
  0.000  0.000 -0.010 -0.020 -0.040 -0.060 -0.080 -0.110 -0.130 -0.160
  0.000  0.010  0.050  0.110  0.180  0.290  0.430  0.600  0.790  1.000
  0.000 -0.010 -0.020 -0.040 -0.060 -0.050 -0.030  0.030  0.120  0.150
Y MODAL COORDINATES
  0.000  0.010  0.030  0.090  0.170  0.290  0.430  0.600  0.790  0.990
  0.000  0.000  0.000  0.000  0.000  0.020  0.060  0.110  0.180  0.250
  0.000  0.030  0.090  0.180  0.270  0.280  0.140 -0.190 -0.700 -0.950
```

SI units are employed by the program and it should be noted that all angles inputed into the computer code are in radians. The use of degrees in the output is for simple identification.

Part of the output from the program DYNAMICS includes the steady-state forces that would exist for a uniform flow field. Rated conditions were choosen for the typical example of the forces and moments. Figure 5.5 shows a comparison between the flatwise and edgewise moment distribution. In the previous chapter, edgewise motion was neglected altogether and the magnitudes of the moments indicate that the assumption was reasonable. The maximum bending moments on the blade occur between the .5 and .7 blade stations. The stress occurring on this section of the blade should be a maximum because the cross-sectional area decreases towards the tip. Figure 5.6 shows the affect that pre-coning the blade 10 degrees has on the bending moment distribution. Centrifugal relief reduces the total moment by more than half, which is a significant reduction of the steady applied loads.

Rated conditions were also chosen to show the typical response of the blade when tower shadow perturbation is disrupting the flow. Figure 5.7 shows the blade root bending moments and Figure 5.8 shows the tip deflection. The blade response has many similarities to the rigid blade analysis in that the shadow response occurs after the blade passes behind the tower and the recovery from the shadow indicates a damped oscillation. Bending moments are not severe because the tower shadow is applied and removed gradually. The gradual loading of the blade is believed to be a realistic model of the physical situation. Also the damped natural frequency of the true geometry is less than exists for an assumed constant chord blade.

FIGURE 3.3

MOMENT DISTRIBUTION

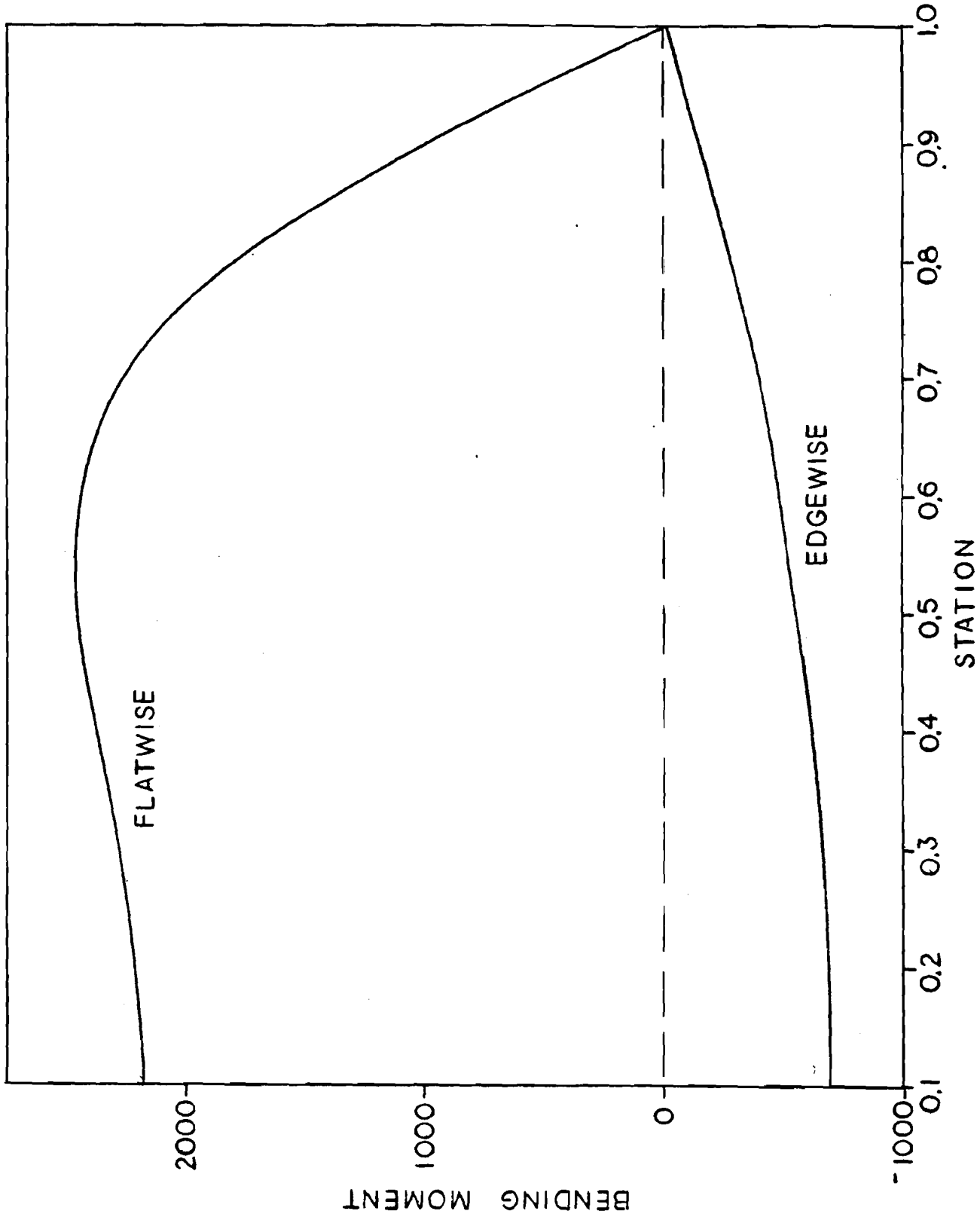

FIGURE 5.6

CENTRIFUGAL RELIEF

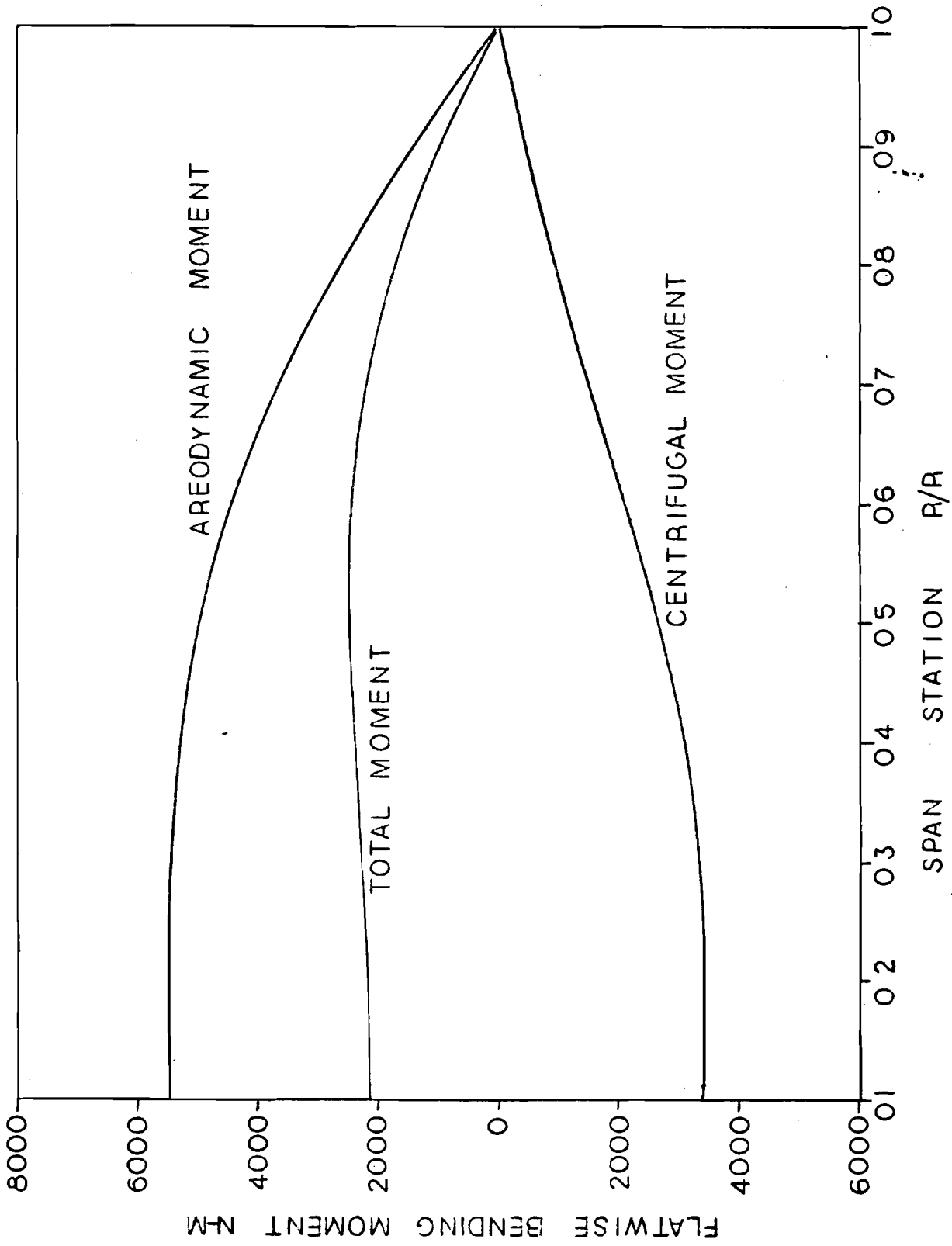

FIGURE 5.7

BLADE TIP MOTION

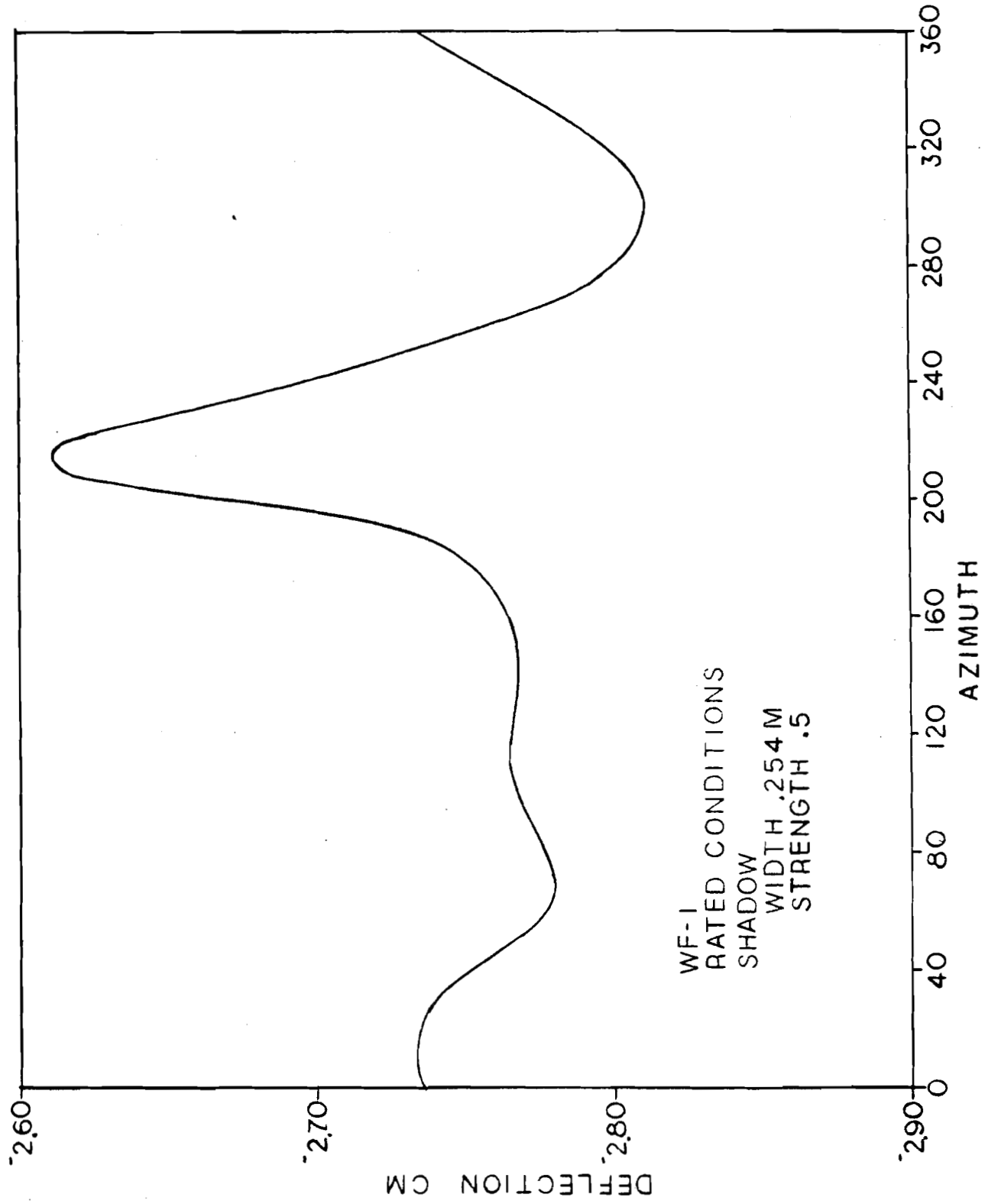

FIGURE 5.8

MODAL PREDICTION

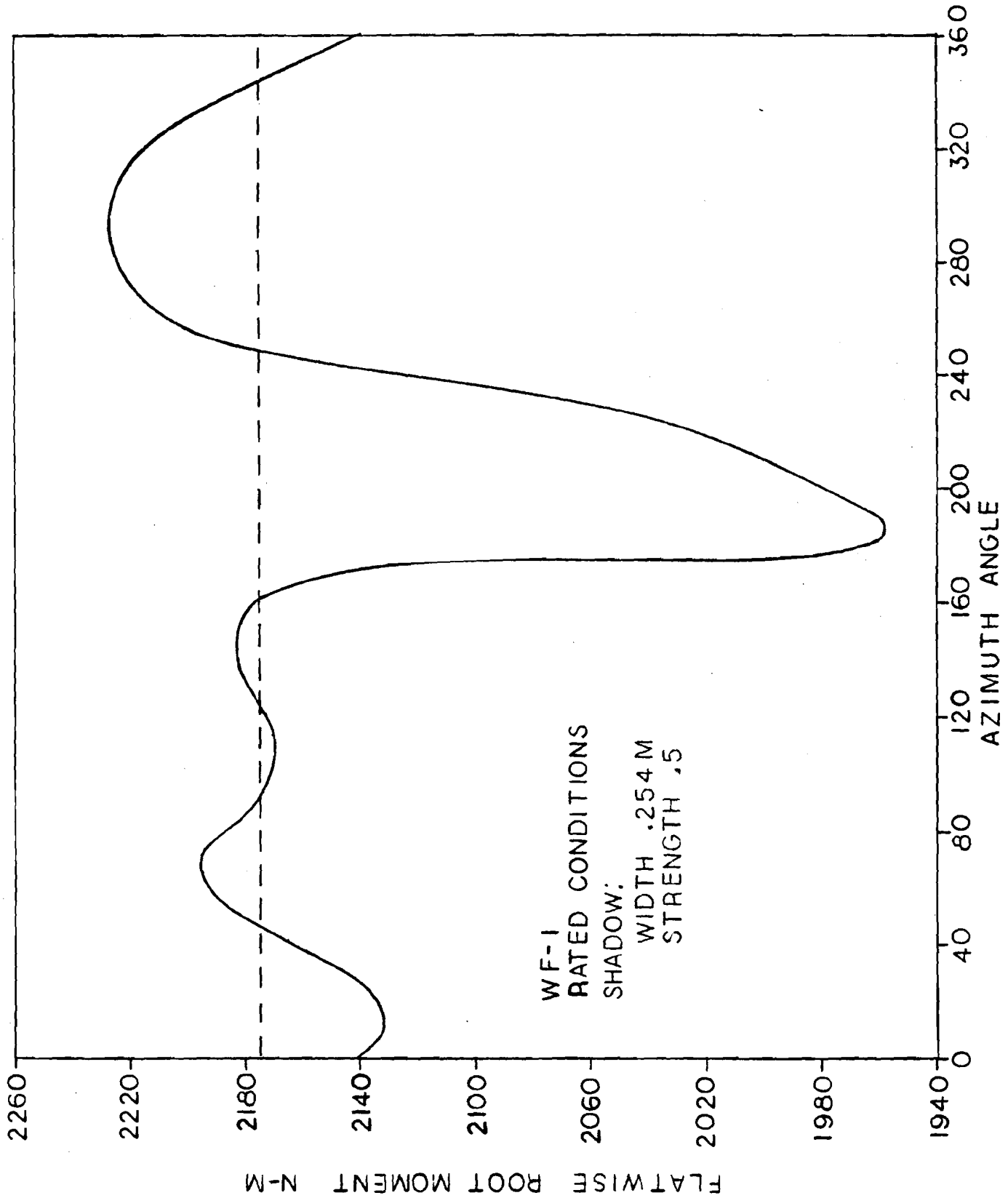

The damping is indicated by the number of oscillations a blade makes during a complete revolution.

Over the entire operating range, tower shadow causes a cyclic response. The magnitude of the oscillations are shown in Figure 5.9, which shows the maximum (M_{max}), minimum (M_{min}) and steaty (M_{st}) moments for the WF-I blade. The steady bending moments increase in region II operation and decrease in region III, while the cyclic tower shadow moment variation increases steadily with wind speed. The magnitude of the moment variation also increases when the wake width becomes larger as shown in Figure 5.10. A doubling of the shadow width is accompanied by a doubling of the cyclic moment variation. Therefore, the common sense approach of small tower causing fewer problems applies to the tower shadow predictions.

To examine the affect that important parameters have on the dynamic model, a sensitivity plot is developed. Figure 5.11 shows the sensitivity of the model to changes in coning angle, wind speed, shdow width, and shadow strength. The ordinate is defined as;

$$\frac{\text{Parameter value}}{\text{Standard Parameter value}} = \frac{P}{P_o}$$

and the abssica is defined in terms of the variation in cyclic bending moments, where the variation is defined as the maximum blade root bending moment minus the minimum blade root bending moment;

$$\frac{\text{Variation of Moment}}{\text{Standard Variation of Moment}} = \frac{M_v}{M_{vo}}$$

Standard conditions are defined for the WF-I as;

Wind speed = 9 m/s (20 mph)

FIGURE 5.9

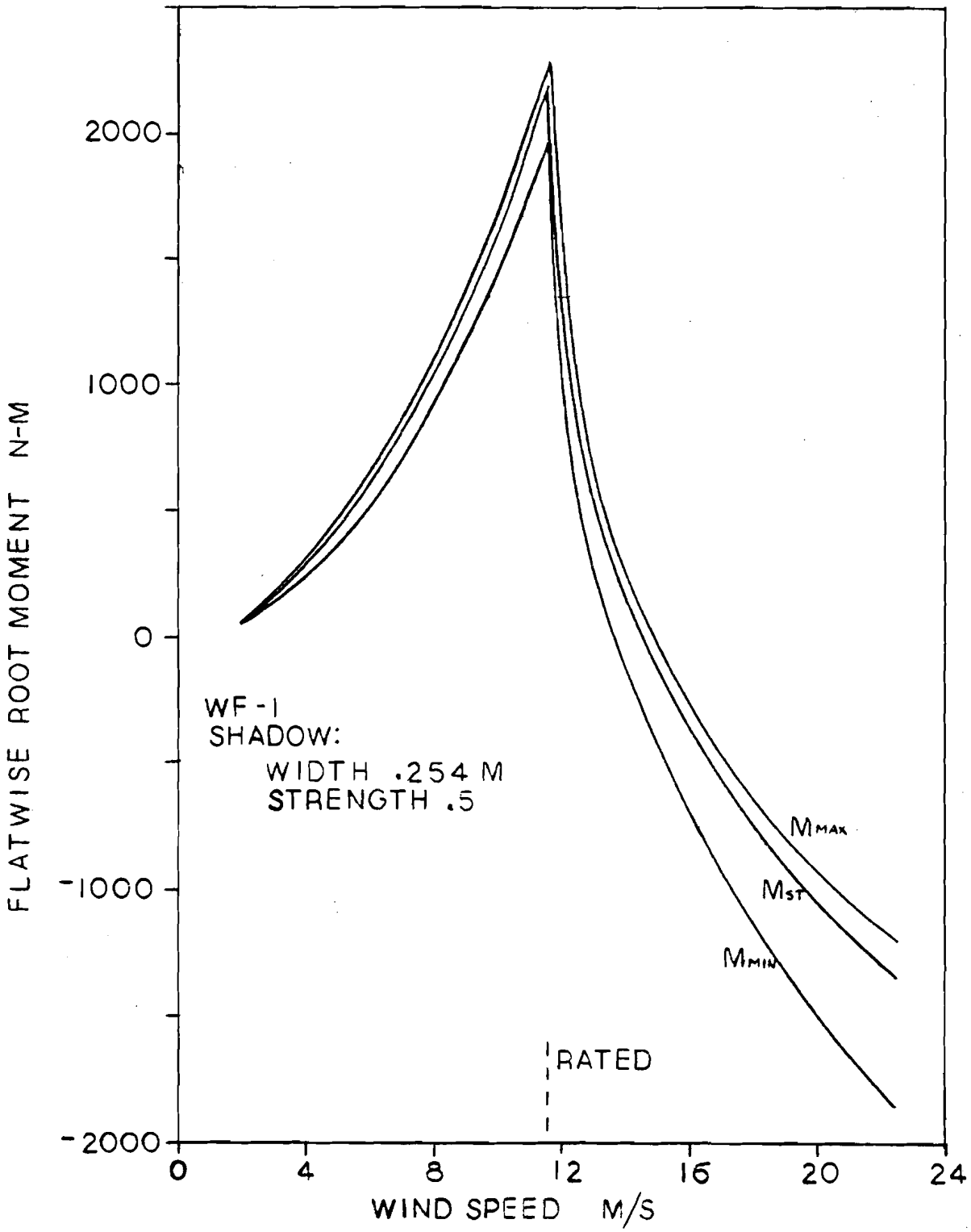
2000
1000
0
-1000
-2000
FLATWISE ROOT MOMENT N-M
WF-1
SHADOW:
WIDTH .254 M
STRENGTH .5
MMAX
MST
MMIN
RATED
0
4
8
12
16
20
24
WIND SPEED M/S

FIGURE 5.10

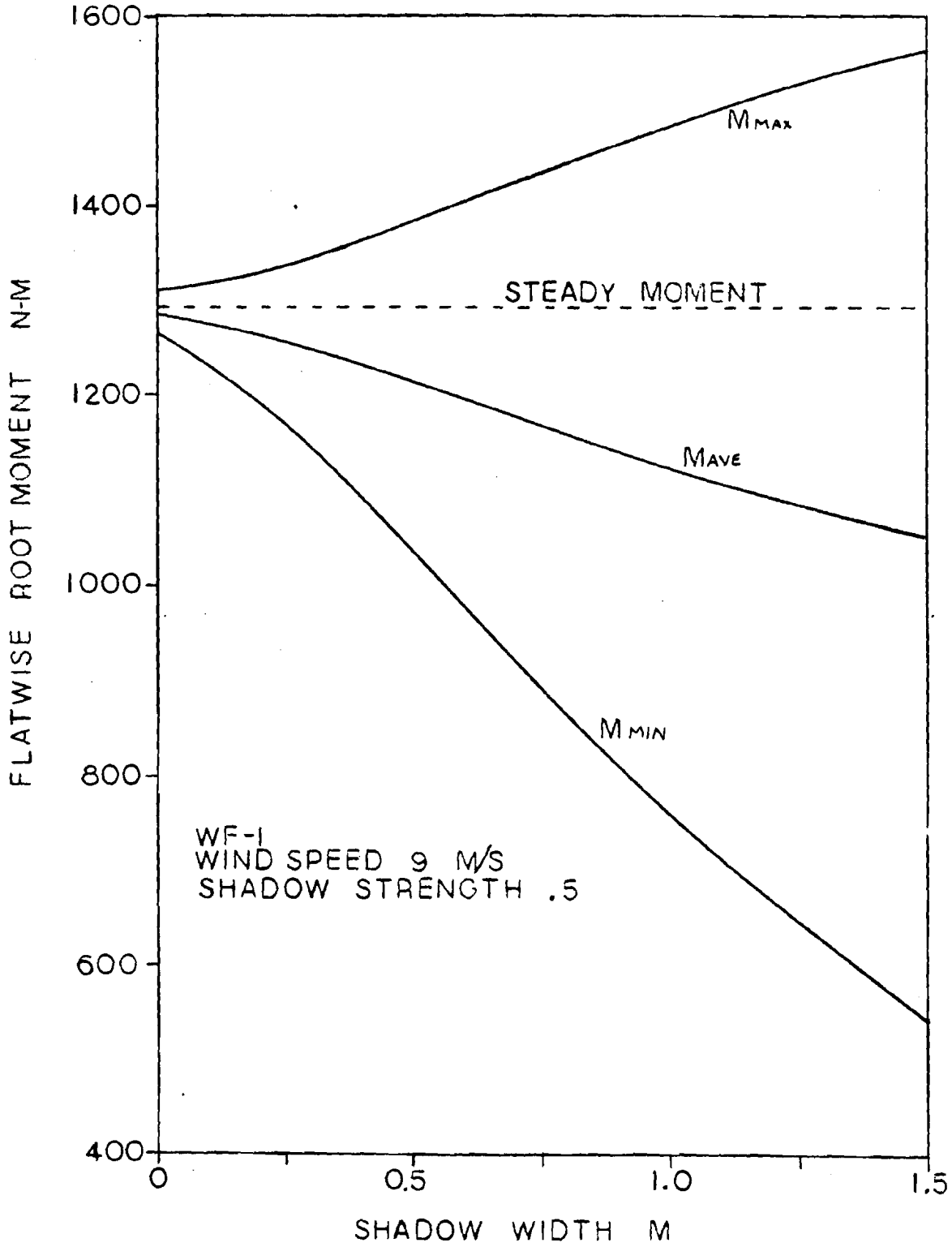
1600
1400
1200
1000
800
600
400
FLATWISE ROOT MOMENT N-M
M MAX
STEADY MOMENT
M AVE
M MIN
WF-1
WIND SPEED 9 M/S
SHADOW STRENGTH .5
0
0.5
1.0
1.5
SHADOW WIDTH M

FIGURE 5.11

SENSITIVITY OF PARAMETERS

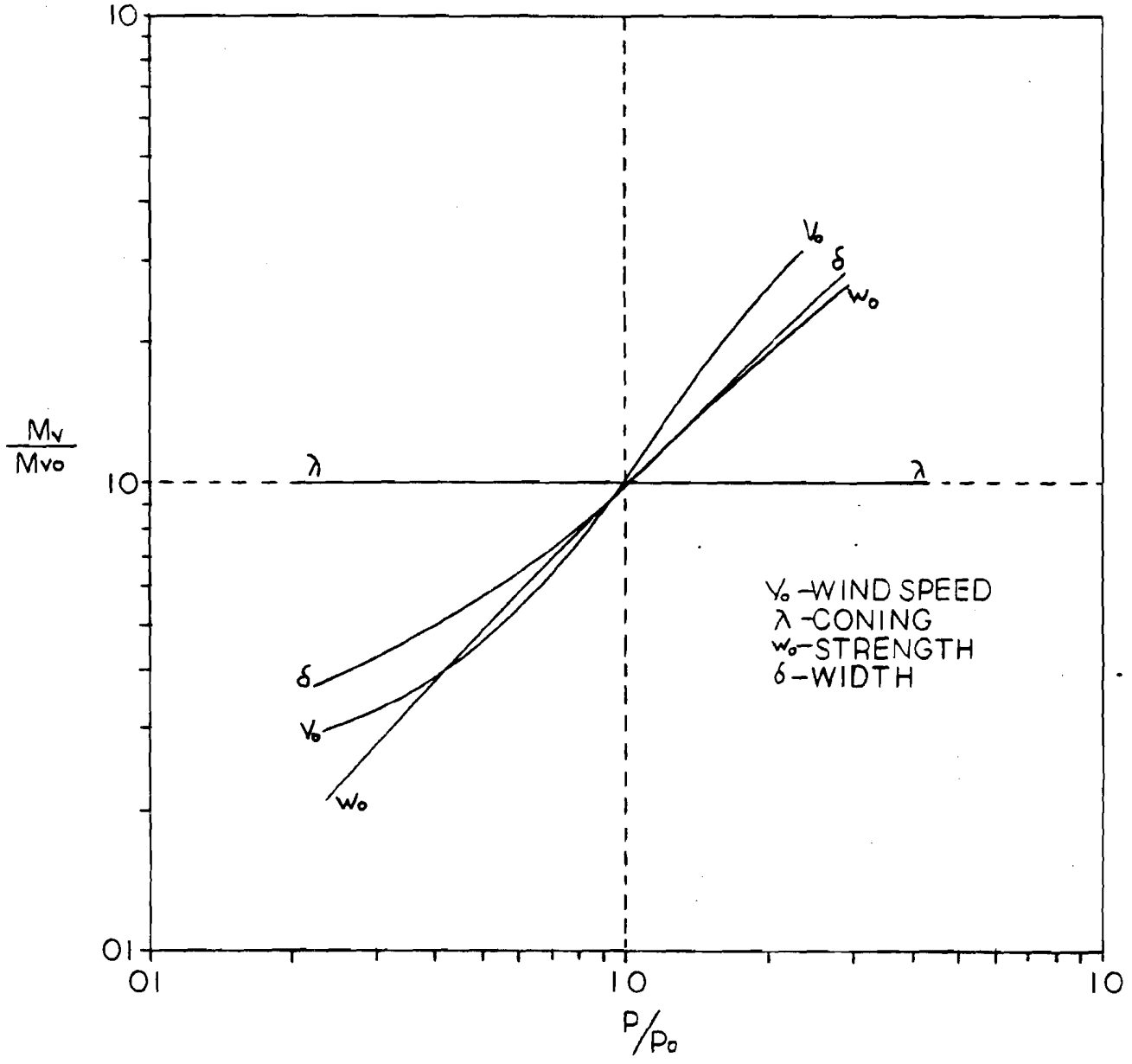

Coning angle = 10°

Shadow width = .254 m (10")

Shadow strength = .5

The results of the sensitivity test indicate that coning angle does not effect the cyclic loading pattern and that windspeed is a dominant variable for high windspeeds. Both windspeed and shadow width have a decreased affect when they have small values. The physical significance of the decreasing affect is that the moment variation is approaching a steady value other than zero. For the shadow width the limiting case is an impulsive load, and for the wind speed, it is the moment variation that occurs at cut-in velocity. In conclusion of this chapter, it should be noted that the wake structure has been defined by a simple model and this model may be changed at any time if more detail is known about the wake or blade response.

CHAPTER 6

CONCLUSIONS AND RECOMMENDATIONS

6.1 Conclusions

The purpose of this study was the evaluate the affect of tower shadow on the wind turbine rotor. Two models were developed for the assessment of rotor blade response. One model involved a simple rigid blade while the other modeled a complex flexible blade. Both models indicated that the tower wake imparts a force that causes the blade to have a damped oscillatory motion with large deflection amplitudes occuring on the upswing of the blade ($\Psi > 180°$). The major discrepancy between the two model predictions involves the magnitude of the resulting forces. Larger cyclic forces are always predicted by the simple rigid model because the shadow is assumed to encompass the entire blade instantaneously, while the complex model assumes a gradual application of the shadow.

Of the two approaches, the rigid system solved by computer code RIGID proved to be easier and less time consuming than its flexible counterpart solved by computer code DYNAMICS. Since the simple model predicts a more drastic response, it serves to make conservative estimates of the blade loading. The more complex model serves the purpose of defining a detailed loading distribution along the blade. For design applications, the simple system will indicate problem areas and the complex system will define the loads at those problem areas.

The computer codes have been documented in the appendices to facilitate their use. These codes many be extended to include force variation due to wind shear and gravity by program modifications that change the applied loads or wind field, not the solution technique. Since the solution technique

has been successful.

6.2 Recommendations

Although the models predict solutions for the wake blade interaction, experimental information is needed to confirm or refute the predictions. Experimental analysis should include both frequency and amplitude analysis of the blade motion.

A frequency analysis is needed to verify the blade natural frequencies and resonant conditions. Of the possible resonant conditions, the 3Ω forcing harmonic occuring in a 7.6 m/s (17 mph) wind speed should be particularly strong because the blades natural frequency coincides with this forcing frequency. A power spectral density analysis should yield most of the frequency information, since the application of this analysis is to establish the frequency composition of data [16].

Experimental data will also yield information about the blade motion and wake structure. The blade motion may not be apparent from the data because the data will contain a large amount of extraneous information. Much of the extraneous data will have frequency components less than or equal to 2Ω. This low frequency information can be eliminated by high pass filtering techniques. Once the extraneous affects have been removed, trends of blade motion may be identified.

For the determination of the wake structure, it will be necessary to vary the tower diameter. This variation can be performed by encompassing the tower with shrouds. The shrouds not only change the wake width but they will alter the wake strength which is related to the ratio of X/D, where X is the distance from the plane of rotation to the tower axis and D is the tower diameter. A method of condensing the large quantity of

information is with the use of non-dimensional parameters. Cyclic moment variations may be non-dimensionalized by

$$\frac{2(M_{max}-M_{min})}{M_{max}-M_{min}} = \frac{M}{M_{ave}}$$

and the windspeed can be expressed in terms of a Reynolds number;

$$\frac{V_o D}{\nu} = R_e$$

The non-dimensional terms allow a plot of the non-dimensional moment versus Reynolds number for various X/D ratios. This type of experimental analysis should facilitate the identification of the wake and the verification of the proposed analytical predictions.

REFERENCES

1. Savino, Joseph M., Wagner, Lee H., and Nash, Mary, Wake Characteristics of a Tower for the DOE-NASA Mod-1 Wind Turbine, April 1978, DOE/NASA/1028-78/17.

2. Perkins, F.W., and Cromack, D.E., Wind Turbine Blade Stress Analysis and Natural Frequencies, UM-WF-TR-78-8.

3. Trichet, Pierre, Study of the Flow Around a Cylinder and of its Near Wake, NASA TT-16844, 1975.

4. Cantwell, Brian Joseph, A Flying Hot Wire Study of the Turbulent Near Wake of a Circular Cylinder at a Reynolds Number of 140,000, Ph.D. Dissertation, California Institute of Technology, Pasadena, California, 1975.

5. Roskko, Anotal, "On the Wake and Drag of Bluff Bodies," Journal of the Aeronautical Sciences, Vol. 22, 1955.

6. Wind Turbine Structural Dynamics, NASA Conference Publication 2034, DOE Publication CONF-771148, 1977.

7. Stoddard, Forrest S., Structural Dynamics, Stability and Control of High Aspect Ratio Wind Turbines, Energy Alternatives Program, University of Massachusetts, Amherst, Mass., UM-WF-TR-78-11.

8. Demarogonas, Andrew D., Vibration Engineering, West Publishing Co., 1976.

9. Cohen, Richard, Yaw Dynamics, Energy Alternatives Program, University of Massachusetts, Amherst, Mass., UM-WF-TR-79.

10. Rivello, Robert M., Theory and Analysis of Flight Structures, McGraw-Hill, New York, 1969.

11. Bigg, John M., Introduction to Structural Dynamics, McGraw-Hill, New York, 1964.

12. Abbott, Ira A., and Van Doenhoff, Albert E., Theory of Wing Sections, Dover Publications, Inc., New York, 1959.

13. Wilson, Robert E. and Lissaman, Peter B.S., Applied Aerodynamics of Wind Power, NTIS, PB-238595, July 1974.

14. Bramwell, A.R.S., Helicopter Dynamics, John Wiley and Sons, New York, 1976.

15. Shapiro, Jacob, Principles of Helicopter Engineering, Temple Press Limited, Bowling Green Lane, London, 1955.

16. Bendat, Julius S. and Piersol, Allen G., Random Data: Analysis and Measurement Procedure, John Wiley and Sons, Inc., New York, 1971.

A P P E N D I X A

A.1 Theorem of Southwell

The Theorem of Southwell mentioned in section 2.3 is discussed here because of its usefullness in accounting for the centrifugal stiffening of a rotating blade. The Theorem states that in an elastic system, the spring forces can be divided into two parts, such that the total potential energy is the sum of two partial potential energies. Thus, the natural frequency (ω_n) of the blade can be approximated by;

$$\omega_n^2 = \omega_1^2 + \omega_2^2 \tag{1}$$

where ω_1 is the natural frequency at standstill and ω_2 is the natural frequency of a blade having no bending resistance. Centrifugal tension is the only stiffening component of ω_2. Rayleigh's method is used to establish the rotating frequency when the blade mode shape is assumed to remain unchanged by blade rotation [14].

Therefore, if the non-rotating mode shape (ϕ_i) is given, then the maximum potential energy due to centrifugal loading is;

$$U_c = \frac{1}{2} \int_{R_o}^{R} G\left(\frac{d\phi_i}{dz}\right)^2 dz \tag{2}$$

where G is the centrifugal tension.

$$G = \int_{z}^{R} m\Omega^2 z\,dz \tag{3}$$

The maximum kinetic energy for a system oscillating at a natural frequency is expressed by;

$$K = \frac{1}{2}\,\omega_i^{\,2} \int_z^R m\,\phi_i^{\,2}\,dz \tag{4}$$

Now, the rotating frequency of the blade is given by equating the energies and solving for ω^2;

$$\omega_i^{\,2} = \frac{\frac{1}{2}\int_{R_o}^{R} G\,(\frac{d\phi_i}{dz})^2\,dz}{\frac{1}{2}\int_{R_o}^{R} m\,\phi_i^{\,2}\,dz} \tag{5}$$

When G is replaced by its integral definition, equation 5 is re-arranged to yield the solution;

$$\omega_i^{\,2} = \frac{r^2\int_{R_o}^{R}\int_{R_o}^{Z} mzdz\;\;(\frac{d\phi_i}{dz})^2\,dz}{\int_{R_o}^{R} m\,\phi_i^{\,2}\,dz} \tag{6}$$

This equation is in the form

$$\omega_i^{\,2} = \alpha_i\, r^2$$

where α_i is the Southwell coefficient given by

$$\alpha_i = \frac{\int_{R_o}^{R}\int_{z}^{R} mz\,dz\;\;(\frac{d\phi_i}{dz})^2\,dz\,dz}{\int_{R_o}^{R} m\,\phi_i^{\,2}\,dz} \tag{7}$$

A.2 Program South

The solution of this equation is performed by function SOUTH. This function uses a data package that consists of a group of stored variables. The stored quantities are shown in the program listing as underscored names, which have the following meaning;

R A D I U S, rotor radius

S P A C E, spacing between blade sections

S T A T I O N, listing of all station spans expressed as r/R

M A S S, mass per unit length at any station span

M O D E X, x coordinates of the mode shape

M O D E Y, y coordinates of the mode shape

To run the program, type SOUTH and the computer will return the solution.

A.3 FLOW CHART FOR PROGRAM SOUTH

SOUTH

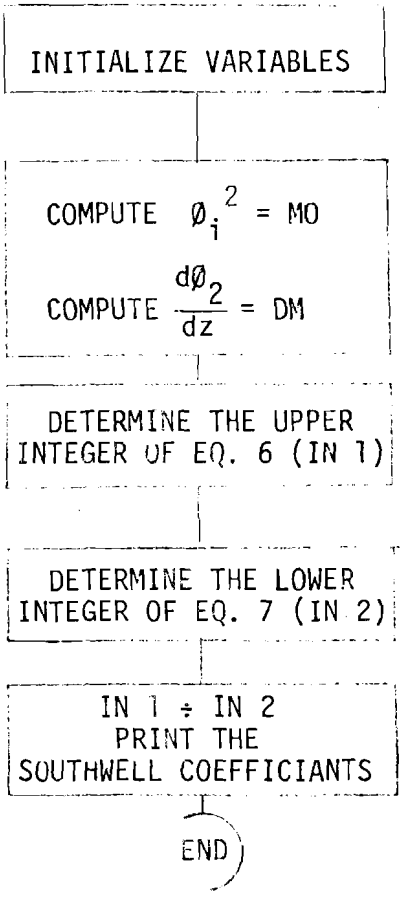

A.4 PROGRAM LISTING

```
      ∇SOUTH[□]∇
      ∇AL←SOUTH;Z;D;N;MO;A;I;DM;M1;MDM;S1;S2;MM;IN1;IN2;T
[1]    Z←RADIUS×STATION
[2]    D←⍴MASS
[3]    N←(¯1↓⍴MODEX)×2
[4]    MO←((MODEY*2)+MODEX*2)*0.5
[5]    A←(N÷2),D
[6]    I←1↓¯1↓⍳D
[7]    DM←A⍴1
[8]    DM[;I]←(MO[;I+1]-MO[;I-1])÷2×SPACE
[9]    DM[;1]←((MO[;2]×4)-MO[;3]+MO[;1]×3)÷2×SPACE
[10]   DM[;D]←((MO[;D]×3)+MO[;D-2]-MO[;D-1]×4)÷2×SPACE
[11]   M1←A⍴MASS
[12]   MDM←M1×DM*2
[13]   S1←S2←A⍴0
[14]   I←¯1↓⍳D
[15]   S1[;I+1]←(MDM[;I]+MDM[;I+1])×SPACE÷2
[16]   I←2
[17]  L1:S2[;I]←S2[;I-1]+S1[;I]
[18]   I←I+1
[19]   →(I≤D)/L1
[20]   S2←S2×A⍴Z
[21]   MM←M1×MO*2
[22]   T←A⍴1,((D-2)⍴2),1
[23]   IN1←+/(T×S2)×SPACE÷2
[24]   IN2←+/(T×MM)×SPACE÷2
[25]   AL←IN1÷IN2
      ∇
```

A.5 TERMINAL SESSION

```
      SOUTH
3.00299629 2.912068217 5.126333881
```

A.6 DATA RECORDS

```
      RADIUS
4.953

      STATION
0.1 0.2 0.3 0.4 0.5 0.6 0.7 0.8 0.9 1

      SPACE
0.4953

      MASS
10.05 6.123 4.766 4.016 3.463 2.696 1.999 1.473 1.025 0.5266

      MODEX
0  0     -0.01 -0.02 -0.04 -0.06 -0.08 -0.11 -0.13 -0.16
0  0.01  0.05  0.11  0.18  0.29  0.43  0.6   0.79  1
0 -0.01 -0.02 -0.04 -0.06 -0.05 -0.03  0.03  0.12  0.15

      MODEY
0 0.01 0.03 0.09 0.17 0.29 0.43  0.6   0.79  0.99
0 0    0    0    0    0.02 0.06  0.11  0.18  0.25
0 0.03 0.09 0.18 0.27 0.28 0.14 -0.19 -0.7  -0.95
```

APPENDIX B

B.1 Aerodynamic Forces

This approach for calculating the lift on a blade element follows the method presented by Stoddard, Structural Dynamics, Stability and Control of High Aspect Ratio Wind Turbines, p. 59-66. To derive the aerodynamic forces, we isolate a blade element dr at radius r, and draw a vector diagram of the velocities perpendicular and tangential to the rotor plane. This is shown in Figure B.1.

The drag is neglected since it is small compared to lift and the lift can be represented as;

$$L = \frac{1}{2} \rho \, C_{\ell\alpha} \, C V_R^2 \, \alpha \qquad (1)$$

where: ρ = air density

$C_{\ell\alpha} = \frac{dC_\ell}{d\alpha}$ = slope of the lift curve

C = chord

α = angle of attack

Significant aerodynamic perturbations will depend on changes in angle of attack α, so V_R will be allowed to remain constant. A further assumption is made, saying that V_R has roughly the same magnitude at U_t. Therefore, $V_R^2 \simeq U_t^2 \simeq (\Omega r)^2$ and lift is now;

$$L = \frac{1}{2} \rho \, C_{\ell\alpha} \, C \, (\Omega r)^2 \, \alpha \qquad (2)$$

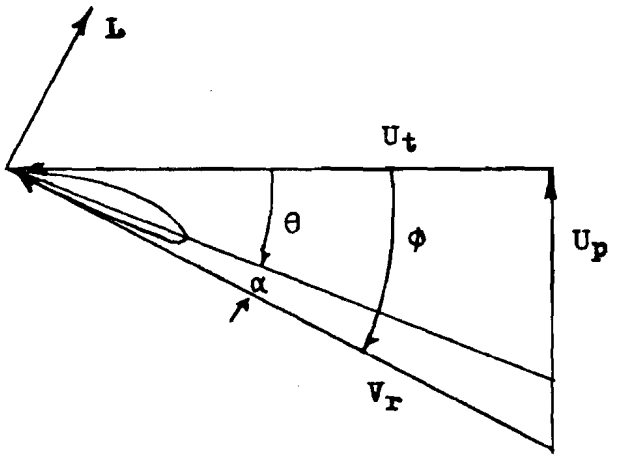

U_p = perpendicular velocity

U_t = tangential velocity

$V_r = U_t^2 + U_p^2$ = resultant velocity

Φ = blade element angle

θ = blade pitch angle

α = angle of attack

L = lift

and;

$$\alpha = \arctan(\phi - \theta) \approx \phi - \theta = \frac{U_p}{U_t} - \theta \tag{3}$$

This gives;

$$L = \frac{1}{2} \rho C_{\ell\alpha} C(\Omega r)^2 \left[\frac{U_p}{U_t} - \theta\right] \tag{4}$$

We now assume linear twist along the blade, so total pitch is;

$$\theta = \theta_o [1 - r/R] + \theta_p \tag{5}$$

with: θ_o = blade twist

θ_p = pitch measured at the tip

Therefore, the lift per unit length for a linearly twisted wind turbine blade at constant Ω is;

$$L = \frac{1}{2} \rho C_{\ell\alpha} C(\Omega r)^2 \left[\frac{U_p}{U_t} - \theta_o \left(1 - \frac{r}{R}\right) - \theta_p\right] \tag{6}$$

The velocities can be written:

$$U_t \approx \Omega r \tag{7}$$

$$U_p \quad [V_o (1-w(\psi)) - v_i] \cos \beta - r\dot{\beta} \tag{8}$$

where: V_o = constant free stream wind

V_i = axial induced velocity

$w(\psi)$ = tower shadow deficit

β = flapping angle

$r\dot{\beta}$ = contribution of the flapping velocity

For small flapping angles, cos $\beta \simeq 1$. Now the lift expression is written;

$$L = \frac{1}{2} \rho C_{\ell\alpha} C \Omega r \left[U_p - \Omega r \theta_o \left(1 - \frac{r}{R} + \frac{\theta_p}{\theta_o}\right)\right] \tag{9}$$

$$L = \frac{1}{2} \rho C_{\ell\alpha} C \Omega r \left[V_o \left(1 - w(\psi) - v_i - r\dot{\beta} - \Omega r \theta_o \left(1 - \frac{r}{R} + \frac{\theta_p}{\theta_o}\right)\right)\right] \tag{10}$$

or non-dimensionally;

$$L = \frac{1}{2} \gamma I \Omega^2 \left(\frac{1}{R^2}\right) \left[\mu_o n(1 - w(\psi)) - n_i n - n^2 \beta^1 - n^2 \theta_o \left(1 + \frac{\theta_p}{\theta_o}\right) + n^3 \theta_o\right] \tag{11}$$

where non-dimensional quantities are:

$$\theta_o = \frac{V_o}{\Omega R} = \frac{1}{\text{tip-speed-ratio}}$$

$$\lambda_i = \frac{v_i}{\Omega R} = \text{non-dimensional induced velocity}$$

$$n = \frac{r}{R} = \text{span station}$$

$$\gamma = \frac{\rho C_{\ell\alpha} CR^4}{I} \quad \text{Lock Number}$$

$$\beta^1 = \frac{d}{d} = \frac{\dot{\beta}}{\Omega}$$

In physical terms, the Lock Number (γ) can be descibed as the ratio of the aerodynamic moment due to a sudden increase of blade pitch to the centrifugal moment due to a sudden increase of a flapping angle [15]. Therefore, if the blade had infinite inertia, its motion would not be effected by changes in aerodynamic forces and the Lock Number would be zero.

A P P E N D I X C

C.1 Program RIGID

This program is used for the analysis of the rigid isolated blade model. The operation of the program is simple since only one data file is needed for the input variables. The input data file is a 5 by 3 matrix arranged in the following order:

Blade mass (kg),	Mass Moment of inertia (kg m^2),	Center of gravity (m)
Radius (m),	Hinge offset (m),	Natural frequency (rod/s)
Pitch (rod),	Twist (rod),	Coning Angle (rod)
Chord (m),	Windspeed (m/s),	Tip-speed-ratio
Snadow Strength,	Shadow width (m),	Axial interference

The program commences by first computing and printing the important structural constants. After the constants have been established, the differential equation is solved using Euler's forward stepping in time integration scheme. Integration proceeds until the transient solution is eliminated from the response. The transient motion fades after four complete cycles, or rotor revolutions. Once integration is complete, the solution is printed out.

The program then asks if you want an input record. If the operator responds with YES, the data record is printed. If the operator responds with NO, the program ends. Following is the flow chart for Program RIGID.

C.2 Program RIGID Flow Chart

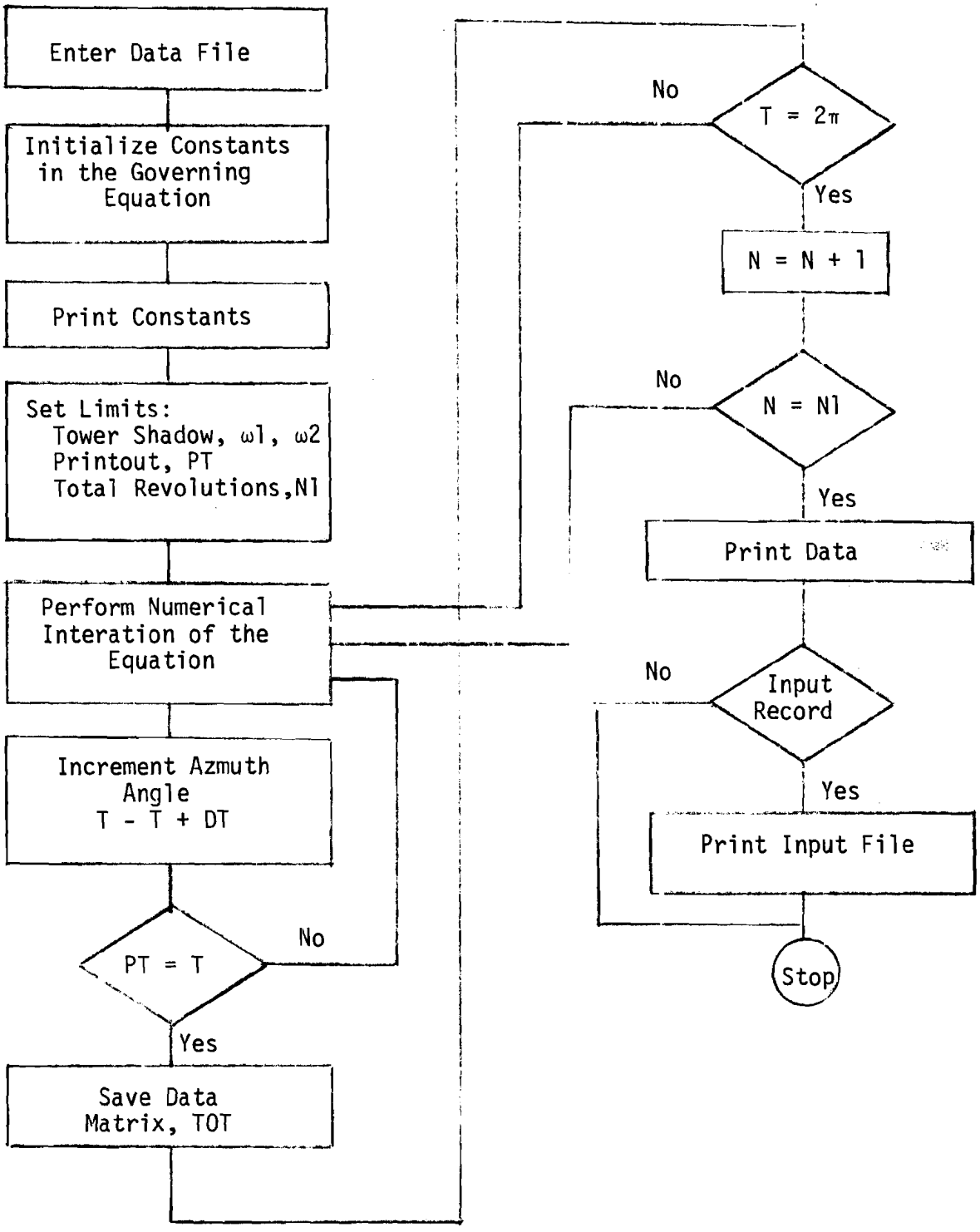

C.3 Program Listing

```
      ∇RIGID[□]∇
      ∇RIGID BLADE;D;T;TOT;KB;E;OM;NFS;LO;MA;MC;MST;BST;MP;DR;SS;DS;W1;W2;DT;
                   N1;N;T1;PT1;PT
[1]     D←BLADE
[2]     KB←D[1;2]×D[2;3]*2
[3]     E←D[1;1]×D[2;2]×D[1;3]÷D[1;2]
[4]     OM←D[4;2]×D[4;3]÷D[2;1]
[5]     NFS←((E×2○D[3;3])+(((2○D[3;3])*2)-(1○D[3;3])*2)+KB÷D[1;2]×OM*2)×OM*2
[6]     LO←(1.2×○2×D[4;1]×D[2;1]*4)÷D[1;2]
[7]     MA←(((1-D[5;3])÷D[4;3]×3)-((D[3;1]÷4)+(D[3;2]÷20)))×(LO×D[1;2]×OM*2)÷2
[8]     MC←((E×1○D[3;3])+(2○D[3;3])×1○D[3;3])×D[1;2]×OM*2
[9]     MST←MA-MC
[10]    BST←MST÷D[1;2]×NFS
[11]    MP←(0.5×LO×D[1;2]×OM*2)÷D[4;3]×3
[12]    DR←LO×OM÷16×NFS*0.5
[13]    P←(2×DR×NFS*0.5)÷OM
[14]    Q←NFS÷OM*2
[15]    R←MST÷D[1;2]×OM*2
[16]    S←MP÷D[1;2]×OM*2
[17]    'WIND SPEED (M/S).............',10 3↑D[4;2]
[18]    'PTICH ANGLE.................',10 3↑D[3;1]×180÷○1
[19]    'TIPSPEED RATIO..............',10 3↑D[4;3]
[20]    'ROTATIONAL SPEED (RPM)......',10 3↑OM×60÷○2
[21]    'NATURAL FREQUENCY...........',10 3↑NFS*0.5
[22]    'DAMPING RATIO...............',10 3↑DR
[23]    'DAMPED NATURAL FREQUENCY....',10 3↑DF←((1-DR*2)*0.5)×NFS*0.5
[24]    'PERIOD OF DAMPED OSCILATION.',10 3↑○2÷DF
[25]    'LOCK NUMBER.................',10 3↑LO
[26]    'SHADOW MOMENT (N-M).........',10 3↑MP
[27]    'STEADY STATE ROOT MOMENT (N-M).',10 3↑MST
[28]    'STEADY STATE DEFLECTION (DEG)..',10 3↑BST×180÷○1
[29]    ''
[30]    SS←D[5;1]
[31]    DS←2×D[5;2]÷D[2;1]
[32]    W1←○1-DS÷2
[33]    W2←○1+DS÷2
[34]    N1←5
[35]    DT←○1×1÷180
[36]    PT1←○1×10÷180
[37]    T1←○2
[38]    T←PT←N←0
[39]    B←BST
[40]    DB←DDB←M←0
```

```
[41]  L2:TOT←1 5⍴T,B,DB,DDB,M
[42]  L1:DB1←DB+DDB×DT
[43]   B1←B+((DB1+DB)÷2)×DT
[44]   DDB1←R-((P×DB1)+(Q×B1)+S×SS×(T≥W1)∧(T≤W2))
[45]   B←B1
[46]   DB←DB1
[47]   DDB←DDB1
[48]   T←T+DT
[49]   PT←PT+DT
[50]   →(PT<PT1)/L1
[51]   PT←0
[52]   M←B×D[1;2]×NFS
[53]   TOT←TOT,T,B,DB,DDB,M
[54]   →(T<T1)/L1
[55]   T←0
[56]   N←N+1
[57]   →(N<N1)/L2
[58]   '      AZMOUTH     DEFLECTION  ROOT MOMENT  ROOT MOMENT'
[59]   '       ANGLE       VARIATION    VARIATION      TOTAL'
[60]   '       (DEG)         (DEG)        (N-M)         (N-M)'
[61]   T←37 4⍴0
[62]   T[;1]←TOT[;1]×180÷○1
[63]   T[;2]←(TOT[;2]-BST)×180÷○1
[64]   T[;3]←(TOT[;5]-MST)
[65]   T[;4]←TOT[;5]
[66]   12 3⍕T
[67]   'DO YOU WANT AN INPUT RECORD'
[68]   EXIT←∧/'YES'=3⍴⍞
[69]   →(EXIT=0)/END
[70]   ''
[71]   ''
[72]   'BLADE MASS (KG).....',10 3⍕D[1;1]
[73]   'MASS MOMENT OF INERTIA (KG M*2)...',10 3⍕D[1;2]
[74]   'CENTER OF GRAVITY (M).....',10 3⍕D[1;3]
[75]   'RADIUS (M).....',10 3⍕D[2;1]
[76]   'HINGE OFFSET (M).....',10 3⍕D[2;2]
[77]   'NATURAL FREQUENCY.....',10 3⍕D[2;3]
[78]   'PITCH (RADIANS).....',10 3⍕D[3;1]
[79]   'TWIST (RADIANS).....',10 3⍕D[3;2]
[80]   'CONING (RADIANS).....',10 3⍕D[3;3]
[81]   'CHORD (M).....',10 3⍕D[4;1]
[82]   'WIND SPEED (M/S).....',10 3⍕D[4;2]
[83]   'TIPSPEED RATIO.....',10 3⍕D[4;3]
[84]   'SHADOW STRENGTH (VS/V).....',10 3⍕D[5;1]
[85]   'SHADOW WIDTH (M).....',10 3⍕D[5;2]
[86]   'AXIAL INTERFERENCE.....',10 3⍕D[5;3]
[87]  END:
      ∇
```

C.4 Terminal Session

RIGID BLADE

WIND SPEED (M/S).....	9.000
PTICH ANGLE.....	-6.000
TIPSPEED RATIO.....	7.500
ROTATIONAL SPEED (RPM).....	130.218
NATURAL FREQUENCY.....	28.814
DAMPING RATIO.....	0.345
DAMPED NATURAL FREQUENCY.....	27.048
PERIOD OF DAMPED OSCILATION....	0.232
LOCK NUMBER.....	11.655
SHADOW MOMENT (N-M).....	4919.515
STEADY STATE ROOT MOMENT (N-M).	2569.422
STEADY STATE DEFLECTION (DEG)..	1.736

AZMOUTH ANGLE (DEG)	DEFLECTION VARIATION (DEG)	ROOT MOMENT VARIATION (N-M)	ROOT MOMENT TOTAL (N-M)
0.000	0.008	11.882	2581.304
10.000	-0.033	-49.199	2520.223
20.000	-0.061	-90.815	2478.607
30.000	-0.076	-112.269	2457.152
40.000	-0.078	-115.446	2453.976
50.000	-0.070	-104.014	2465.408
60.000	-0.056	-82.588	2486.834
70.000	-0.038	-55.964	2513.458
80.000	-0.019	-28.500	2540.921
90.000	-0.002	-3.692	2565.730
100.000	0.011	16.063	2585.485
110.000	0.020	29.504	2598.926
120.000	0.025	36.413	2605.835
130.000	0.025	37.404	2606.826
140.000	0.023	33.671	2603.093
150.000	0.018	26.710	2596.132
160.000	0.012	18.074	2587.496
170.000	0.006	9.176	2578.598
180.000	-0.067	-99.590	2469.831
190.000	-0.313	-463.144	2106.278
200.000	-0.581	-860.360	1709.062
210.000	-0.721	-1067.243	1502.179
220.000	-0.743	-1099.729	1469.693
230.000	-0.671	-992.558	1576.864
240.000	-0.533	-789.595	1779.827
250.000	-0.362	-536.517	2032.905
260.000	-0.186	-274.913	2294.509
270.000	-0.026	-38.182	2531.240

280.000	0.102	150.676	2720.098
290.000	0.189	279.527	2848.948
300.000	0.234	346.150	2915.572
310.000	0.241	356.315	2925.737
320.000	0.217	321.311	2890.733
330.000	0.173	255.366	2824.787
340.000	0.117	173.280	2742.702
350.000	0.060	88.518	2657.940
360.000	0.008	11.882	2581.304

DO YOU WANT AN INPUT RECORD
YES

BLADE MASS (KG).....	15.440
MASS MOMENT OF INERTIA (KG M*2)...	102.150
CENTER OF GRAVITY (M).....	2.227
RADIUS (M).....	4.950
HINGE OFFSET (M).....	0.495
NATURAL FREQUENCY.....	25.000
PITCH (RADIANS).....	-0.105
TWIST (RADIANS).....	0.262
CONING (RADIANS).....	0.175
CHORD (M).....	0.263
WIND SPEED (M/S).....	9.000
TIPSPEED RATIO.....	7.500
SHADOW STRENGTH (VS/V).....	0.500
SHADOW WIDTH (M).....	0.254
AXIAL INTERFERENCE.....	0.000

10 3+BLADE

15.440	102.150	2.227
4.950	0.495	25.000
-0.105	0.262	0.175
0.263	9.000	7.500
0.500	0.254	0.000

A P P E N D I X D

D.1 Program DYNAMICS

This is the main program used to solve the coupled differential equations of motion for a flexible wind turbine blade. Operation of the program commences by typing DYNAMICS. The program responds by asking if initial conditions are to be specified. If NO, the initial conditions are assigned internally. If YES, the operator is asked to input the necessary parameters in modal coordinates. After initial conditions have been assigned, the operator is asked to input the number of rotor revolutions before printout begins, and the total number of rotor revolutions desired. For the steady state forced response, operational experience indicates that the transient motion is diminished after four rotor revolutions.

The majority of the input data consists of stored variables. These stored variables are given underscored names. The input data is assigned as follows:

W I N D; wind speed, m/s

T I P S P E E D; tip-speed-ratio

P I T C H; blade pitch angle, radians

C O N E; coning angle, radians

W I D T H; tower shadow width, m

S T R E N G T H; tower shadow strength, ν/V

R A D I U S; blade radius, m

S P A C E; spacing between stations, m

S T A T I O N; station spans expressed as r/R

C H O R D; chord distribution, m

T W I S T; blade twist distribution, radians

A X I A L; axial interference factor at each station span

R A D I A L; radial interference factor at each station span

M A S S; blade mass distribution, kg

F R E Q; non-rotating natural frequencies, radians/sec.

M O D E X; X coordinates of the mode shape

M O D E Y; Y coordinates of the mode shape

The sotred variables must be specified in SI units before program operation commences.

Following is the flow chart for Program DYNAMICS.

D.2 Program DYNAMICS Flow Chart

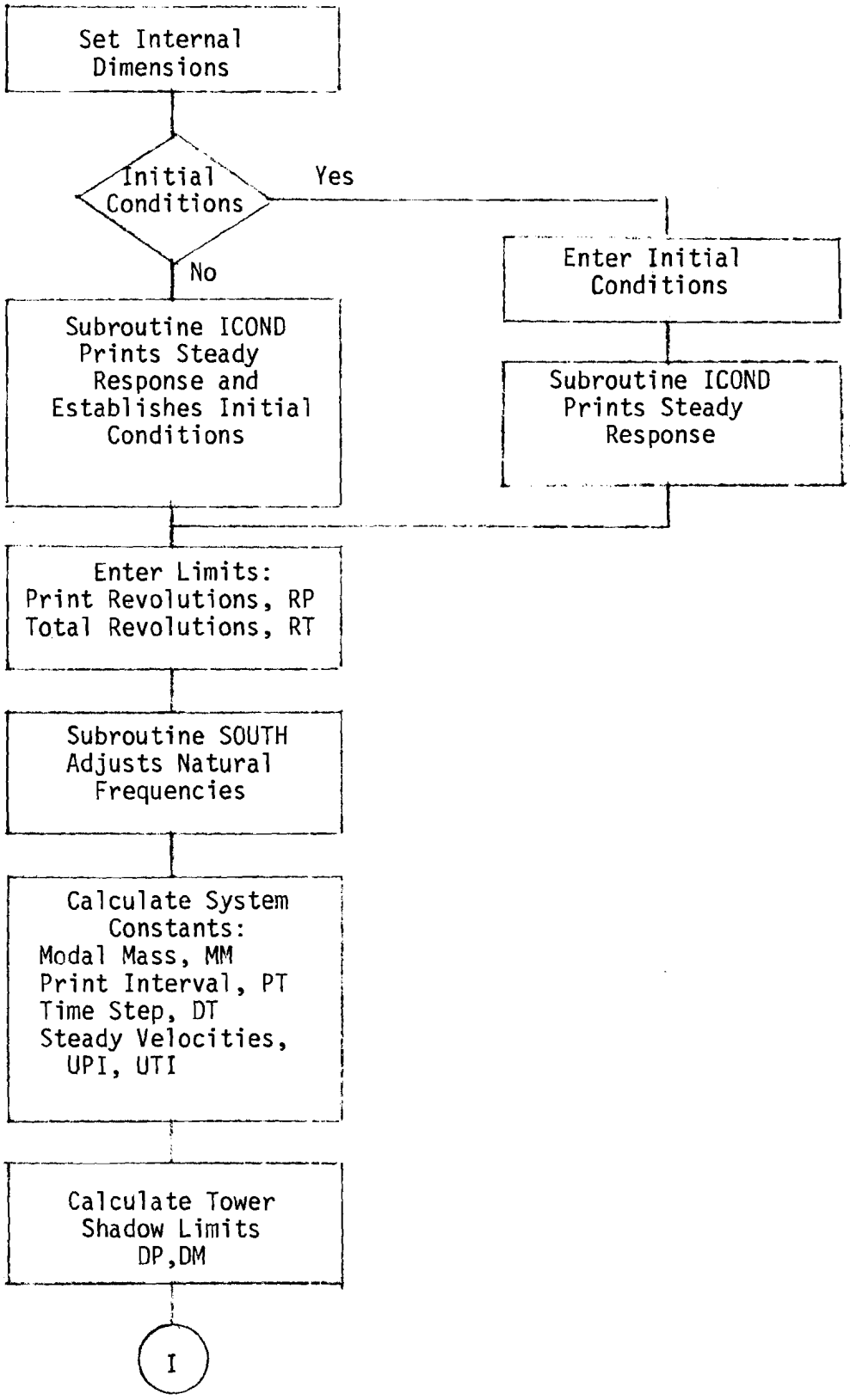

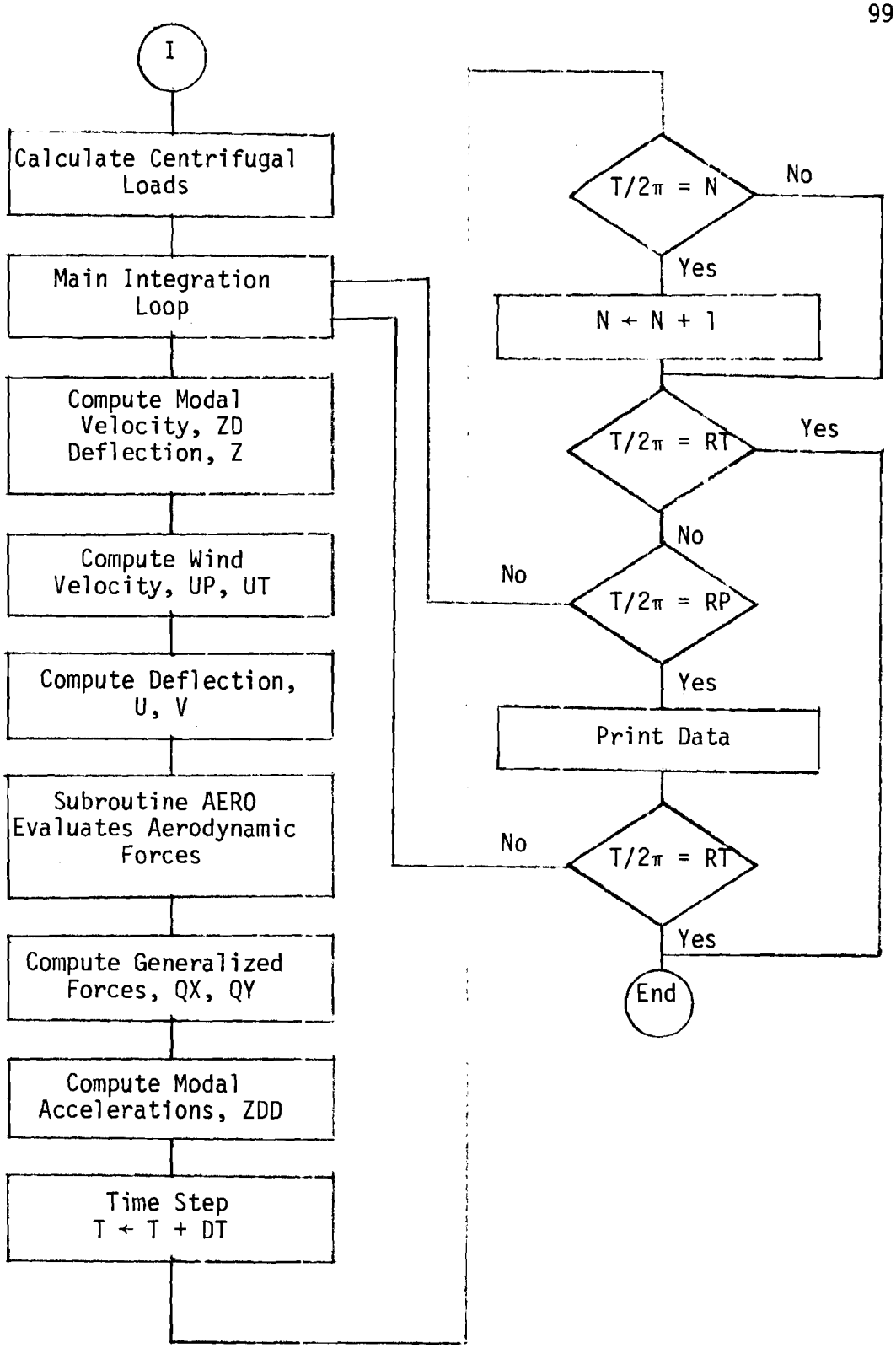
I
Calculate Centrifugal Loads
Main Integration Loop
Compute Modal Velocity, ZD Deflection, Z
Compute Wind Velocity, UP, UT
Compute Deflection, U, V
Subroutine AERO Evaluates Aerodynamic Forces
Compute Generalized Forces, QX, QY
Compute Modal Accelerations, ZDD
Time Step T ← T + DT
T/2π = N
No
Yes
N ← N + 1
T/2π = RT
Yes
No
T/2π = RP
No
Yes
Print Data
T/2π = RT
No
Yes
End

D.3 Program Listing

```
      ∇DYNAMICS[□]∇
      ∇DYNAMICS
[1]    MX←MODEX
[2]    MY←MODEY
[3]    D←1↓⍴MX
[4]    N←¯1↓⍴MX
[5]    A←N,D
[6]    'DO YOU WANT TO SPECIFY INITIAL CONDITIONS'
[7]    REPLY←∧/'YES'=3↑□
[8]    →(REPLY≠0)/INITIAL
[9]    DEF←INCOND
[10]   Z←(2,N)↑DEF
[11]   ZD←ZDD←(2,N)⍴0
[12]   NS←PT←T←0
[13]   →START
[14]  INITIAL:'ENTER INITIAL CONDITIONS OF THE MODAL SYSTEM'
[15]   'DISPLACEMENT'
[16]   Z←□
[17]   'VELOCITY'
[18]   ZD←□
[19]   'ACCELERATION'
[20]   ZDD←□
[21]   'AZIMUTH ANGLE'
[22]   T←□
[23]   'NUMBER OF COMPLETED REVOLUTIONS'
[24]   NS←□×○2
[25]   DEF←INCOND
[26]   PT←0
[27]  START:'NUMBER OF REVOLUTIONS BEFORE PRINT OUT'
[28]   RP←□
[29]   'TOTAL REVOLUTIONS'
[30]   RT←□
[31]   ''
[32]   N←1+T÷○2
[33]   OM←TIPSPEED×WIND÷RADIUS
[34]   F1←((FREQ*2)+(OM*2)×SOUTH)*0.5
[35]   TRAP←A⍴1,((D-2)⍴2),1
[36]   MM←+/((MX*2)+MY*2)×(A⍴MASS)×TRAP×SPACE÷2
[37]   MS←MM×F1*2
[38]   PN←(20×○1÷180)
[39]   DT←(1×○1÷180)÷OM
```

```
[40]   UP1←¯1×WIND×(1-AXIAL)
[41]   UT1←RADIUS×STATION×OM×(1+RADIAL)
[42]   DELT←WIDTH÷2×RADIUS×STATION
[43]   DELT←(DELT)1)+DELT×(DELT⍳1)
[44]   DP←DELT+⍳1
[45]   DM←(⍳1)-DELT
[46]   FC←MASS×STATION×RADIUS×(OM*2)×3⍟CONE
[47]  LOOP:
[48]   ZD←ZD+ZDD×DT
[49]   Z←Z+(ZD×DT)+ZDD×DT*2
[50]   UP←UP1+(¯1×,(ZD[2;]+.×MY))+WIND×STRENGTH×(DM⍳T-NS)-(DP⍳T-NS)
[51]   UT←UT1+(¯1×,(ZD[1;]+.×MX))
[52]   U←,Z[1;]+.×MX
[53]   V←,Z[2;]+.×MY
[54]   F←UP AERO UT
[55]   QX←+/(TRAP×MX×A⍲F[1;])×SPACE÷2
[56]   QY←+/(TRAP×MY×A⍲F[2;]+FC)×SPACE÷2
[57]   ZDD[1;]←(QX÷MM)-(F1*2)×,Z[1;]
[58]   ZDD[2;]←(QY÷MM)-(F1*2)×,Z[2;]
[59]   T←T+DT×OM
[60]   CYCLE←T÷⍳2
[61]   →((CYCLE÷N)<1)/L1
[62]   NS←T
[63]   N←N+1
[64]  L1:→(CYCLE>RT)/END
[65]   →(CYCLE⍳RP)/LOOP
[66]   PT←PT+DT×OM
[67]   →(PT<PN)/LOOP
[68]   'AZIMUTH ANGLE',5 0⍕(T-RP×⍳2)×180÷⍳1
[69]   'DEFLECTIONS (CM)'
[70]   'U',7 3⍕U×10
[71]   'V',7 3⍕V×10
[72]   'FORCE DISTRIBUTION (N/M)'
[73]   'X',7 0⍕FTX←F[1;]+(-1×MASS×,ZDD[1;]+.×MX)
[74]   'Y',7 0⍕FTY←F[2;]+(¯1×MASS×,ZDD[2;]+.×MY)+FC
[75]   'BENDING MOMENTS (N-M)'
[76]   'Y',7 0⍕BMY←BENDING FTX
[77]   'X',7 0⍕BMX←¯1×BENDING FTY
[78]   ''
[79]   PT←0
[80]   →(CYCLE<RT)/LOOP
[81]  END:'END OF PROGRAM'
      ∇
```

D.4 Terminal Session

```
      DYNAMICS
DO YOU WANT TO SPECIFY INITIAL CONDITIONS
NO
STEADY DEFLECTION (CM)
U  0.000 ¯0.001 ¯0.006 ¯0.014 ¯0.023 ¯0.037 ¯0.054 ¯0.076 ¯0.099 ¯0.124
V  0.000 ¯0.011 ¯0.033 ¯0.120 ¯0.244 ¯0.461 ¯0.753 ¯1.145 ¯1.619 ¯2.049
STEADY BENDING MOMENTS (N-M)
Y   ¯416   ¯412   ¯397   ¯370   ¯331   ¯281   ¯220   ¯150    ¯74      0
X   1294   1310   1352   1406   1458   1461   1348   1071    617      0
STEADY CENTRIFUGAL MOMENT DUE TO CONING (N-M)
X  ¯2007  ¯1985  ¯1905  ¯1754  ¯1522  ¯1222   ¯892   ¯559   ¯245      0
STEADY AERODYNAMIC MOMENTS (N-M)
X   3301   3295   3257   3160   2980   2683   2240   1630    862      0
NUMBER OF REVOLUTIONS BEFORE PRINT OUT
□:
      4
TOTAL REVOLUTIONS
□:
      5.2


AZIMUTH ANGLE   20
DEFLECTIONS (CM)
U  0.000 ¯0.001 ¯0.007 ¯0.015 ¯0.025 ¯0.040 ¯0.059 ¯0.082 ¯0.106 ¯0.134
V  0.000 ¯0.011 ¯0.033 ¯0.120 ¯0.244 ¯0.461 ¯0.753 ¯1.145 ¯1.618 ¯2.048
FORCE DISTRIBUTION (N/M)
X    ¯24    ¯38    ¯45    ¯47    ¯48    ¯49    ¯49    ¯47    ¯43    ¯34
Y    140    126    100     75     44    ¯39   ¯130   ¯218   ¯277   ¯314
BENDING MOMENTS (N-M)
Y   ¯448   ¯444   ¯429   ¯400   ¯360   ¯306   ¯240   ¯163    ¯80      0
X   1297   1314   1355   1409   1460   1463   1349   1072    616      0

AZIMUTH ANGLE   40
DEFLECTIONS (CM)
U  0.000 ¯0.001 ¯0.006 ¯0.012 ¯0.021 ¯0.033 ¯0.048 ¯0.067 ¯0.087 ¯0.110
V  0.000 ¯0.011 ¯0.033 ¯0.121 ¯0.246 ¯0.464 ¯0.757 ¯1.150 ¯1.624 ¯2.055
FORCE DISTRIBUTION (N/M)
X    ¯24    ¯38    ¯43    ¯42    ¯41    ¯40    ¯39    ¯37    ¯34    ¯28
Y    140    126    100     75     43    ¯39   ¯130   ¯218   ¯276   ¯314
BENDING MOMENTS (N-M)
Y   ¯369   ¯365   ¯350   ¯324   ¯288   ¯244   ¯190   ¯130    ¯64      0
X   1299   1315   1357   1410   1461   1463   1348   1070    616      0
```

AZIMUTH ANGLE 60
DEFLECTIONS (CM)

U	0.000	-0.001	-0.006	-0.013	-0.023	-0.036	-0.053	-0.073	-0.096	-0.121
V	0.000	-0.011	-0.033	-0.121	-0.245	-0.463	-0.756	-1.151	-1.627	-2.059

FORCE DISTRIBUTION (N/M)

X	-24	-38	-44	-44	-44	-44	-43	-42	-38	-31
Y	140	126	101	76	45	-38	-130	-219	-278	-316

BENDING MOMENTS (N-M)

Y	-404	-400	-385	-358	-320	-271	-212	-144	-71	0
X	1301	1317	1359	1413	1464	1468	1354	1076	619	0

AZIMUTH ANGLE 80
DEFLECTIONS (CM)

U	0.000	-0.001	-0.007	-0.015	-0.026	-0.041	-0.060	-0.084	-0.110	-0.138
V	0.000	-0.011	-0.033	-0.121	-0.244	-0.463	-0.755	-1.149	-1.625	-2.057

FORCE DISTRIBUTION (N/M)

X	-24	-38	-46	-48	-49	-51	-50	-49	-45	-35
Y	140	126	101	76	44	-39	-131	-219	-278	-316

BENDING MOMENTS (N-M)

Y	-461	-458	-442	-413	-372	-317	-249	-169	-83	0
X	1303	1320	1361	1415	1467	1470	1356	1077	620	0

AZIMUTH ANGLE 100
DEFLECTIONS (CM)

U	0.000	-0.001	-0.006	-0.014	-0.023	-0.037	-0.054	-0.075	-0.098	-0.124
V	0.000	-0.011	-0.033	-0.120	-0.244	-0.461	-0.752	-1.144	-1.618	-2.048

FORCE DISTRIBUTION (N/M)

X	-24	-38	-44	-45	-45	-45	-44	-43	-39	-32
Y	140	126	100	75	44	-38	-129	-217	-276	-315

BENDING MOMENTS (N-M)

Y	-413	-410	-394	-367	-329	-279	-219	-149	-74	0
X	1293	1309	1351	1405	1456	1459	1346	1070	616	0

AZIMUTH ANGLE 120
DEFLECTIONS (CM)

U	0.000	-0.001	-0.006	-0.013	-0.021	-0.034	-0.050	-0.069	-0.090	-0.114
V	0.000	-0.011	-0.033	-0.120	-0.243	-0.459	-0.750	-1.141	-1.613	-2.041

FORCE DISTRIBUTION (N/M)

X	-24	-38	-43	-43	-42	-42	-40	-39	-35	-29
Y	140	126	101	76	45	-37	-128	-216	-275	-314

BENDING MOMENTS (N-M)

Y	-381	-378	-363	-336	-300	-254	-198	-135	-67	0
X	1284	1300	1342	1396	1448	1453	1341	1067	615	0

AZIMUTH ANGLE 140
DEFLECTIONS (CM)

U	0.000	-0.001	-0.007	-0.014	-0.024	-0.038	-0.056	-0.078	-0.102	-0.129
V	0.000	-0.011	-0.033	-0.120	-0.243	-0.460	-0.751	-1.143	-1.616	-2.046

FORCE DISTRIBUTION (N/M)

X	-24	-38	-45	-46	-46	-47	-47	-45	-41	-33
Y	140	126	101	76	45	-38	-129	-217	-277	-315

BENDING MOMENTS (N-M)

Y	-431	-427	-412	-384	-344	-293	-229	-156	-77	0
X	1292	1308	1350	1404	1456	1460	1348	1071	617	0

AZIMUTH ANGLE 160
DEFLECTIONS (CM)

U	0.000	-0.001	-0.007	-0.015	-0.025	-0.039	-0.057	-0.080	-0.104	-0.131
V	0.000	-0.011	-0.033	-0.120	-0.244	-0.462	-0.754	-1.146	-1.621	-2.051

FORCE DISTRIBUTION (N/M)

X	-24	-38	-45	-47	-47	-48	-48	-46	-42	-33
Y	140	126	100	75	44	-39	-130	-218	-277	-315

BENDING MOMENTS (N-M)

Y	-439	-435	-420	-392	-352	-299	-234	-160	-78	0
X	1298	1314	1356	1410	1461	1464	1351	1073	617	0

AZIMUTH ANGLE 180
DEFLECTIONS (CM)

U	0.000	-0.001	-0.006	-0.013	-0.022	-0.035	-0.051	-0.071	-0.093	-0.117
V	0.000	-0.011	-0.033	-0.120	-0.243	-0.460	-0.752	-1.146	-1.621	-2.052

FORCE DISTRIBUTION (N/M)

X	9	2	-12	-24	-34	-42	-45	-45	-41	-26
Y	180	209	197	151	95	-19	-132	-236	-302	-310

BENDING MOMENTS (N-M)

Y	-358	-359	-357	-345	-320	-279	-220	-149	-70	0
X	1175	1199	1273	1380	1486	1528	1426	1133	638	0

AZIMUTH ANGLE 200
DEFLECTIONS (CM)

U	0.000	-0.001	-0.005	-0.011	-0.018	-0.029	-0.042	-0.059	-0.077	-0.097
V	0.000	-0.009	-0.028	-0.107	-0.219	-0.422	-0.698	-1.074	-1.532	-1.941

FORCE DISTRIBUTION (N/M)

X	-24	-37	-41	-39	-36	-34	-33	-32	-30	-27
Y	140	129	108	91	67	-14	-109	-204	-271	-315

BENDING MOMENTS (N-M)

Y	-326	-323	-308	-284	-252	-213	-168	-116	-59	0
X	1163	1179	1223	1284	1352	1381	1298	1048	611	0

AZIMUTH ANGLE 220
DEFLECTIONS (CM)

U	0.000	-0.001	-0.007	-0.016	-0.027	-0.043	-0.064	-0.088	-0.115	-0.146
V	0.000	-0.010	-0.031	-0.112	-0.228	-0.432	-0.708	-1.078	-1.527	-1.933

FORCE DISTRIBUTION (N/M)

X	-24	-39	-47	-51	-52	-54	-54	-53	-47	-36
Y	140	125	98	73	43	-35	-121	-203	-258	-302

BENDING MOMENTS (N-M)

Y	-490	-486	-470	-441	-396	-337	-264	-179	-87	0
X	1206	1223	1264	1316	1367	1371	1266	1008	584	0

AZIMUTH ANGLE 240
DEFLECTIONS (CM)

U	0.000	-0.001	-0.007	-0.015	-0.025	-0.039	-0.058	-0.081	-0.105	-0.133
V	0.000	-0.011	-0.032	-0.118	-0.239	-0.453	-0.741	-1.130	-1.599	-2.024

FORCE DISTRIBUTION (N/M)

X	-24	-38	-45	-47	-48	-49	-49	-47	-42	-33
Y	140	127	103	80	50	-34	-127	-217	-277	-313

BENDING MOMENTS (N-M)

Y	-444	-441	-425	-397	-356	-302	-236	-160	-78	0
X	1273	1289	1331	1387	1443	1452	1344	1070	615	0

AZIMUTH ANGLE 260
DEFLECTIONS (CM)

U	0.000	-0.001	-0.005	-0.011	-0.018	-0.028	-0.041	-0.057	-0.074	-0.093
V	0.000	-0.012	-0.035	-0.125	-0.252	-0.474	-0.769	-1.165	-1.642	-2.077

FORCE DISTRIBUTION (N/M)

X	-24	-37	-41	-39	-36	-34	-32	-30	-27	-23
Y	140	125	97	70	36	-46	-135	-220	-276	-313

BENDING MOMENTS (N-M)

Y	-315	-311	-296	-272	-240	-200	-155	-105	-53	0
X	1326	1342	1383	1434	1480	1474	1352	1069	613	0

AZIMUTH ANGLE 280
DEFLECTIONS (CM)

U	0.000	-0.001	-0.006	-0.014	-0.023	-0.037	-0.054	-0.075	-0.098	-0.124
V	0.000	-0.011	-0.034	-0.124	-0.252	-0.476	-0.775	-1.177	-1.663	-2.104

FORCE DISTRIBUTION (N/M)

X	-24	-38	-44	-45	-45	-45	-45	-43	-39	-31
Y	140	126	101	75	43	-42	-135	-225	-284	-320

BENDING MOMENTS (N-M)

Y	-413	-409	-394	-367	-328	-278	-218	-148	-73	0
X	1341	1358	1399	1453	1504	1505	1386	1099	631	0

AZIMUTH ANGLE 300
DEFLECTIONS (CM)

U	0.000	-0.001	-0.008	-0.017	-0.028	-0.045	-0.066	-0.092	-0.120	-0.152
V	0.000	-0.011	-0.034	-0.123	-0.248	-0.470	-0.767	-1.166	-1.648	-2.085

FORCE DISTRIBUTION (N/M)

X	-24	-39	-47	-51	-53	-55	-56	-55	-50	-39
Y	140	126	100	75	43	-41	-133	-222	-282	-320

BENDING MOMENTS (N-M)

Y	-505	-501	-485	-455	-411	-351	-277	-189	-93	0
X	1328	1345	1386	1440	1490	1492	1374	1091	627	0

AZIMUTH ANGLE 320
DEFLECTIONS (CM)

U	0.000	-0.001	-0.006	-0.013	-0.022	-0.036	-0.052	-0.073	-0.095	-0.120
V	0.000	-0.011	-0.033	-0.120	-0.243	-0.460	-0.751	-1.142	-1.615	-2.044

FORCE DISTRIBUTION (N/M)

X	-24	-38	-44	-44	-43	-44	-43	-41	-38	-31
Y	140	126	100	75	44	-38	-129	-216	-275	-314

BENDING MOMENTS (N-M)

Y	-401	-397	-382	-355	-318	-270	-211	-144	-72	0
X	1288	1305	1346	1400	1451	1455	1342	1067	615	0

AZIMUTH ANGLE 340
DEFLECTIONS (CM)

U	0.000	-0.001	-0.005	-0.012	-0.020	-0.032	-0.047	-0.065	-0.084	-0.106
V	0.000	-0.011	-0.032	-0.117	-0.239	-0.453	-0.740	-1.128	-1.597	-2.021

FORCE DISTRIBUTION (N/M)

X	-24	-38	-42	-41	-40	-39	-37	-36	-33	-27
Y	140	127	102	78	48	-34	-125	-214	-274	-313

BENDING MOMENTS (N-M)

Y	-357	-353	-339	-313	-278	-235	-184	-125	-62	0
X	1262	1278	1320	1375	1429	1437	1330	1060	612	0

AZIMUTH ANGLE 360
DEFLECTIONS (CM)

U	0.000	-0.001	-0.007	-0.015	-0.025	-0.040	-0.059	-0.082	-0.107	-0.135
V	0.000	-0.011	-0.032	-0.118	-0.240	-0.455	-0.744	-1.133	-1.603	-2.029

FORCE DISTRIBUTION (N/M)

X	-24	-38	-46	-48	-48	-50	-49	-48	-43	-34
Y	140	126	101	76	46	-36	-128	-215	-275	-314

BENDING MOMENTS (N-M)

Y	-452	-449	-433	-405	-363	-309	-242	-165	-81	0
X	1279	1295	1337	1391	1443	1448	1338	1064	613	0

AZIMUTH ANGLE 380
DEFLECTIONS (CM)

U	0.000	-0.001	-0.007	-0.015	-0.025	-0.040	-0.059	-0.082	-0.106	-0.134
V	0.000	-0.011	-0.033	-0.120	-0.244	-0.461	-0.753	-1.145	-1.619	-2.048

FORCE DISTRIBUTION (N/M)

X	-24	-38	-45	-47	-48	-49	-49	-47	-43	-34
Y	140	126	100	75	44	-39	-130	-218	-277	-314

BENDING MOMENTS (N-M)

Y	-448	-444	-429	-400	-360	-306	-240	-163	-80	0
X	1297	1314	1355	1409	1460	1463	1349	1072	616	0

AZIMUTH ANGLE 400
DEFLECTIONS (CM)

U	0.000	-0.001	-0.006	-0.012	-0.021	-0.033	-0.048	-0.067	-0.087	-0.110
V	0.000	-0.011	-0.033	-0.121	-0.246	-0.464	-0.757	-1.150	-1.624	-2.055

FORCE DISTRIBUTION (N/M)

X	-24	-38	-43	-42	-41	-40	-39	-37	-34	-28
Y	140	126	100	75	43	-39	-130	-218	-276	-314

BENDING MOMENTS (N-M)

Y	-369	-365	-350	-324	-288	-244	-190	-130	-64	0
X	1299	1315	1357	1410	1461	1463	1348	1070	616	0

AZIMUTH ANGLE 420
DEFLECTIONS (CM)

U	0.000	-0.001	-0.006	-0.013	-0.023	-0.036	-0.053	-0.073	-0.095	-0.121
V	0.000	-0.011	-0.033	-0.121	-0.245	-0.463	-0.756	-1.151	-1.627	-2.059

FORCE DISTRIBUTION (N/M)

X	-24	-38	-44	-44	-44	-44	-43	-42	-38	-31
Y	140	126	101	76	45	-38	-130	-219	-278	-316

BENDING MOMENTS (N-M)

Y	-404	-400	-385	-358	-320	-271	-212	-144	-71	0
X	1301	1317	1359	1413	1464	1468	1354	1076	619	0

END OF PROGRAM

A P P E N D I X E

E.1 Function ICOND

This program is a self-contained package that computes turbine forces and deflections for an undisturbed flow field. The program uses the same data used by program DYNAMICS for all computations. The computed parameters are printed and assigned to a matrix that can be used as initial conditions for DYNAMICS. The program uses functions SOUTH, AERO, and BENDING for internal computation.

Following is the flow chart for the Program Function ICOND.

E.2 Function ICOND Flow Chart

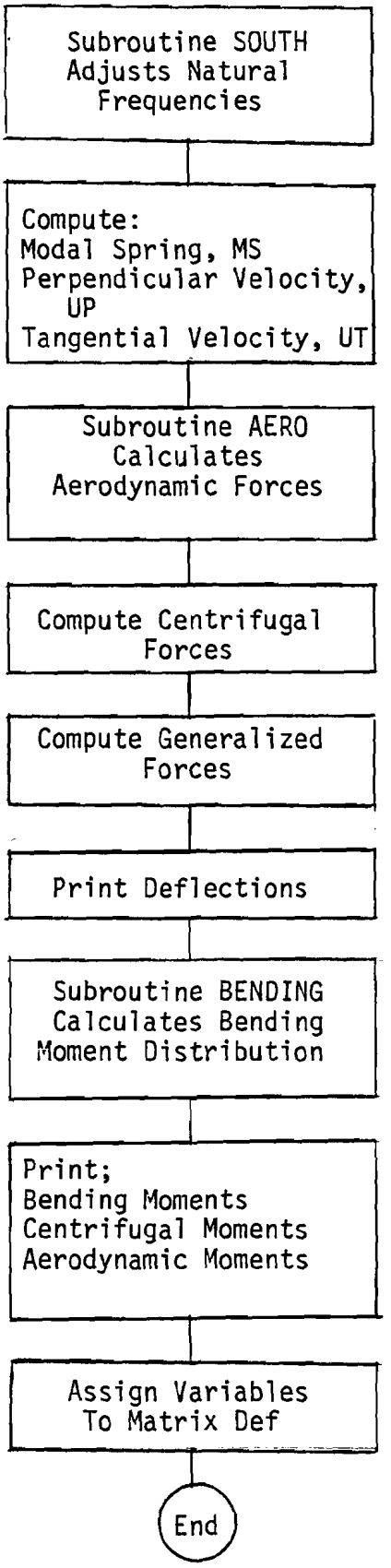

E.3 Program Listing

```
      ∇INCOND[□]∇
      ∇DEF←INCOND;MX;MY;K;OM;F2;D;T;MS;UP;UT;U;V;U1;V1;FA;FC;QX;QY;ZX;ZY;
[1]    MX←MODEX
[2]    MY←MODEY
[3]    OM←TIPSPEED×WIND÷RADIUS
[4]    F2←((FREQ*2)+(OM*2)×SOUTH)
[5]    D←1↓⍴MX
[6]    T←(⍴MX)⍴1,((D-2)⍴2),1
[7]    MS←(+/((MX*2)+MY*2)×((⍴MX)⍴MASS)×T×SPACE÷2)×F2
[8]    UP←¯1×WIND×(1-AXIAL)
[9]    UT←RADIUS×STATION×OM×(1+RADIAL)
[10]   K←0
[11]   FA←UP AERO UT
[12]   FC←MASS×(OM*2)×STATION×RADIUS×3○CONE
[13]   QX←+/(T×MX×(⍴MX)⍴FA[1;])×SPACE÷2
[14]   QY←+/(T×MY×(⍴MX)⍴FA[2;]+FC)×SPACE÷2
[15]   ZX←QX÷MS
[16]   ZY←QY÷MS
[17]   'STEADY DEFLECTION (CM)'
[18]   'U',7 3⍕(ZX+.×MX)×10
[19]   'V',7 3⍕(ZY+.×MY)×10
[20]   'STEADY BENDING MOMENTS (N-M)'
[21]   'Y',7 0⍕BMY←BENDING FA[1;]
[22]   'X',7 0⍕BMX←¯1×BENDING FA[2;]+FC
[23]   'STEADY CENTRIFUGAL MOMENT DUE TO CONING (N-M)'
[24]   'X',7 0⍕BENDING FC×¯1
[25]   'STEADY AERODYNAMIC MOMENTS (N-M)'
[26]   'X',7 0⍕¯1×BENDING FA[2;]
[27]   ZX←D⍴ZX
[28]   ZY←D⍴ZY
[29]   DEF←(2,D)⍴ZX,ZY
[30]   M←(2,D)⍴BMX,BMY
[31]   DEF←DEF,M
      ∇
```

A P P E N D I X F

F.1 Function AERO

Aerodynamic forces are computed by this program. The program requires input of the velocities perpendicular (U_p) and tangential (U_T) to the plane of rotation. The lift and drag calculations are based on two dimensional airfoil theory. Presently, the program contains lift coefficient (C_ℓ) and drag coefficient (C_D) curve fits for a 4415 airfoil. These curve fits are polynomials of the form:

$$y = C_n X^n + \ldots + C_3 X^3 + C_2 X^2 + C_1 X^1 + C_0 X^0$$

Alteration of the polynomial for a different airfoil section is accomplished by changing the coefficients. The coefficients are listed internally as CLC and CDC.

The program output is a matrix (F) that contains:

Perpendicular force

Tangential force

Angle of attack

Lift coefficient

Drag coefficient

Relative pitch

Relative velocity

for each station along the blade.

Following is the flow chart for the Program Function AERO.

F.2 Function AERO Flow Chart

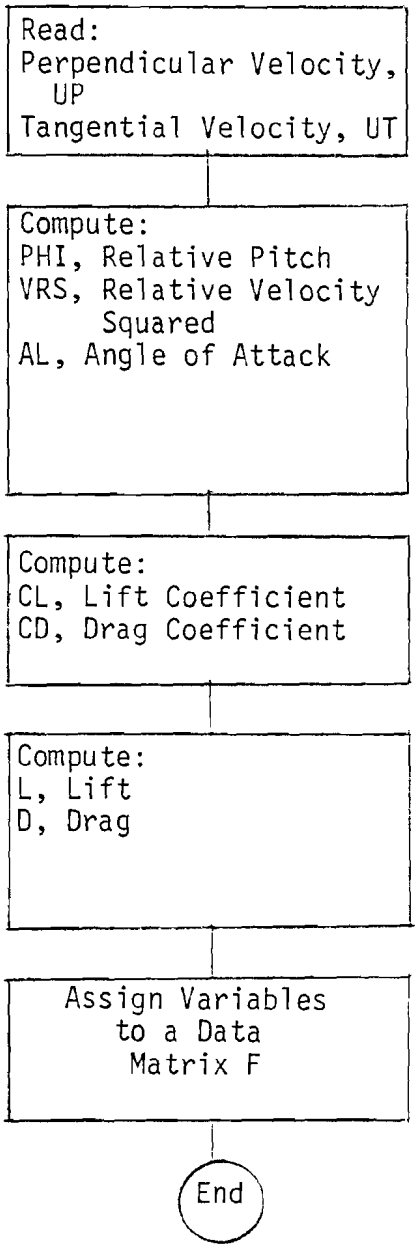

F.3 Program Listing

```
      ∇AERO[□]∇
      ∇F←UP AERO UT;PHI;VRS;AL;CLC;CDC;CD;CL;RHO;L;D
[1]    PHI←(¯3○(UP÷UT))×¯1
[2]    VRS←((UP*2)+UT*2)
[3]    AL←((⍴PHI),1)⍴PHI-TWIST+PITCH
[4]    CLC←¯3.6826 5.4301 0.41124
[5]    CDC←0.19095 3.4623E¯5 0.33515 ¯8.5943E¯5 0.010511
[6]    CL←(AL⊥CLC)×(,AL≥¯0.34907)∧(,AL≤0.34907)
[7]    CD←(2×(DL=0))+(AL⊥CDC)×DL←(,AL≥¯1.571)∧(,AL≤1.571)
[8]    RHO←1.2
[9]    L←0.5×RHO×CHORD×VRS×CL
[10]   D←0.5×RHO×CHORD×VRS×CD
[11]   F←(7,(⍴UP))⍴0
[12]   F[2;]←((L×2○PHI)+D×1○PHI)×¯1
[13]   F[1;]←(D×2○PHI)-L×1○PHI
[14]   F[3;]←AL
[15]   F[4;]←CL
[16]   F[5;]←CD
[17]   F[6;]←PHI
[18]   F[7;]←VRS×0.5
      ∇
```

A P P E N D I X G

G.1 Function BENDING

BENDING computes the bending moments for any load distribution when the forces are equally spaced along the blade and are given in terms of force per unit length. The spacing between stations is stored as the variable S P A C E. Care must be taken as to the sign of the computed bending moments.

Following is the flow chart for the Program Function BENDING.

G.2 Function BENDING Flow Chart

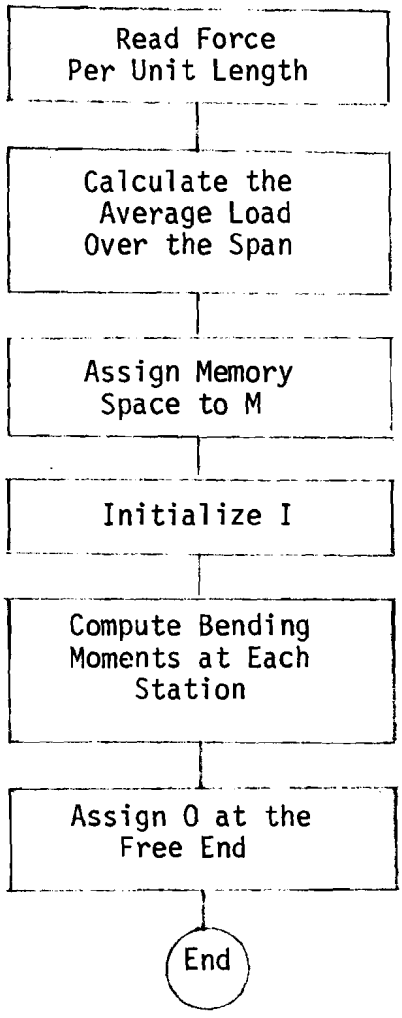

G.3 Program Listing

```
      ∇BENDING[□]∇
      ∇M←BENDING F;I;K;H
[1]    H←SPACE
[2]    F←((1↓F)+(¯1↓F))×H÷2
[3]    M←F
[4]    I←1
[5]   NEW:K←I+(⌊1+(⍴F)-I)-1
[6]    M[I]←H×+/(0.5+K-1)×F[K]
[7]    →(I=⍴F)/L
[8]    I←I+1
[9]    →NEW
[10]  L:M←M,0
      ∇
```

A P P E N D I X H

H.1 Function DATA

DATA is used to print an input record for program DYNAMICS. The input record is listed when the operator types DATA.

Following is the program listing for DATA.

H.2 Program Listing

```
      ∇DATA[□]∇
      ∇DATA
[1]    'WIND SPEED (M/S).............',7 3↑WIND
[2]    'TIP SPEED RATIO..............',7 3↑TIPSPEED
[3]    'PITCH ANGLE (DEG)............',7 3↑PITCH×180÷○1
[4]    'CONING ANGLE (DEG)...........',7 3↑CONE×180÷○1
[5]    'SHADOW WIDTH (M).............',7 3↑WIDTH
[6]    'SHADOW STRENGTH V/V..........',7 3↑STRENGTH
[7]    'BLADE RADIUS (M).............',7 3↑RADIUS
[8]    'STATION SPAN'
[9]    7 3↑STATION
[10]   'CHORD DISTRUBUTION (M)'
[11]   7 3↑CHORD
[12]   'TWIST DISTRIBUTION (DEG)'
[13]   7 3↑TWIST×180÷○1
[14]   'AXIAL INTERFERENCE FACTOR'
[15]   7 3↑AXIAL
[16]   'RADIAL INTERFERENCE FACTOR'
[17]   7 3↑RADIAL
[18]   'MASS DISTRIBUTION (KG)'
[19]   7 3↑MASS
[20]   'NATURAL FREQUENCY (RADIANS/SECOND)'
[21]   17 3↑FREQ
[22]   'X MODAL COORDINATES'
[23]   7 3↑MODEX
[24]   'Y MODAL COORDINATES'
[25]   7 3↑MODEY
      ∇
```

H.3 Terminal Session

```
      DATA
WIND SPEED (M/S).............  9.000
TIP SPEED RATIO..............  7.500
PITCH ANGLE (DEG)............ -6.000
CONING ANGLE (DEG)........... 10.000
SHADOW WIDTH (M).............  0.254
SHADOW STRENGTH V/V.........  0.500
BLADE RADIUS (M).............  4.953
STATION SPAN
  0.100  0.200  0.300  0.400  0.500  0.600  0.700  0.800  0.900  1.000
CHORD DISTRUBUTION (M)
  0.411  0.445  0.384  0.311  0.259  0.223  0.192  0.168  0.137  0.107
TWIST DISTRIBUTION (DEG)
 45.000 25.600 15.700 10.400  7.400  4.500  2.700  1.400  0.400  0.000
AXIAL INTERFERENCE FACTOR
  0.090  0.140  0.180  0.200  0.210  0.230  0.240  0.250  0.250  0.270
RADIAL INTERFERENCE FACTOR
  0.140  0.050  0.027  0.016  0.011  0.008  0.006  0.005  0.004  0.003
MASS DISTRIBUTION (KG)
 10.050  6.123  4.766  4.016  3.463  2.696  1.999  1.473  1.025  0.527
NATURAL FREQUENCY (RADIANS/SECOND)
           28.430              64.450              99.550
X MODAL COORDINATES
  0.000  0.000 -0.010 -0.020 -0.040 -0.060 -0.080 -0.110 -0.130 -0.160
  0.000  0.010  0.050  0.110  0.180  0.290  0.430  0.600  0.790  1.000
  0.000 -0.010 -0.020 -0.040 -0.060 -0.050 -0.030  0.030  0.120  0.150
Y MODAL COORDINATES
  0.000  0.010  0.030  0.090  0.170  0.290  0.430  0.600  0.790  0.990
  0.000  0.000  0.000  0.000  0.000  0.020  0.060  0.110  0.180  0.250
  0.000  0.030  0.090  0.180  0.270  0.280  0.140 -0.190 -0.700 -0.950
```

APPENDIX I

I.1 Tower Shrouds

The investigation into tower shadow cannot be considered complete until experimental verification of the blade interaction with the wake confirms predicted behavior. To facilitate the experimental procedures, tower shrouds have been constructed to increase the diameter of the WF-1 pole tower. Two diameter increases, 20" and 30", were chosen to give a representative example of tower shadow. Figure A.1 shows the orientation of an installed 30" diameter shroud.

The major factors in the design of the shrouds was the tower geometry (Figure A.2 and A.3) and the accessability of the nacell; access to the nacell must be maintained because of experimental procedures. These constraints lead to the choice of a split shroud, which has an upper and a lower portion.

I.2 20" Diameter Shroud

The smaller diameter shroud will not encompass the tower and the rungs. Therefore, clearance holes have been cut that allow for the protrusion of the rungs. The shroud is supported by U-bolts attaching the top plate of each section to a semi-circular rung, Figure A.4. The front section of the shroud is removeable to permit easy access to the rungs. Modified hinges support the removeable front section. Details of the hinges are shown in Figure A.5.

I.3 30" Diameter Shroud

The 30" diameter shroud is large enough to encompass both the tower and rungs. Therefore, the shroud must be hinged on one side and latched on the other side to permit access to the nacell. The latches are rope

controlled since there is no way to reach the upper latches from the tower. Details about the construction and assembly of this shroud are shown in Figures A.6 and A.7.

ENERGY ALTERNATIVE PROGRAM

TURBINE SHEET

DWG. NO.

DATE 10/78 DRN BY [illegible] SCALE

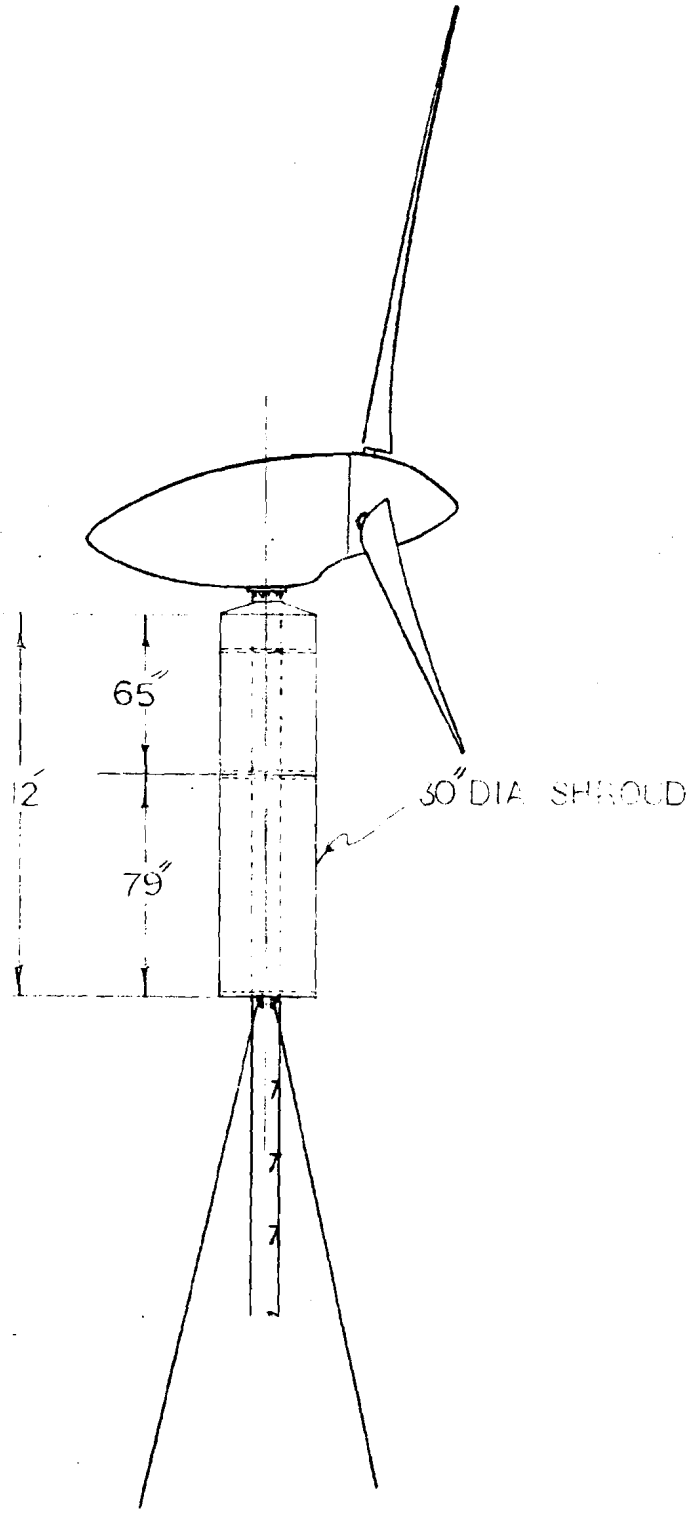

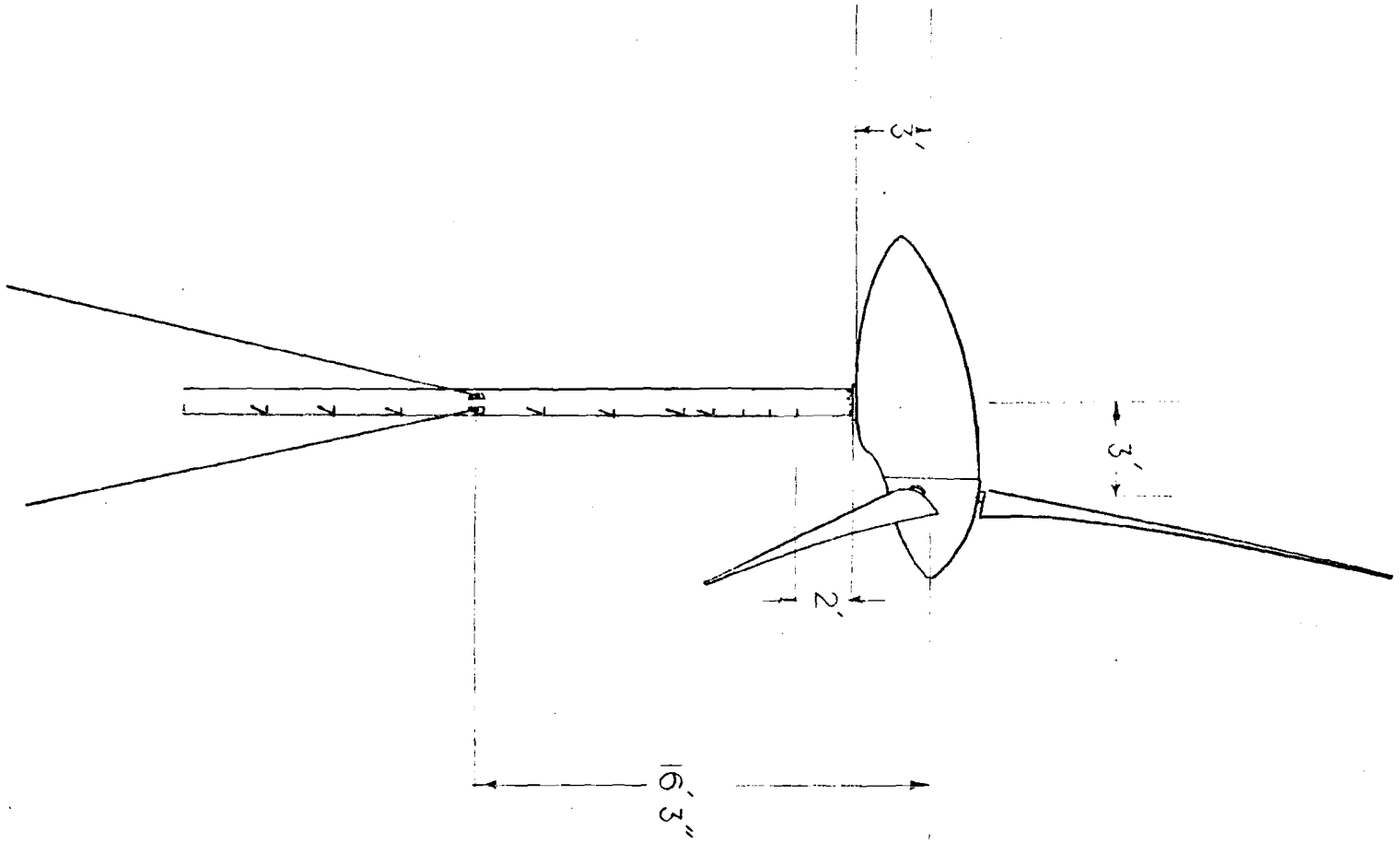

ENERGY ALTERNATIVE PROGRAM

[illegible]

DWG. NO. 123

DATE [illegible] DRN BY [illegible] SCALE

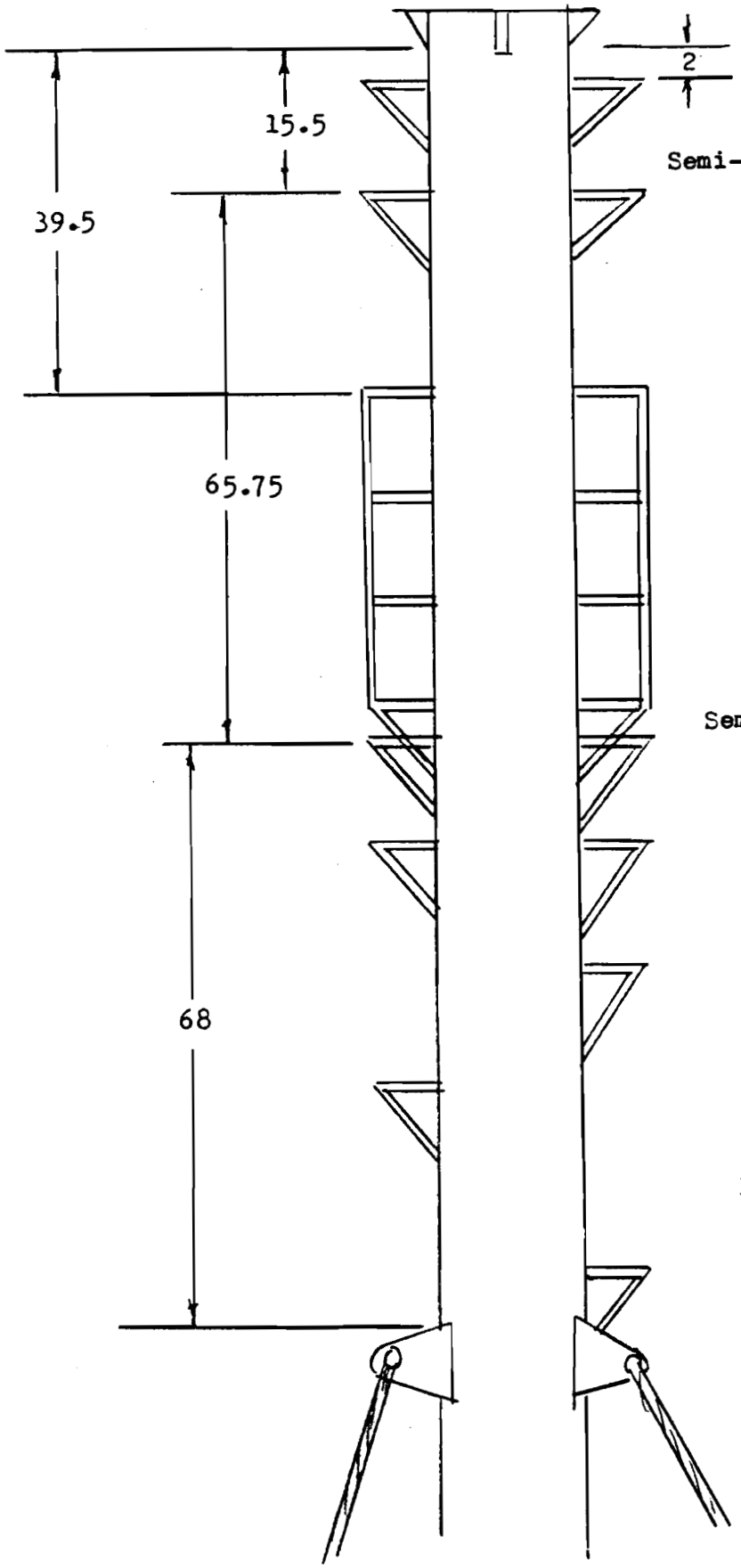
2
15.5
39.5
65.75
68
Semi-circular rung
Ladder
Semi-circular rung
Dimensions in inches

20" Diameter Shroud

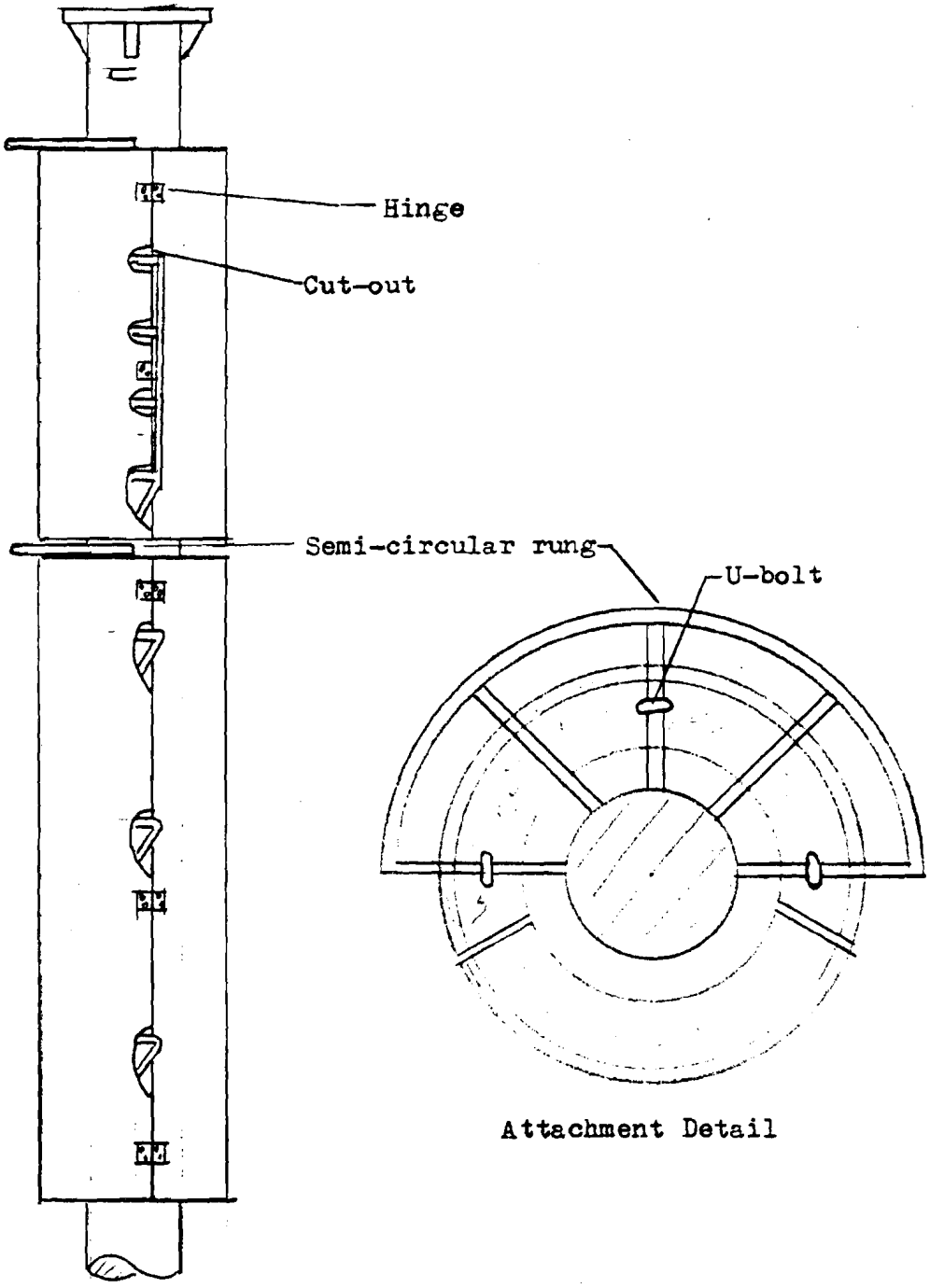

Attachment Detail

Hinge Detail

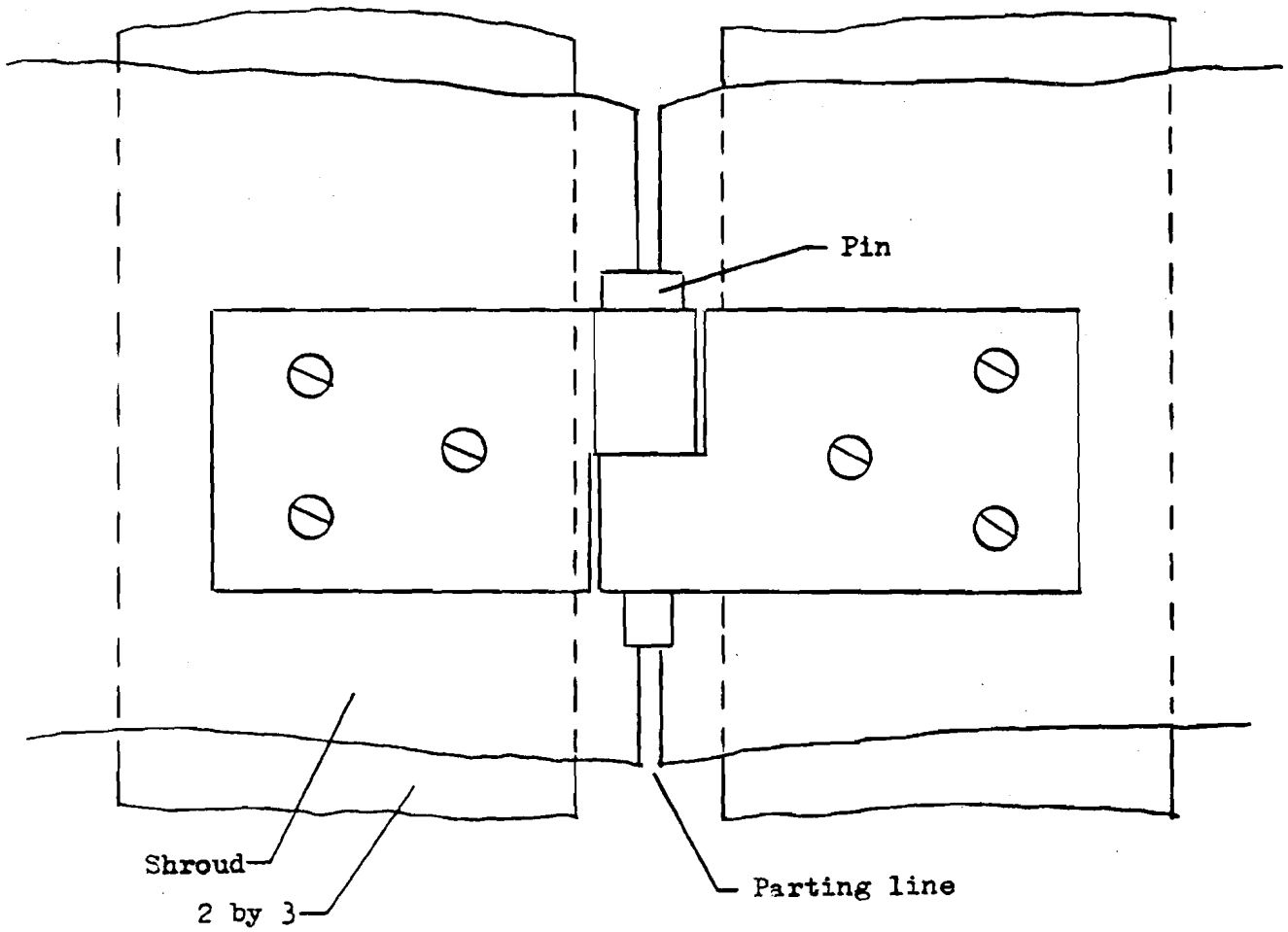

Material 1/2 Drop hinge

SIDE VIEW
SECTION

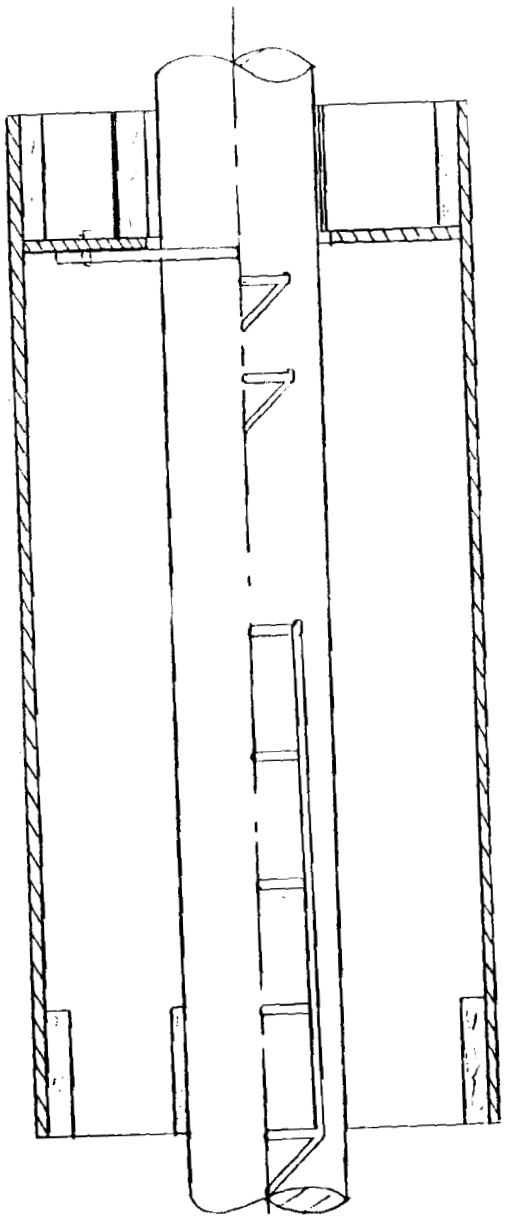

TOP VIEW

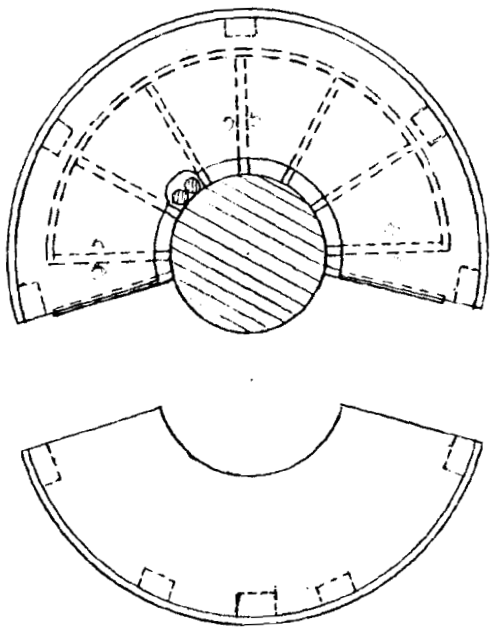

UPPER SHROUD
ASSEMBLY

30" Diameter Shroud

Outside

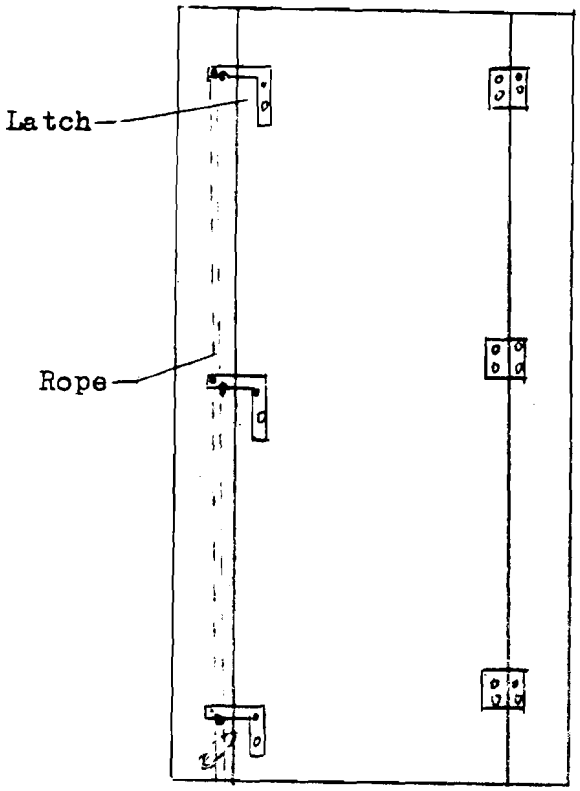

Inside

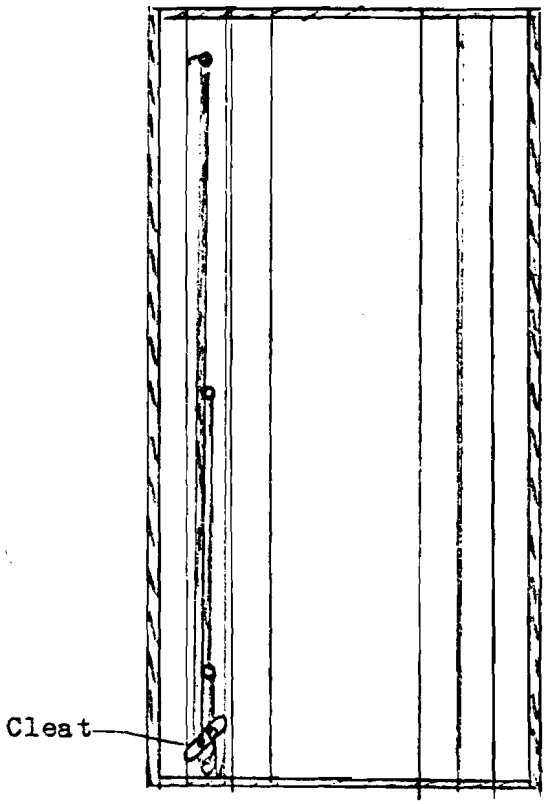

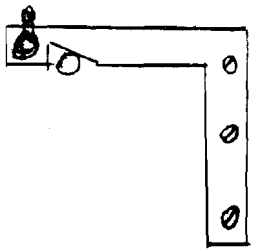

Latch detail